Effect of rock stiffness on subsidence phenomena

Angelo Cannata

Department of Environment, Land and Infrastructure Engineering

POLITECNICO DI TORINO

This dissertation is submitted for the degree of

Master of Science in Petroleum Engineering

Supervisor: Vera Rocca

March 2018

Contents

List of Figures

List of Tables

Chapter 1

Introduction

In the oil and gas field the exploitation of the subsoil during the primary production phase can lead to compaction phenomena of deposits in depth, due to the decrease in pressure of the interstitial fluids contained within them, which can be transmitted up to the surface. These phenomena are called induced subsidence and consist of a lowering of the ground level. It is important to study the development of these phenomena on the surface in terms of vertical displacements and in terms of superficial extension in order to prevent damage to pre-existing infrastructures around the extraction wells.

The Italian peninsula and its surrounding areas have been subjected to a complex geological evolution that originated several oil and gas systems that are mainly located in the Adriatic Basin. In particular, the North-East area of Basin is affected by both natural subsidence phenomena, such as the Venetian Lagoon, and due to the exploitation of deposits by man. In this area there are mainly biogenic gas reservoir at moderate depths that increase the probability of occurrence of the phenomenon.

Usually the study of induced subsidence phenomena is done by analytical approaches or numerical models, the last has the advantage to take into consideration the lithostratigraphic sequence and the geometry of the area of interest to which mechanical properties are assigned, including the stiffness moduli. In order to retrieve the values of the stiffness moduli necessary for carrying out the analyses, laboratory tests and / or in situ tests may be used.

The thesis work is focus on studying how the mechanical response of a typical gas reservoir present in the Adriatic Basin evolves over time as a function of the stiffness modulus assigned, and the consequent impact in terms of subsidence evolution. In particular, different scenarios were simulated and analysed, considering basically static pseudo elastic parameters, dynamic pseudo elastic parameters and a transition curve between them. In order to fully understand the mechanical behavior of soils one should take into account their discrete nature, but in numerical and analytical models they are treated according to the laws of continuous mechanics. In Chapter 2, after a brief discussion of the elastic linear Isotropic model ILE, we focused on the factors influencing the elastic parameters of soils and rocks because the geomechanical classification of the reservoirs lies between Rock and Soil Mechanics. Among these factors, the degree of saturation, cementation, degree of consolidation, depth, the strain amplitude plays an important role. The whole field of deformations can be subdivided into three subdomains where the stiffness modulus has different trends:

1. Very Small Strain Domain within which the mechanical response can be assumed elastic and the stiffness modulus, called Dynamic, can be assumed costant;

2. Small or Medium Strain Domain where the mechanical response can be assumed to be still elastic since the plastic deformations are limited, but not linear where the stiffness modulus can be expressed through a decay law;

3. Larger Strain Domain where the contribution of plastic strains becomes grater than the elastic strains reducing the mechanical resistance of the material. In this field the stiffness modulus is called static.

Static and dynamic moduli can be measured through laboratory tests and in situ tests as described in the chapter.

In Chapter 3 we briefly described the Italian geological context. So we focused our study on a typical offshore biogenic gas field in the North East of the Adriatic Basin, creating numerical models of synthetic case study through the use of a mechanical simulation software within the Petrel E&P software platform (Schlumberger).

We studied different cases. Each case has been analysed through three different mechanical configurations:

1. static configuration;

2. dynamic configuration;

3. dynamic initial configuration with additional information about the decay of the stiffness modulus inside the reservoir.

The aim of thesis work is to assess the effect on compaction and subsidence phenomena of deformation behavior of a reservoir clastic gas bearing formation during gas exploitation.

Preliminary sensitivities were perform to assess the effect of:

1. timesteps: we changed the timestep to see which was the best resolution of the results;

2. sampling points of the E decay curve: we used three different decay curves in terms of number of sampling points in order to reduce the approximation error of the software;

3. different reservoir shapes: we studied a base case with a lens shaped reservoir. Subsequently we changed the shape of the reservoir by creating a disk-shaped and sphere-shaped reservoir.

All the results obtained from the different scenarios were then compared and critically analysed.

Finally, in Chapter 4 there are the main conclusions of the thesis work and some tips on further possible sensitivity analysis that could be developed in future.

Chapter 2

Literature review

To fully understand the mechanical behavior of the lands, one must take into account their discrete nature, but in the mathematical models, they are treated as continuous medium. Therefore it is necessary to know the basic concepts of continuum mechanics, such as the state of stress and strain. In this way, it is possible to treat the land with the same methodology with which all the engineering materials are described. These materials, and therefore also the rocks, have a behavior defined by two main aspects: the way how deformation occurs under stress and the maximum value of the strength that can be sustained before failure.

The lands have a discrete nature that makes their behavior nonlinear and inelastic, but there are particular circumstances where it is possible to consider the hypothesis of elastic behavior which represents only the first phase of the behavior of a material which in fact presents a threshold of stresses called the elasticity limit where, above it, it has no more elastic but inelastic elastic features. This threshold is represented by the yield stress in ductile materials while it is associated with the breaking of the material for brittle materials, called brittle failure. The simplest mathematical model that describes the elastic behavior is linear and refers to isotropic materials and is known as an elastic linear isotropic model that we will explain below. Furthermore, it is important to note that the theory of elasticity allows to obtain solutions in a closed form, so although there are limitations in the application of this theory. In fact, elastic models are very used to have an initial estimation. The results will be affected in some cases by a too simplified approach, but they are quick to obtain and require input parameters easily available from literature or routine tests.

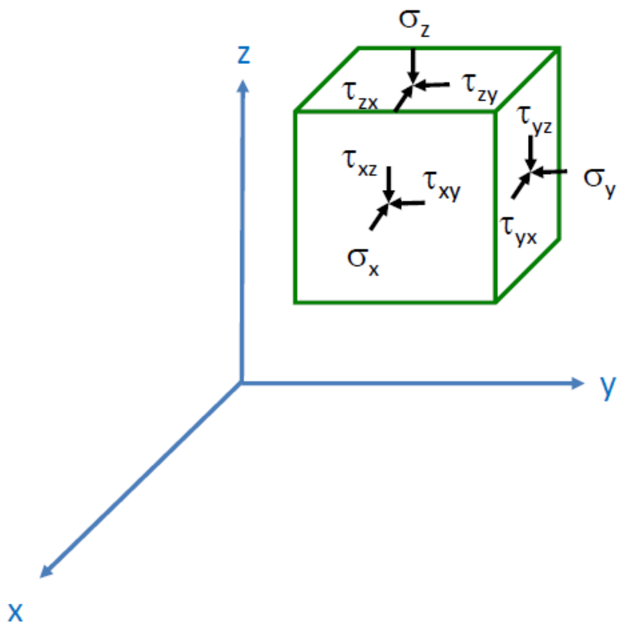

Figure 2.1: Stresses acting on a small element of volume

2.1 Elastic constitutive law

With the concept of the elastic body, we define a deformable body whose energy of deformation, that is the work done from outside to bring it to a certain state of deformation, or in a certain stress state, does not depend on the loading process, but only from the final state. The behavior of these bodies during their deformation is described by linear or non-linear elastic constitutive law. The first is the simplest case which states that stress $d\sigma_{ij}$ and increase of strain $d\varepsilon_{kh}$ are related through the relationship

$$d\sigma_{ij} = C_{ijkh} d\varepsilon_{kh}$$

where C is called stiffness tensor and is made up by independent scalar quantities called elastic constants. Conventionally the subscript i identifies the direction normal to the surface on which the stress acts, while the second j identifies the axis where it is projected; therefore using this nomenclature, the term $d\sigma_{ij}$ means the stress acting on the face having normal i and acting in j direction as schematized in Figure 2.1.

In continuum mechanics, a body is in equilibrium when all the forces acting on it are balanced and for the Cauchy reciprocal theorem the stress tensor is symmetrical or $\sigma_{ij} = \sigma_{ji}$ reducing the elements of the stress tensor from 9 to 6. For this reasons the independent elastic constants are 36.

The linear elastic constitutive law allows thus to calculate the stress tensor known the strain tensor and vice versa. Generally speaking for anisotropic materials, the matrix of the elastic coefficients is symmetrical and therefore 21 elements of this are needed to characterize the material. When the elastic constants are independent of the choice of the reference system, that is, if the elastic characteristics of the material do not depend on the direction in which I go to calculate them, then the material is isotropic. For these Isotropic Linear Elastic (ILE) materials the matrix of elastic coefficients is made up of three elements to be determined of which only two of them are independent, while the third element is obtained from these two. In addiction if the mechanical characteristics of the material are constant in all points, we define it homogeneous.

2.1.1 Isotropic Linear Elastic Model

If we focus on an Isotropic Linear Elastic Model (ILE), the simplest constitutive law is written with the following hypotheses:

- linear field, which implies that the stress is proportional to the strain;
- elastic field, the material returns to its original shape when the loads are removed, the unloading path is the same as the loading path and there is no dependence on the rate of loading or straining;
- isotropic material, the mechanical response is independent of the orientation of the applied stress.

This model well represents the engineering materials up to their elastic limit.

As described before, in order to characterize completely the mechanical response of an isotropic material only two elastic coefficients are needed, and a third can be obtained through the first two. In this case, the matrix of elastic coefficients takes the following form:

$$[C] = \begin{bmatrix} C_{11} & C_{12} & C_{12} & 0 & 0 & 0 \\ C_{12} & C_{11} & C_{12} & 0 & 0 & 0 \\ C_{12} & C_{12} & C_{11} & 0 & 0 & 0 \\ 0 & 0 & 0 & C_{44} & 0 & 0 \\ 0 & 0 & 0 & 0 & C_{44} & 0 \\ 0 & 0 & 0 & 0 & 0 & C_{44} \end{bmatrix}$$

These elastic constants (C_{11}, C_{12}, C_{44}) are defined through elastic parameters called the elastic modulus or Young's modulus E and the Poisson's coefficient υ and therefore the generalized constitutive law of an ILE material can be written in terms of E and υ as:

$$\begin{bmatrix} \sigma_x \\ \sigma_y \\ \sigma_z \\ \tau_{xy} \\ \tau_{yz} \\ \tau_{zx} \end{bmatrix} = \frac{E(1-\upsilon)}{(1+\upsilon)(1-2\upsilon)} \begin{bmatrix} 1 & \frac{\upsilon}{1-\upsilon} & \frac{\upsilon}{1-\upsilon} & 0 & 0 & 0 \\ \frac{\upsilon}{1-\upsilon} & 1 & \frac{\upsilon}{1-\upsilon} & 0 & 0 & 0 \\ \frac{\upsilon}{1-\upsilon} & \frac{\upsilon}{1-\upsilon} & 1 & 0 & 0 & 0 \\ 0 & 0 & 0 & \frac{1-2\upsilon}{2(1-\upsilon)} & 0 & 0 \\ 0 & 0 & 0 & 0 & \frac{1-2\upsilon}{2(1-\upsilon)} & 0 \\ 0 & 0 & 0 & 0 & 0 & \frac{1-2\upsilon}{2(1-\upsilon)} \end{bmatrix} \begin{bmatrix} \varepsilon_x \\ \varepsilon_y \\ \varepsilon_z \\ \gamma_{xy} \\ \gamma_{yz} \\ \gamma_{zx} \end{bmatrix}$$

This is known as the generalized Hooke's Law. Definitely the elastic parameters necessary to characterize an isotropic material are two, the elastic modulus and the Poisson's coefficient, while the third parameter can be calculated from these two.

2.2 Elastic parameters

Let's now see in detail how these elastic parameters are defined and how they are linked to each other.

The Young modulus E represents the stiffness of the material and on the ε-σ plane is the positive angular coefficient of the straight line passing through the origin which describes the loading process and can be calculated as

$$E = \frac{\sigma_z}{\varepsilon_z}$$

The Poisson modulus or transverse contraction coefficient ν represents the ratio between the dilations induced in the orthogonal directions to the stress applied ε_x and dilatation in the direction of stress ε_z

$$\nu = -\frac{\varepsilon_x}{\varepsilon_z}$$

The third parameter that takes part in the characterization of anisotropic material is chosen according to the case to be analyzed and can be one of the following:

- shear elasticity modulus G can be calculated knowing the previous elastic moduli, in fact, it is given by

  $$G = \frac{E}{2(1+\nu)}$$

  and it is the ratio of an applied shear stress to a corresponding shear strain;

- Bulk modulus K, is the stiffness of a material in hydrostatic compression

$$K = \frac{p}{\varepsilon_v} = \frac{E}{3(1-2\nu)}$$

$$p = \frac{\sigma_x + \sigma_y + \sigma_z}{3}$$

$$\varepsilon_v = \varepsilon_1 + \varepsilon_2 + \varepsilon_3 = \frac{\Delta V}{V}$$

  where p is the mean normal stress equal to one third of the trace of the stress tensor and ε_v is the volumetric strain (the ratio of volumetric variation ΔV to initial volume V) equal to the trace of the strain tensor; these traces are invariants of the tensors or independent by the reference system and for this reason they are used.

- Oedometric modulus E_{oed}, is the stiffness in confined uniaxial compression (no lateral strains occur)

$$E_{oed} = \frac{E(1-\nu)}{(1+\nu)(1-2\nu)} = \frac{1}{C_m}$$

  where C_m is the uniaxial compressibility;

- Lamè constant λ, defined as

$$\lambda = \frac{\nu E}{(1+\nu)(1-2\nu)}$$

Clearly, all these elastic parameters are influenced by several factors that we now see in detail.

2.2.1 Factors affecting the elastic parameters

This thesis work deals on issues related to the world of reservoirs geomechanics, which characteristics can vary greatly due to their lithological nature, depth and in situ state of stress. Generally for these reasons the geomechanical classification of the reservoirs lies between Rock and Soil Mechanics, [6]. So a preliminary knowledge of these two worlds allows us to better identify the case study and the orders of magnitude that we might expect to obtain from the analysis.

Soils are a natural aggregate of mineral particles linked together by normal and tangential contact forces that can be separated by simple mechanical action. Based on their granulometry they can be classified into four groups:

- gravels, characterized by grains from 2 mm to 8-10 cm;

- sands, with particles between 0.06 and 2 mm;
- silts, with particles between 0.002 and 0.06 mm;
- clays, with particles smaller than 0.002 mm.

Rocks are natural, hard and compact aggregates of particular minerals linked together by permanent and strong bonds, which can be considered as a continuous system. The easiest way to classify rocks is based on their composition, texture, and origin as:

- sedimentary rocks, i.e. deriving from the decomposition of pre-existing rocks as a result of chemical and mechanical activities of atmospheric agents and theirs mechanical behavior depends on diagenetic phenomena, that is the degree of compaction, cementation and recrystallization, i.e. an increase in the original crystals;
- magmatic rocks, which derive from the solidification of magma and whose mechanical characteristics vary considerably according to the speed of cooling, or rather, slowly cooling the minerals have time to organize themselves in ordered structures resulting stiffer;
- metamorphic rocks deriving from the transformation of rocks due to strong pressures and/or temperatures or reactions with magmatic fluids without a complete fusion of the minerals that constitute them. These processes often lead to a recrystallization phase.

The type of bond existing in soils and rocks is the main difference the mechanical response, in fact, the latters are characterized by elastic moduli of about three orders of magnitude higher than soils.

Usually, the rocks are affected by discontinuity, fracture or surfaces of weakness, which identify blocks of rocky matrix or intact rock and the whole is called rock mass.

The great variability of the characteristics and of the physical and mechanical properties is reflected both in the intact rock microscale and in the macroscale of the fractured rock mass. Therefore the factors affecting the mechanical response will have a different role depending on the scale factor considered

The stiffness value of the intact rock represents an upper limit of the rock mass values because both contain pores and interstices but the rock mass also has discontinuities that degrade its mechanical response. The bigger the discontinuities, the lower the stiffness.

The problem, therefore, is to determine the characteristics of deformability of the rock mass, that is to identify the scale factor (reduction factor) that must be taken into account when the intact rock or the rock mass are considered (see Figure 2.2).

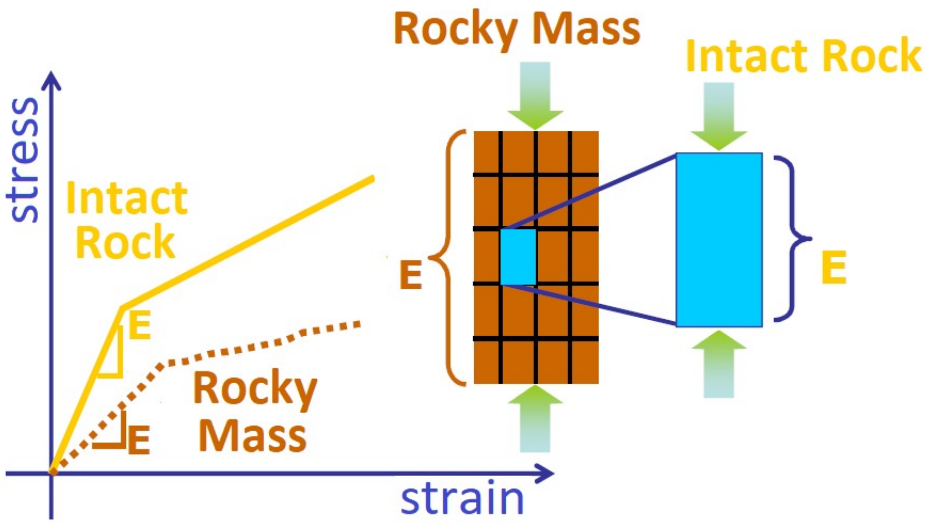

Figure 2.2: Scale factor [2]

Porous media such as soils and some rocks have a mechanical behavior that depends on solid matrix, discontinuities present inside like voids, pores or fractures.

The presence of pores, voids or fractures is taken into account by the porosity that is defined as the ratio between the volume of voids and the total volume of the element considered indicated as ϕ for rocks, while for soils is called void ratio e representing the relationship between the volume of voids and the volume of solids. Higher the porosity or void ratio, greater the deformability of rocks and soils.

A parameter related to porosity is density. The rock density or bulk density ρ_{bulk} is given by the density of the matrix ρ_{matrix} (solid part) multiplied by the fraction of the volume occupied by the matrix plus the density of the fluid ρ_{fluid} contained in its pores multiplied by the fraction of volume occupied by the fluid:

$$\rho_{bulk} = \phi\rho_{fluid} + (1-\phi)\rho_{matrix}$$

The mineral particles of the porous medium subjected to external actions slip and rotate between them, but they can be considered non-deformable. For these reasons, materials with high porosity values or voids ratio, and therefore low density like soils, have lower elastic moduli compared to ones having a greater density like rocks. Generally, the range of porosity of rocks can vary between 15% and 30% while clastic, volcanic and altered sedimentary rocks may have higher values.

The pores of the medium can contain fluids inside them, If these are only in gaseous phase the material is defined dry, if they are only in liquid phase it is called saturated, instead in the case in which liquid and gaseous phase coexist the material is defined unsaturated. Moreover, in this last case, if the fluids are also immiscible, capillary phenomena occur that influence the values of the effective stress of which we will discuss later. The easiness with which these fluids are able to circulate inside the porous materials is defined permeability K which is independent of the type of fluid but is an intrinsic characteristic of a porous medium and depends on:

- Granulometry. The smaller are the grains size and the lower is the permeability. For example, gravels and sands do not hold liquids while clays have a high water retention capacity.
- Density. If we consider a constant granulometry, if the density increases the permeability decreases.
- Shape and orientation of the particles. The permeability can vary according to the direction of the fluid flow.

Generally rocks have a lower permeability than soils while in rock masses the permeability is given by their discontinuities. The latters can be considered so big to assume that their permeability values tend to infinity. For this reason fluids move more easily within the discontinuities.

Density is influenced by the depth at which the considered medium is located through the concept of geostatic stress. In the absence of applied external loads, the initial in-situ stresses are represented by geostatic (or lithostatic) stresses, or by the stress present in the subsoil in its natural state induced by its own weight. These stresses depend also by the granulometric characteristics of the ground and on the stress history with which we commonly refer to the sequence of stress, in terms of entity and duration, which have affected the deposit from the beginning of its formation to the current conditions.

The value of the total vertical stress state σ_{v0} at depth z, in the case of a deposit made up of several horizontal layers characterized by different density values ρ_i considered constant within each layer, is given by:

$$\sigma_{v0} = \sum_i g\rho_i \Delta z_i$$

being Δz_i the thickness of the i-th layer and g the gravity acceleration constant. The higher the depth the bigger will be the weight on the considered layer which tends to compact the medium more and more. For these reasons as depth increases the medium become stiffer and stiffer and vice versa.

The main events of the stress history of a deposit are divided into phenomena of loading, or compression such as deposition, and of discharge, for example erosion. To understand such phenomenologies it is necessary to introduce the concept of effective stress enunciated by Terzaghi (1936):

"All measurable effects of a change of stress, such compression, distortion and a change of shearing resistance, are exclusively due to changes in the effective stresses.

The effective stress σ' is equal to the difference between the total stress σ and the interstitial pressure u, $\sigma' = \sigma - \alpha u$"

where α is a correction factor that measures the effectiveness of the pore pressure in counteracting the total applied load. The value of α , which varies between 0 and 1, depends on the pore geometry and the physical properties of the constituents of the solid system. In the extreme cases when α is equal to 0, the pore pressure has no effect on the behavior of the rock, and when $\alpha = 1$ the pore pressure is 100% effective in counteracting the applied load. We assume $\alpha = 1$ for soils, while values lower than unity are characteristic of rocks. The coefficient α in isotropic linear elastic rocks is equal to the so-called Biot coefficient:

$$\alpha = 1 - \frac{K'}{K_s}$$

where K' is the drained bulk modulus of the solid skeleton and K_s is the bulk modulus of the solid phase.

The term compression is used to describe the variation of the voids ratio associated with a variation of the effective stress, without any indications about the duration of this variation. Generally, it is assumed to calculate these variations in the monoaxial case along the z-axis as they are predominant along this direction. On the other hand, if we want to consider the transient phenomenon which couples the fluid flow and the deformation of the solid phase we talk about consolidation.

The compressibility expresses the easiness of a material to deform as a result of a change in the stress equilibrium. In porous media we can distinguish two types of compressibility, pore compressibility C_p and bulk compressibility C_b:

$$C_p = -\frac{1}{V_{pores}}\frac{dV_{pores}}{dP}$$

$$C_b = -\frac{1}{V_b}\frac{dV_b}{dP}$$

Where V_{pores} is the volume of the pores and V_b is the bulk volume of the rock.

Depending on the type of phase contained in the pores, the compressibility varies considerably, in particular, it varies approximately between $2 \div 4\ 10^{-4} psi^{-1}$ for gases, $0.5 \div 4\ 10^{-5} psi^{-1}$ for oils, $2 \div 4\ 10^{-6} psi^{-1}$ for water and rocks.

In ideal cases, i.e. in absence of interaction between fluid molecules, we can consider water and rock as incompressible respect to gases. Therefore in this condition, the compressibility of a saturated porous medium will be lower than unsaturated medium due to the absence of gaseous phases. As a consequence, the elastic modulus will be greater in saturated materials, while in non-saturated ones it will vary according to the percentage of gaseous phase with respect to the liquid one.

Generally, the deposits after the sedimentation and consolidation phase can undergo a subsequent stress history which can be described by means the Over Consolidation Ratio OCR which is the ratio between the maximum historical vertical effective stress or the over-consolidation stressσ'_p and the current vertical effective stress σ'_{v0}

$$OCR = \frac{\sigma'_p}{\sigma'_{v0}}$$

We define Normalconsolidated a material with $OCR = 1$ and overconsolidated if $OCR > 1$. Under the same conditions, the deformability of a overconsolidated material is considerably lower than a normal-consolidated deposit, this happens because the reduction of the volume of voids will be lower in the first case. Moreover, the over-consolidated deposits behave in an approximately elastic way, whereas the normal-consolidated behaves like elastoplastic materials. Assigning to the yield stress the meaning of boundary of the elastic domain, we can say that if the induced stresses do not exceed this threshold, the corresponding deformations will be relatively modest and also in the elastic; on the contrary, overcoming this threshold the strains become significant and predominantly plastic.

It is possible to assume that in very permeable materials with big grains strains and load application occur simultaneously. In contrast for low permeable materials with small grains, the time required to reach the final equilibrium condition after the application of the load is extremely long and therefore not negligible. The latter condition is defined undrained condition beacuse the overpressure generated inside the fluid by the applied load cannot be dissipated instantaneously. Furthermore, in this condition, a saturated deposit is not subjected to any volume variation and the engineering problem must be addressed in terms of total stresses, i.e. considering the element as a single-phase system. Finally, we define "drained" conditions when the induced overpressures on a saturated medium are instantly dissipated and the mechanical response is given only by the solid matrix.

2.2.2 Static and Dynamic elastic moduli

Another factor affecting the values of the elastic parameters is the deformation threshold at which the material is subjected. In fact, the strain amplitude at which the deposit is subjected, we can define three different domains, where it's possible to observe different rheological behaviors (Figure 2.3):

1. Very Small Strain Field where the mechanical behavior is linear elastic;
2. the Field of Small or Medium Strain where the mechanical response can be assumed to be still elastic since the plastic deformations are limited, but not linear;
3. Field of Larger Strain where the contribution of plastic strains becomes grater than the elastic strains.

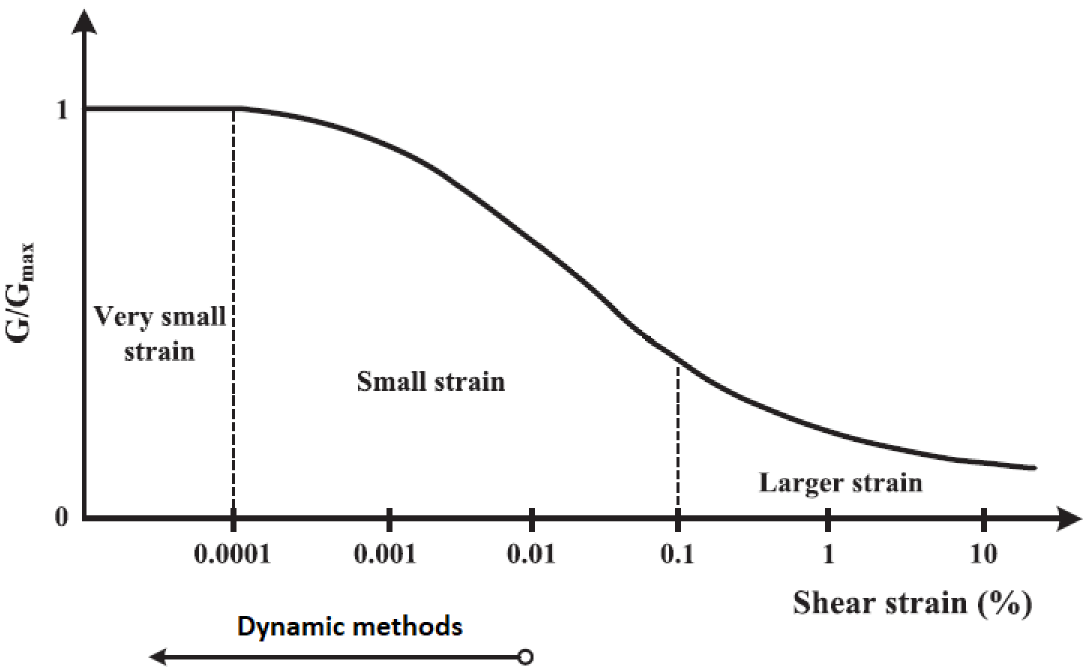

Figure 2.3: Theoretical decay curve

To understand the difference between the static and dynamic moduli we must introduce the concept of strain rate, that is how much time is necessary to reach a predetermined strain or the velocity at which this strain occurs. In a general way we talk about static conditions if applying a stress the strain occurs in terms of hours while we refer to dynamic conditions if the strain occurs within minutes or seconds. Furthermore, if the same material is subjected to different stresses, that is, in terms of stress magnitude, different strains are obtained.

By subjecting a material to an uni-axial compression load slowly enough, a curve of the deformation trend is obtained on the stress-strain plane containing all the domains described above, as visible in Figure 2.4. The elastic linear relationship between the applied stress and the deformation produced in the direction of application of the force is called the static elastic modulus. We define the static elastic modulus as the ratio between the applied stress and the induced deformation in the same direction of the applied stress, as well as the angular coefficient of the traced curve on the stress-strain plane up to the yield stress.

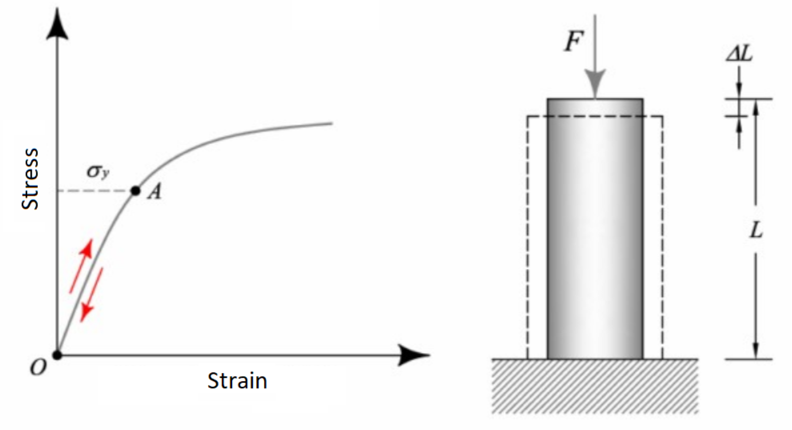

Figure 2.4: Theoretical stress-strain curve from uni-axial compression load

When a material is excited by a small force, that is, in the field of small strains, sonic waves are generated and propagated within it. The propagation velocities of these longitudinal and transversal elastic waves, respectively V_p e V_s , through the material, depend on its density and stiffness, defined respectively through the dynamic elastic modulus E_d and the dynamic shear modulus G_d , through the following formulas

$$E_d = 2\rho_{bulk} V_p^2 (1+\nu)$$

$$G_d = \rho_{bulk} V_s^2$$

The equations used to calculate dynamic moduli assume the material ideal or homogeneous, isotropic linear elastic rock. Reservoir rocks, of course, are not ideal and also heterogeneous.

The values of the seismic wave velocities, and consequently also those of the dynamic moduli, will be different depending on the type of formations, lithotypes and also in general increase going in depth and with age.

The values with which the longitudinal seismic waves cross the subsoil vary from hundreds of m/s for the superficial aerated layers, up to about 6000-7000 m/s for the densest and most compact rocks (igneous and metamorphic rocks). Some reference values are shown in the Table 2.1.

For soils the velocity values of the longitudinal waves vary within a range that goes from 1400 m/s for loose soils to a maximum of 2000 m/s for very dense soils, while for rocks this range varies between 1000 m/s and 6000 m/s. Moreover, the V_p not only provides the value of the dynamic elastic modulus, but also allows to obtain informations about the rock quality. In fact, values lower than about 1000 m/s are a clue of phenomena such as alteration, porosity and discontinuity of the rock. In general, the clay-rich and sedimentary rocks are the most vulnerable to the processes of physical alteration while the igneous and metamorphic rocks are chemically unstable and therefore subject to chemical alteration. In both cases these materials have values below 1000 m/s (threshold value) indicating a degradation of the rock. If the rocks have negligible porosity and values of V_p are lower than the threshold value, this means that there are discontinuities inside them. Or in porous materials it is always true that the speed of the compressional waves is lower than the same material assuming negligible porosity. In addition the type of fluid, or more generally the degree of saturation, alters these velocity values thus affecting the dynamic elastic modules, since the latters are directly proportional to the square of V_p, varying significantly.

In particular, it has been seen that the velocity of the shear waves is independent from the degree of saturation, and more in general from any kind of fluids because the latters have a shear strength negligible. On the other hand, the velocity of the longitudinal waves depends on it. V_p values, in fact, are 1500 m/s in water while 330 m/s in air (see Table 1). This means that on average for the same material, a saturated porous medium will have a higher propagation velocity than a unsaturated one and even more for dry medium and therefore, the dynamic Young modulus of the former will be greater than the second medium. Generally in these last cases, in order to obtain more accurate results, it is best practice to retrieve the dynamic shear modulus G experimentally and, known the Poisson's coefficient, it's possible to calculate the dynamic Young modulus through the following formula

$$E_d = 2G_d(1+\nu)$$

As a first approach, we can say that static and dynamic moduli have the same meaning but not the same values. In fact, usually the dynamic Young modulus is greater than the static one, but it's not always true. As visible in Table 2.2, as we said before, due to the high variability of physical properties, i.e. porosity, mineral structure, cementation, etc. , and the anisotropic characteristic of some lithotypes both the static and dynamic values of the same deposit are not fixed but vary within a wide range.

			SATURATED					UNSATURATED		DRY	
			V_p [m/s]	V_s [m/s]	ν (Poisson)	Density ρ [g/cm^3]	G_d [kg/cm^2 x 10^5]	V_p [m/s]	ν (Poisson)	V_p [m/s]	V_s [m/s]
SOILS	Sand	loose	1450 - 1550	100 - 250	0.48 - 0.50	1.5 - 1.8	0.0015 - 0.0110	180 - 450	0.3 - 0.35	150 - 1000	100 - 500
		medium	1500 - 1750	200 - 350	0.47 - 0.49	1.7 - 2.1	0.0070 - 0.0250	320 - 650	0.2 - 0.3		
		dense	1700 - 2000	350 - 700	0.45 - 0.48	1.9 - 2.2	0.0230 - 0.1	550 - 1300	0.15 - 0.3		
	Clay	loose	1450 - 1550	80 - 180	0.47 - 0.5	1.6 - 2.0	0.0010 - 0.0065			100 - 600	40 - 300
		medium	1500 - 1700	180 - 300	0.47 - 0.5	1.7 - 2.1	0.0055 - 0.0190				
		dense	1600 - 1900	300 - 500	0.47 - 0.5	1.8 - 2.3	0.0160 - 0.0450				
	Silt		1450	40 - 250						100 - 600	40 - 300
	Gravel		1450	80 - 450						150 -1000	100 - 500

		φ [%]	V_p [m/s]	V_s [m/s]	ν (Poisson)	Unit weight [gr$_f$/cm^3]	Dynamic elastic moduli E_d [kg/cm^2 x 10^5]
INTACT ROCKS	Andesite	10 - 15			0.23 - 0.32	2.2 - 2.35	
	Amphibolite	-				2.9 - 3.0	4.6 - 10.5
	Sandstone	5 - 25	1400 - 4200	1200 - 1800	0.1 - 0.4	2.3 - 2.6	0.5 - 5.6
	Basalt	0.1 - 2	4500 - 6500	300 - 900	0.19 - 0.38	2.7 - 2.9	4.1 - 8.7
	Limestone	5 - 20	2500 - 6000	1200 - 3000	0.12 - 0.33	2.3 - 2.6	0.8 - 9.9
	Coal	10				1.0 - 2.0	
	Quartzite	0.1 - 0.5	5000 - 6500		0.08 - 0.24	2.6 - 2.7	
	Dolerite	0.1	5500 - 7000		0.28	2.9	6.0 - 9.8
	Diorite	-				2.7 - 2.85	2.5 - 4.4
	Dolostone	0.5 - 10	5000 - 6000		0.29 - 0.34	2.5 - 5.6	2.2 - 8.6
	Schist	3			0.01 - 0.31	2.5 - 2.8	
	Gabbro	0.1 - 0.2	4500 - 6500		0.12 - 0.20	3.0 - 3.1	
	Gneiss	0.5 - 1.5	3100 - 5500	1700 - 3500	0.08 - 0.40	2.7 - 3.0	2.5 - 10.5
	Granite	0.5 - 1.5	4500 - 6000	1700 - 3500	0.1 - 0.4	2.6 - 2.7	1.0 - 8.4
	Greywacke	3				2.8	2.3 - 10.7
	Marble	0.3 - 2	3500 - 6000	2000 - 3500	0.1 - 0.4	2.6 - 2.8	
	Argillite	2 - 15	1400 - 3000		0.25 - 0.29	2.2 - 2.6	1.0 - 7.0
	Slate	0.1 - 1	3500 - 5000	2000 - 3500	0.25 - 0.30	2.5 - 2.7	
	Rhyolite	4 - 6				2.4 - 2.6	
	Salt	5	4500 - 6000		0.22	2.1 - 2.2	
	Tuff	14 - 40		500 - 700	0.24 - 0.29	1.9 - 2.3	
	Chalk	5	3000 - 4000	230 - 1100		2.3	
	Conglomerate		2500 - 5000				
	Marlstone		1800 - 3200				1.0 - 4.9
	Anhydrate					2.96	
	Siltstone			2400 - 2700	0.25		0.7 - 6.5

Table 2.1: Wave velocities and the related moduli. Data collected from [6] [11]

In order to provide a preliminary comparison between the moduli, the ratio between the minimum value of the dynamic modulus and the minimum value of the static modulus for each type of material was calculated from the Table 2.2, and the ratios of the maximum values were calculated in the same way. These ratios have been calculated in order to give an approximate and qualitative idea of the differences in orders of magnitude between the two moduli but not usable for practical purposes, due to the fact that the data collected do not refer to measurements carried out under the same laboratory conditions. Generally the values of these ratios are widely larger in the case of soils than rocks. This might mean that the difference between static and dynamic moduli is more pronounced in soil than in rocks. Furthermore, for the same material, in most cases, the ratios between the minimum values are larger than the ones obtained from the maximum values. Instead, this might mean that as the stiffness of the material increases the difference between the two moduli decreases.

			Static elastic moduli E_s [kg/cm^2 x 10^2]	Dynamic elastic moduli E_d [kg/cm^2 x 10^2]	Ed_MIN / Es_MIN calculated	Ed_MAX/ Es_MAX calculated
SOILS	Sand	loose	1.0 - 3.0		4,5	10,9
		medium	3.0 - 5.0	20	6,9	14,8
		dense	5.0 - 8.0		13,4	36,6
	Clay	loose	0.05 - 0.5	3.5	59,4	38,6
		medium	0.5 - 1.2	7.0	32,0	46,7
		dense	1.2 - 6.0	14.0	39,2	22,2
	Silt	loose	0.25 - 0.8			
		medium	1.0 - 2.0			
		dense	2.0 - 8.0			
	Gravel	loose	3.0 - 8.0			
		medium	8.0 - 10.0	30.0		
		dense	10.0 - 20.0			

		φ [%]	Static elastic moduli E_s [kg/cm^2 x 10^2]	Dynamic elastic moduli E_d [kg/cm^2 x 10^2]	Ed_MIN / Es_MIN calculated	Ed_MAX/ Es_MAX calculated
INTACT ROCKS	Andesite	10 - 15	3000 - 4000			
	Amphibolite	-	1300 - 9200	4600 - 10500	3,5	1,1
	Sandstone	5 - 25	300 - 6100	500 - 5600	1,7	0,9
	Basalt	0.1 - 2	3200 - 10000	4100 - 8700	1,3	0,9
	Limestone	5 - 20	1500 - 9000	800 - 9900	0,5	1,1
	Coal	10				
	Quartzite	0.1 - 0.5	2200 - 10000			
	Dolerite	0.1	6900 - 9600	6000 - 9800	0,9	1,0
	Diorite	-	200 - 1700	2500 - 4400	12,5	2,6
	Dolostone	0.5 - 10	400 - 5100	2200 - 8600	5,5	1,7
	Schist	3	600 - 3900			
	Gabbro	0.1 - 0.2	100 - 6500			
	Gneiss	0.5 - 1.5	1700 - 8100	2500 - 10500	1,5	1,3
	Granite	0.5 - 1.5	1700 - 7700	1000 - 8400	0,6	1,1
	Greywacke	3	4700 - 6300	2300 - 10700	0,5	1,7
	Marble	0.3 - 2	2800 - 7200			
	Argillite	2 - 15	300 - 2200	1000 - 7000	3,3	3,2
	Slate	0.1 - 1	500 - 3000			
	Rhyolite	4 - 6	1000 - 5000			
	Salt	5	500 - 2000			
	Tuff	14 - 40	300 - 7600			
	Chalk	5	1500 - 3600			
	Conglomerate		1000 - 9000			
	Marlstone		400 - 3400	1000 - 4900	2,5	1,4
	Anhydrate		1500 - 7600			
	Siltstone		5300 - 7500	700 - 6500	0,1	0,9

Table 2.2: Static and Dynamic Moduli for soils and rocks. Typical rocks and soil in oil field are written in red. Data collected from [6]

These ideas could be confirmed by experimental tests performed by Yagi et al. [26] where the static and dynamic moduli were measured on clay and mortar specimens. The latters was used because it was difficult to obtain a uniform rock samples, and different sand cement ratio was used to simulate different stiffnesses of the same rock. As shown in the Figure 2.5, it has been observed that for soil E_d increases as E_s increases, and it seems that the relationship between E_d and E_d/E_s is represented by an hyperbola, where for low stiffness values the difference between static and dynamic moduli is very high and very low for high stiffness values. While, in general, for mortars, the E_d/E_s ratio is much smaller than that of soils.

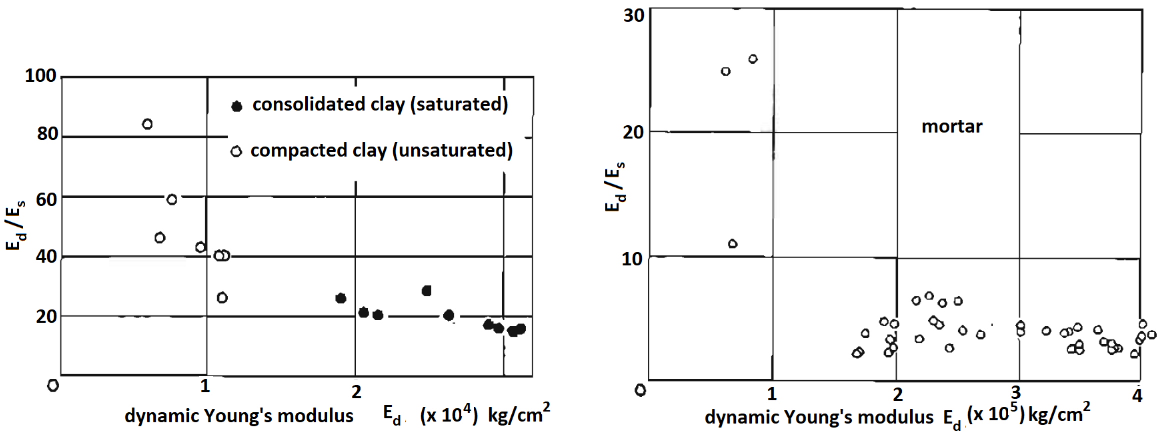

Figure 2.5: Leftside, the relationship between Young's modulus ratio E_d/E_s and dynamic Young's modulus for clay; rightside, the relationship between Young's modulus ration and dynamic Young's modulus for mortar [26]. Pay attention to the different orders of magnitude on the x axes.

For the aforementioned considerations, either for soils or rocks, if the material is the same, stiffness moduli rise as depth increases. This means that the difference between the static and dynamic moduli of a same material reduces as the depth increases. A similar observation can be done about the degree of consolidation since, by definition, an over-consolidated material possesses a stiffness modulus higher than that of the same normal-consolidated material. We can deduce that as OCR ratio increases, the difference between static and dynamic moduli decreases.

2.2.2.1 Lab Tests

Rock mechanical properties such as Poisson's ratio, shear modulus, Young's modulus, bulk modulus, and compressibility can be obtained from laboratory measurements, which allow direct measurements of strength parameters and elatic behaviour on recovered core material from discrete depths.

The static elastic parameters can be obtained from static laboratory tests such as the uniaxial unconfined compression test, the triaxial test and the edometric test. While the dynamic ones can be obtained from Cyclic Torsional Shear tests, Resonant Column and through the cyclic triaxial test.

The simple uniaxial compression test (Figure 2.6) consists in placing a cylindrical specimen in a normal press and breaking it by simple compression without any lateral confinement. This test allows to determine:

- the uniaxial or unconfined compressive strength (UCS) C_o or σ_c or the ultimate strength of a rock, that is, the maximum value of stress attained before failure;
- the Young modulus E;
- the Poisson ratio.

In conventional instruments, the variable is represented by the force, whose intensity and speed of application can be controlled. The axial deformations produced on the specimen are measured by comparators or strain gauge bands. During the test, the pairs of axial stress-strain values or radial deformations are recorded. The initial part of the plotted stress-strain curve can be assumed linear and also that the Hooke's law is valid $E = \dfrac{\sigma}{\varepsilon} = constant$.

Although it is assumed that the fracture in the rock occurs when the unconfined compressive strength (UCS) is reached, experimentally it has been verified that the breaking process and the generation of micro-cracks begin at stresses below to C_o, in particular between 50% and 95% of its value (Brady and Brown, 1985).

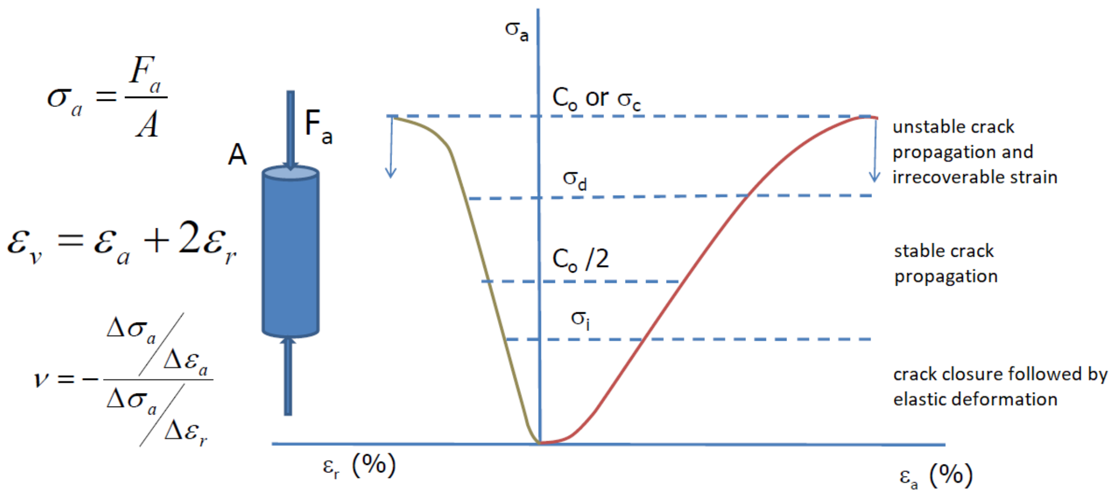

Figure 2.6: Uniaxial compression test

The triaxial compression test allows to represent the conditions of the rocks in depth, i.e. subjected not only to the overlying load but also to the horizontal stresses called confinement stresses by applying a uniform hydraulic pressure around the specimen making possibile the control the radial and axial stresses independently, thus allowing the realization of any stress paths.

This test allows to determine the failure envelope or the resistance line of the material on the stress-strain plane from which it is possible to extrapolate two resistance parameters to build a failure criterion (Mohr-Coulomb criterion), the cohesion c and the friction angle φ', discussed later in the Section **??**, and then the static elastic modulus E and the Poisson's coefficient are obtained.

The test is carried out on specimens similar to those of the uniaxial test, which are introduced into steel cylinders in which a hydraulic pressure is applied to the walls of the specimen. This is surrounded by a waterproof and flexible membrane to isolate it from the liquid under pressure. The deformations are measured through strain gauge bands fixed directly on the specimen.

Using the triaxial cell, different types of tests can be carried out, based on the material and on in-situ conditions to be reproduced, which can be identified using a code composed by two or three letters as shown in Figure 2.8.

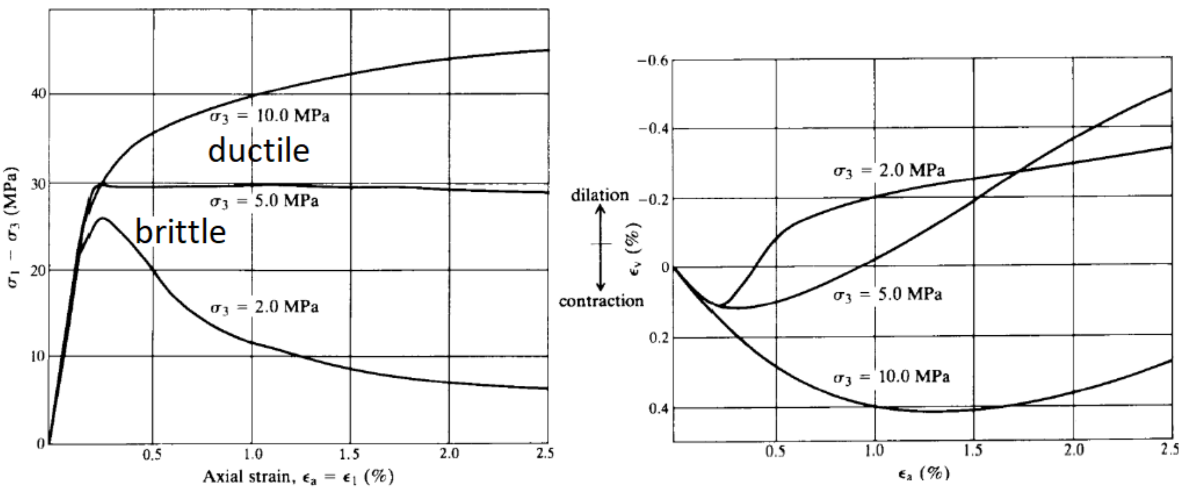

Figure 2.7: Typical triaxial compression test curve and the influence of the confining pressure and consequent change in failure mechanism, from brittle to ductile. In the figure below is visible the dilation phenomena if the confining pressure (2.0 Mpa) is low [7]

The first phase can be carried out in two different ways: consolidating the specimen (letter C) or leaving it unchanged (letter U). In the C case the consolidation can be done in three different ways, that is applying an isotropic effective stress state (I), or a pre-established anisotropic state (A), or applying in -situ state of stress (K_0). Once the desired confining pressure level is reached, this confining pressure is kept constant and only the axial load is increased until failure of the specimen occurs. During the loading phase of the specimen, shear stresses are generated which can generate dilation phenomena which are a volume variation. This phenomenon physically represents the effect of the mutual interlocking between particles that start to slide. In general, and therefore also for high depth rocks, the dilatation phenomenon decreases as confining pressure increases. Furthermore, increasing the confinement pressure the mechanical response changes from brittle to ductile. The loading phase is called second phase and it can be done in drained (D) conditions, allowing to measure the volume variation, or in undrained (U) conditions measuring the overpressure due to the fact that the change in volume is impeded. In addition, every drained test is analyzed in term of effective stress while every undrained test is analyzed in terms of total stress. For example, using the term CID, the specimen is subjected firstly to an isotropic consolidation and after is brought to failure in drained condition; This kind of test is performed in order to simulate the reservoir conditions during production, which are permeable rocks and fluids are easly drained. While, in oil and gas industry, CIU or CK_0U tests are used to simulate the performance of sealing rocks which are not permeable. In case of Normal Consolidated clay, which are very low permeable, it is usually to perfom UU tests.

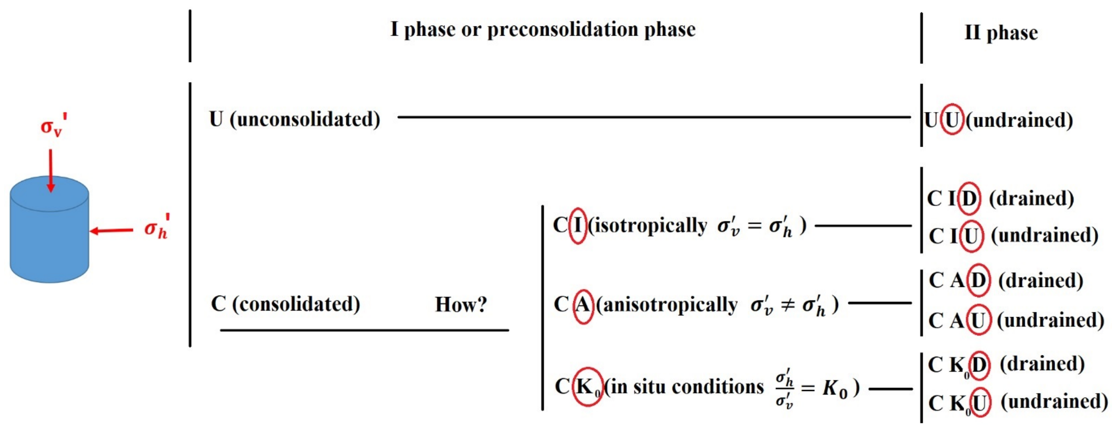

Figure 2.8: Kind of tests on triaxial cell

The edometric tests are the most widely used tests to determine the compressibility parameters and the history of a deposit in terms of OCR.

A cylindrical saturated sample is confined laterally by a rigid ring in such a way that only axial deformation is permitted (see Figure 2.9). Furthermore, two porous stones are used in contact with the upper and lower surfaces of the specimen, allowing the flow of water, i.e. allowing the specimen to consolidate. The reduction in volume of the specimen corresponds to a variation in the voids ratio, which implies the expulsion of an equivalent volume of interstitial water.

The specimen is loaded by a uni-axial load in a geometrical way (i.e. 5, 10, 20, 40, 80, 160, ..., etc kPa) by measuring the voids ratio in Figure 2.10. Each loading step is maintained constant for long times after which the load is removed, terminating in this way the so-called first loading cycle, branch from A to D shown in the same figure. A second load cycle is carried out not exceeding the maximum value of the effective stress to which the specimen was subjected during the first cycle, the branch from D to E, to analyze the purely elastic behavior of the material.

The stiffness of the sample increases as the applied axial force increases and the number of cycles performed increases, while the compressibility decreases.

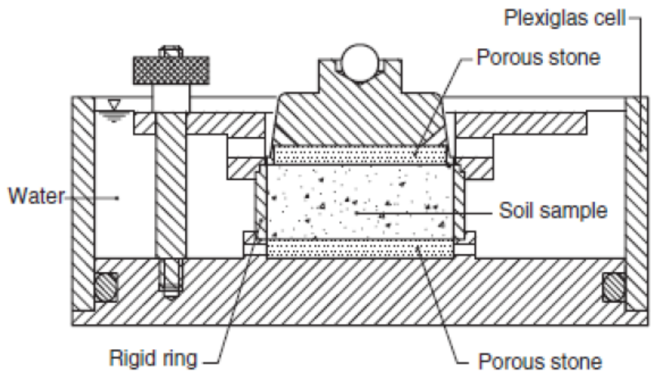

Figure 2.9: Oedometer test [17]

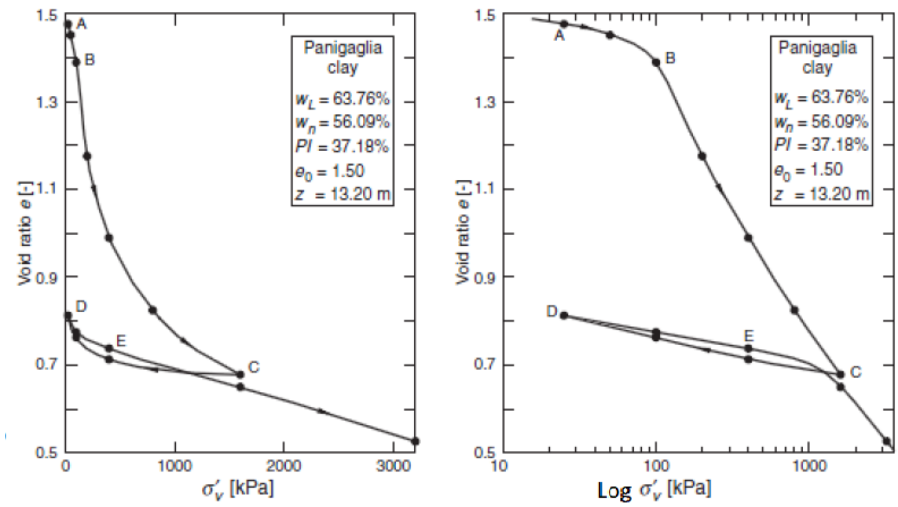

Figure 2.10: Examples of results obtained from an Oedometric test

Speaking about dynamic tests, these allow to determine experimentally the decay curve that represents the variation of the secant stiffness modulus G as a function of the deformation level γ, shown in Figure 2.12.

Due to the fact that the material has not a ideal beahaviour, we need to introduce a G_t tangent modulus

$$G_t = \frac{d\tau}{d\gamma}$$

which describes the variation of the stress due to a small variation of deformation around the current state, or a G_{sec} secant modulus

$$G_{sec} = \frac{\tau}{\gamma}$$

that identifies a mean stiffness in a stress interval determined from a reference zero as shown in Figure 2.11, where G_0 means G_t or G_{sec} at the beginning.

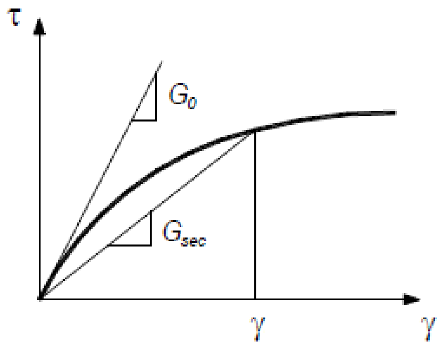

Figure 2.11: G moduli variations as function of deformations

It is clear that the two values of the moduli coincide in the initial phase of the test ($G_{sec}/G_t = 1$), while as deformation increases more and more the two values become very different.

It's possible to distinguish from the decay curve 2.12 three zones:

1. Very Small Strain Domain where a linear threshold (ε_t or γ_t used for E or G respectively according to the kind of test) of the order of $10^{-5}\%$ exists , below which the stiffness can be assumed constant;

2. Over ε_t range in the Small or Medium Strain Domain the behavior is non linear but still elastic. Here the stiffness modulus decreases significantly as deformations become larger and larger and now every loading cycle is characterized by hysteresis

phenomena until creep phenomena start to occur and it means that the upper limit of this region is reached. This boundary is called critical strain threshold ε_{crit};

3. Beyond ε_{crit} the Larger Strain Domain exists where the total deformation is given by an elastic and plastic contributions. The further we move away from ε_{crit}, the more the plastic deformations are predominant over the elastic ones. This is a transitional region where the behaviour is not well defined.

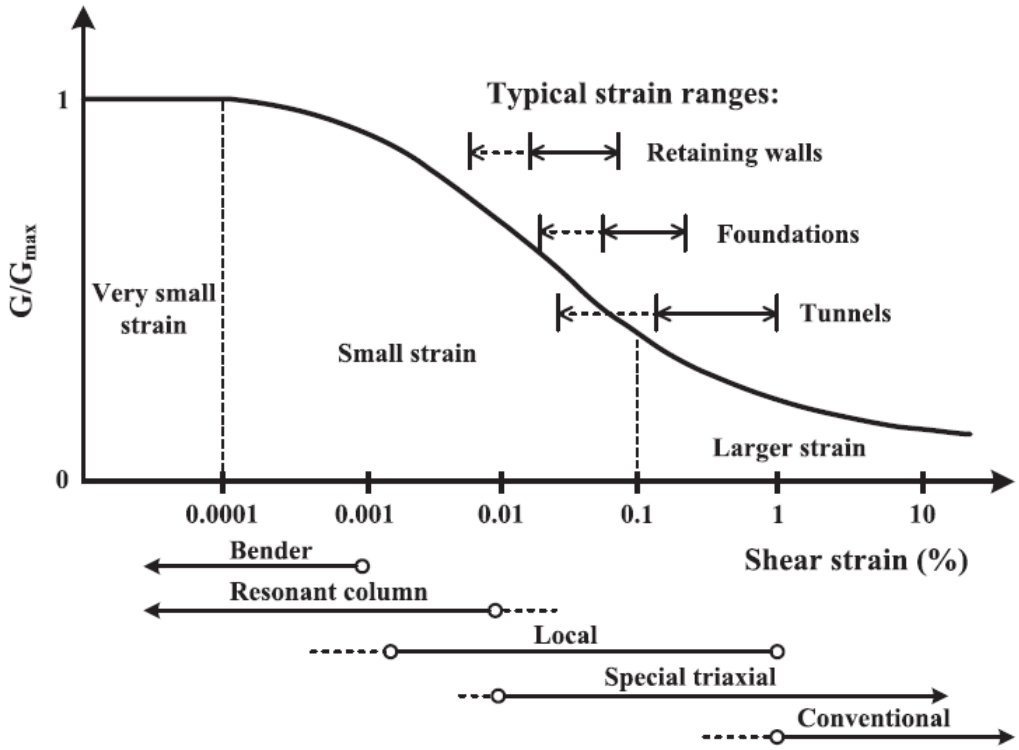

Figure 2.12: Normalised stiffness degradation curve [18]

It is possible to notice how at each test is associated a deformation levels according to the measurements of interest. Obviously, each test has its own resolution (Figure 2.12).

The resonant column test is based on the application of the concept of resonance to a cylindrical sample subjected to torsional excitation. The test is generally carried out by the application of constant amplitude cyclic stresses and variable frequency at the top of a specimen which is embedded at the bottom base. Monitoring the induced rotations the frequency of resonance can be detected and then it is possible to retrieve, through a mathematical inversion process, the shear modulus G. Varying the amplitude of the stress and therefore the average deformation induced on the sample, is possible to reconstruct the G modulus decay curves.

In the case of cyclic torsional shear test, using a similar kind of stress of the resonant column, secant shear modulus and is determined directly from the cyclic stress-strain curve.

The cyclic triaxial test is performed in a similar way as the standard triaxial test. The difference remains in the application of the load that now occurs cyclically in a range where failure doesn't occur. This is the only dynamic test that allows an evaluation of Young's modulus and its decay curve experimentally. In order to obtain the relative G decay curve is necessary to fix one value for the Poisson's coefficient and then apply the realtionship $E_d = 2G_d(1+\nu)$.

Performing the standard triaxial test on a specimen and reaching the failure condition in a static way, it is also possible to reconstruct the decay curve of the modulus for high deformation values, although in this case, it is difficult to obtain the values corresponding to the small deformations. However, a more satisfactory approach is to make use of local instrumentation which can be attached directly to the sample while performing a standard test. These local transducers employed in the triaxial cell are reliable and simple to install directly on the specimen. The main advantages of this type of instrumentations are that the small strain behavior of a material can now be investigated to a high level of accuracy and remain undamaged at strains of up to 35%.

So laboratory tests are useful because:

- allow a better control of measurement accuracy;
- a well-defined correspondence between the applied effective stress and strain;
- the possibility of exploring a very wide range of strains;
- the ability to control the stress path, or to give a voluntary stress history to the specimen.

On the other hand, there are some disadvantages in the use of laboratory tests including:

- disturbance of rock samples during the drilling, recovery and storage operations that weakens the sample structure and limits the representativeness of the real behavior;
- samples of the same deposit but of different sizes may have a different mechanical response.

2.2.2.2 Factors affecting the decay curve

As a first approach we can state that the thresholds of the decay curve are not fixed but may vary according to the nature of the material, the stress history and the conditions at which the tests are performed.

Generally the very small strain domain is more extended in strongly cemented materials and also easier to detect than soils. In fact for the latters this region is not always recognizible. In the case of cemented materials drained tests show an extensive range where the behaviour is nearly linear elastic and the failure is brittle. In this case the other two domains don't exist but they are engulfed in the very small strain domain. This means that the stiffness modulus is nearly constant for the entire load cycle if the peak strength is not exceeded, a trend that best approximates the ideal case. Instead in undrained tests these linear thresholds may not be recognizible regardless of the nature of the material either cemented or uncemented.

ε_{crit} are case dependent, Table 2.3, but from Lo Presti et al. (1989) it appears that this value is smallest in loose uniform clean sand and increases when active clay minerals or some chemical bonding are present. In the Small Strain Domain it is important to take into account the degree of consolidation of the material. In fact, static laboratory tests on slightly Overconsolidated materials have shown that if a high-resolution instrument is not used for small strains, the stiffness modulus measured in this field is greatly underestimated [12, 14].

Soil	ε_{crit} %	Reference
Toyoura sand	0.001	Teachavorasinskun (1989)
Loose clayey sand (PI=3)	0.007	Georgiannou (1988)
Magnus till (PI=18)	0.01	Jardine (1985)
Bothkennar clay (PI=70)	0.02	Smith (1992)
London clay (PI=45)	0.04	Takahashi (1981)
Intact Chalk	0.06	Jardine, Brooks & Smith (1985)

Table 2.3: Variation of ε_{crit} with soil type, [13]

Beyond the critical strain threshold rapid changes in secant and tangent moduli can occur according to the yielding point of the material which is dependent on the OCR (see Figure 2.13). In fact beyond the yielding point we have a fast increment of the plastic strains and at the same time the contribution of the elastic strain becomes negligible. In general the OCR ratio allows to identify a threshold called Bounding Surface BS beyond which there are only unrecoverable strains. This BS is reached earlier by Normally consolidated materials than the Overconsolidated ones.

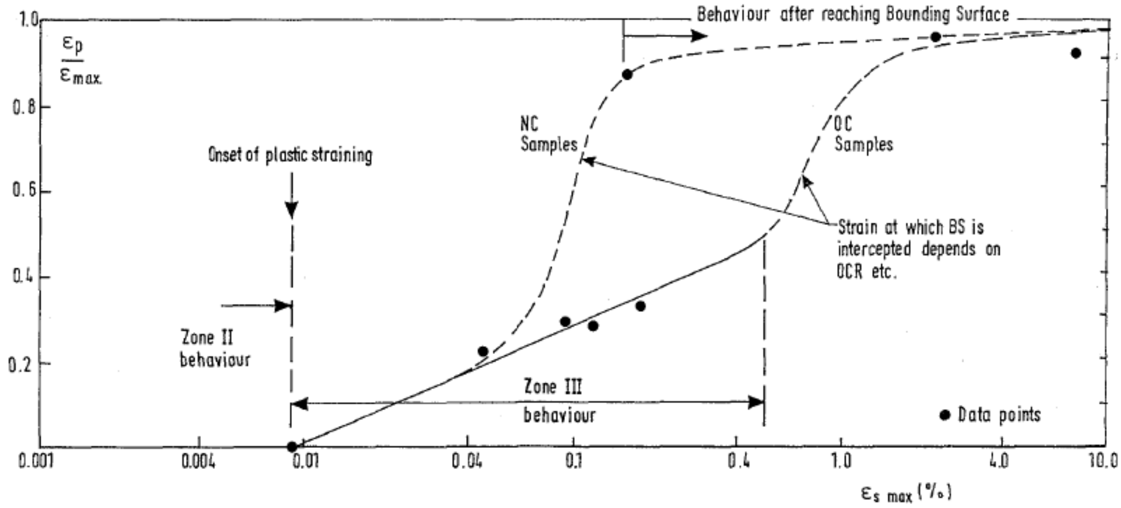

Figure 2.13: Relationships between permanent and total strains for Magnus Till, [13]

The decay curve varies in magnitude and shape depending on the type of the material. An example is visible in the Figure 2.14 where the decay curves of different types of soils are shown. It is possible to observe how the high and low plasticity clay and sand have a stiffness modulus lower than gravel but they have a linear elastic threshold clearly identifiable respect to the gravel in the very small strain field. Moreover, it is possible to notice on the right of the Figure how the decay of the curve is more pronounced for gravel and sand, while the stiffness of the low and high plasticity clay assume a limited variation in the whole deformation field, i.e. the decay of the curve is lower.

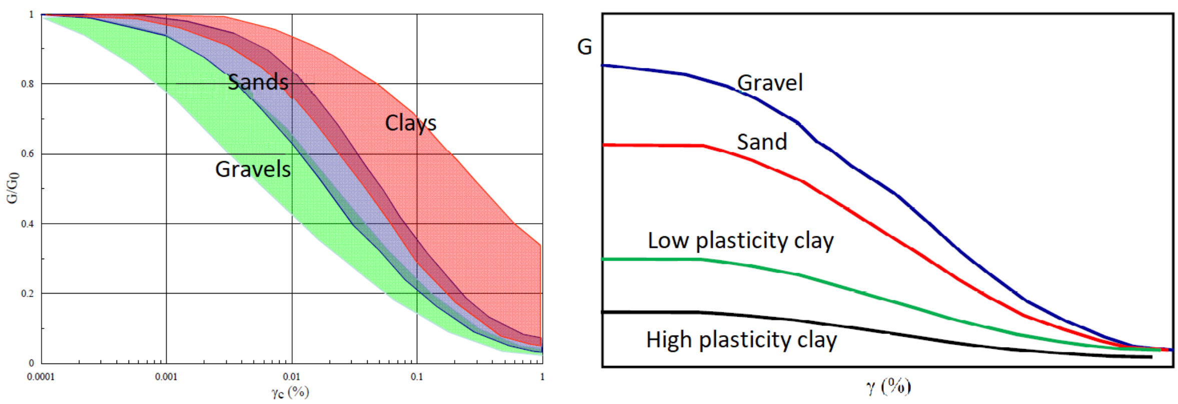

Figure 2.14: $G/G_0 - \gamma$ curves and relative range for different kind of soil, [10]

Another parameter affecting the decay curve is the number of cycles done on the specimen, Figure 2.15. As the number of cycles increases, the degradation of the material increases and therefore the corresponding stiffness modulus decreases. If the number of cycles are equal, the cyclic degradation increases if the strain amplitude increases. While cyclic degradation reduces if the OCR ratio increases, [10].

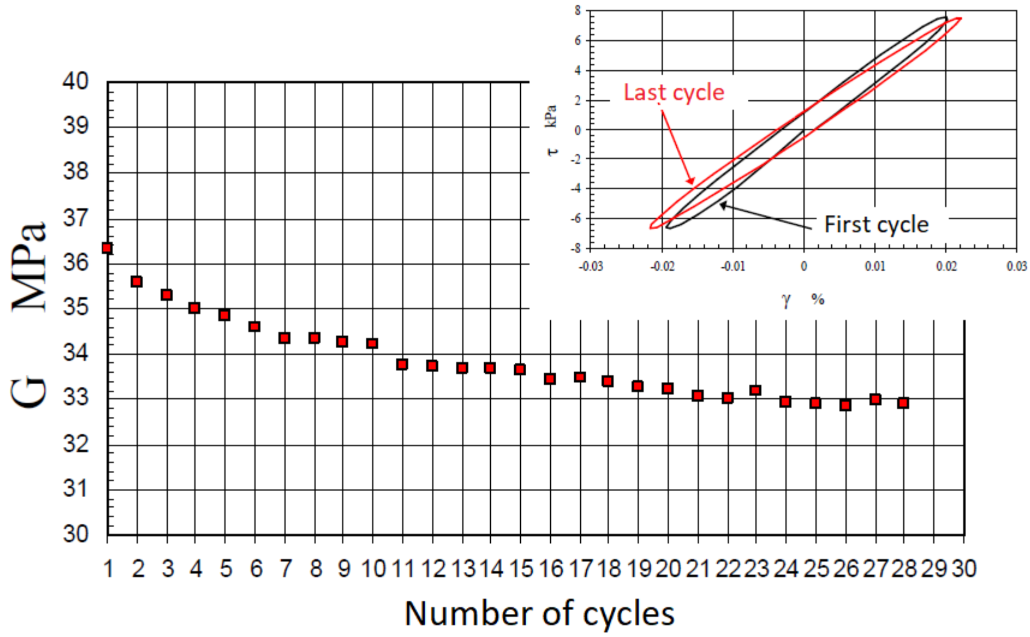

Figure 2.15: Influence of the number of cycles (Degradation), [10]

The confinement pressure also affects the decay curve. From the Figure 2.16 it is possible to notice that if the material is the same, the decay of the curve is delayed or anticipated as the confining pressure increases or decreases respectively.

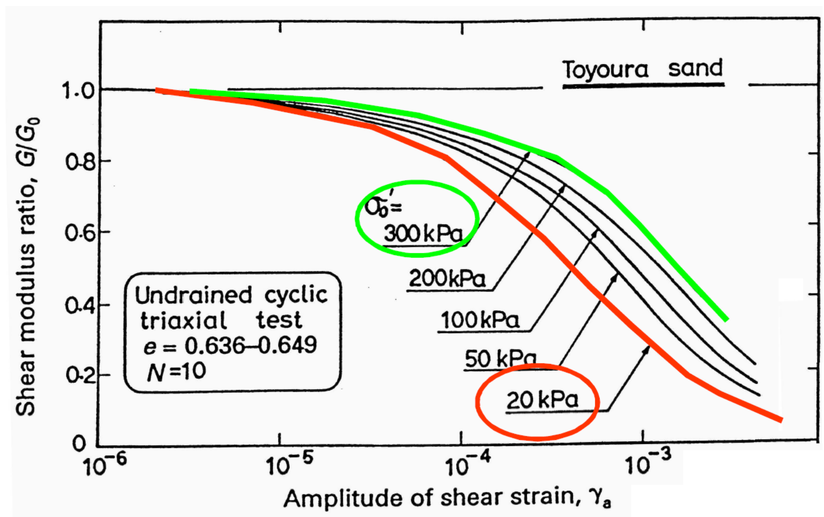

Figure 2.16: Influence of confining pressure on Toyoura sand, [10]

2.2.2.3 Effects of stress cycles

Plona and Cook [22] have emphasized the importance of stress cycles in order to understand the relationship between static and dynamic moduli. Performing an unconfined uniaxial compression test on very permeable and dry rock, Castlegate sandstone.

In Figures 2.17 and 2.18 stress-strain curves relating to static and dynamic measurements and the related values are shown. About static tests, it is possible to notice the large load-unload cycle called major cycle within which 10 load-unload cycles called minor cycles are contained. It is clear that the difference between the two moduli is greater when the static elastic moduli are taken from the big cycle, especially at very low stress. From this point of view, the difference between the two moduli is due to the strain-rate with which the tests are carried out. While the difference between the static and dynamic elastic moduli is negligible when the static moduli are retrieved from the minor cycles within the big cycle mostly at high stress, confirming what was said in the Subsection 2.2.2. This last case shows that the static and dynamic moduli thus obtained are dependent on the amplitude of the load-unload cycles. In fact, reducing more and more the amplitude of the minor cycles of stress, hysteresis phenomena are not present and the minor cycles reproduce exactly the definition of the elastic modulus.

Finally, from [22] static and dynamic values of the elastic modulus differ approximately of 10% and not as usually thought by an order of magnitude (as shown in Figure 2.5).

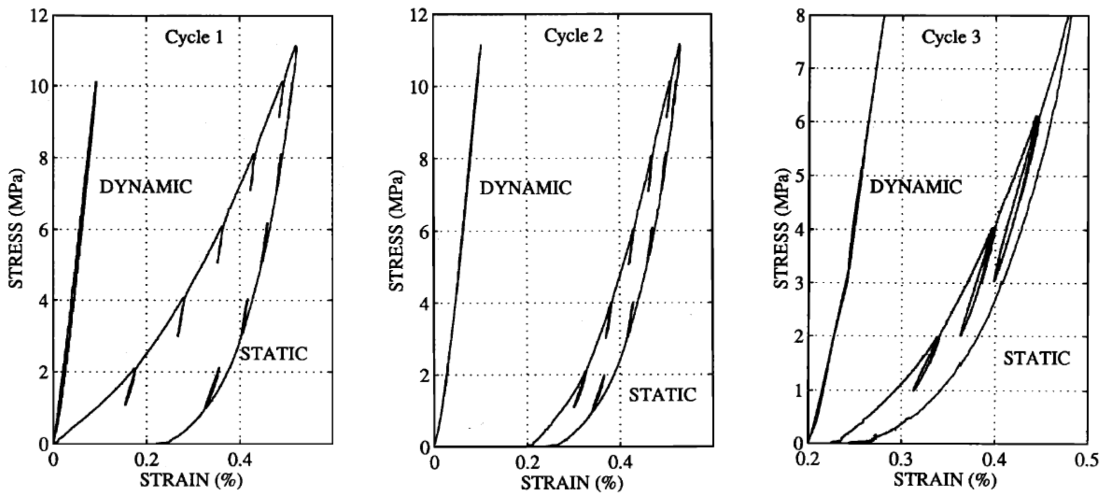

Figure 2.17: Static and Dynamic moduli retrieved from Unconfined Compressional test on Castlegate Sandstone: first major load and unload cycle [22]

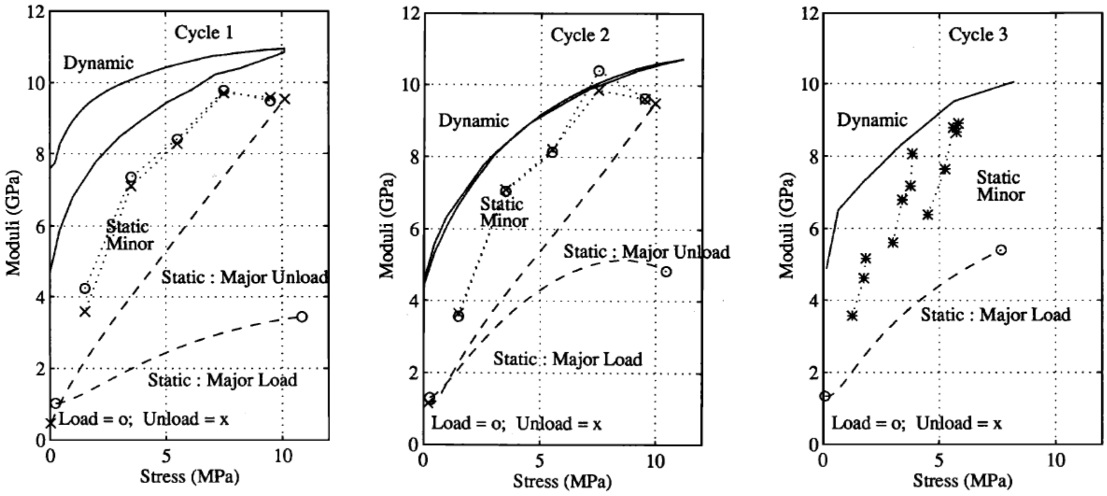

Figure 2.18: Static and dynamic moduli vs stress [22]

2.2.2.4 In situ tests

The Radioactive Marker Technique RMT is a in situ test based on measurement of the vertical distance between radioactive bullets called markers shot radially into the formation at regular intervals every 10.5 m inside a vertical monitoring well before casing operations, Figure 2.19.

The markers having a bullet-shaped and made of steel, contain a radioactive source (low-emission isotopes Cs^{137} or Co^{60}) sealed inside them to avoid problems of environmental contamination.

Then two pairs of gamma ray detectors spaced again appoximately of 10.5 meters are lowered at the bottom of the well. The positions of each marker can be determined by these specialised wireline Gamma Ray (GR) logs, which are run at regular time intervals to estimate the possible temporal changes in the distance between the markers. In fact, moving a set of radioactivity detectors at a constant speed results in a correlation of the GR count rate versus time, which can be transformed in distance [19].

Marker spacing is periodically surveyed in terms of few years, depending on the reservoir depressurisation. During the measurements, the static reservoir pressure is recorded for each interval, which is necessary for the estimation of the effective uniaxial compressibility C_m retrieved by

$$C_m = \frac{\overline{\Delta h}}{\overline{h_0}\Delta p}$$

where $\overline{\Delta h} = \overline{h_t} - \overline{h_0}$ is the average vertical deformation (expansion if positive, compaction if negative) of the marker interval; $\overline{h_0}$ and $\overline{h_t}$ are the average distance between two adjacent markers at the initial time and at time t, respectively; and Δp is the fluid pressure variation (rise if positive, drawdown if negative) occurred within the monitored depth interval over the time period 0-t [9].

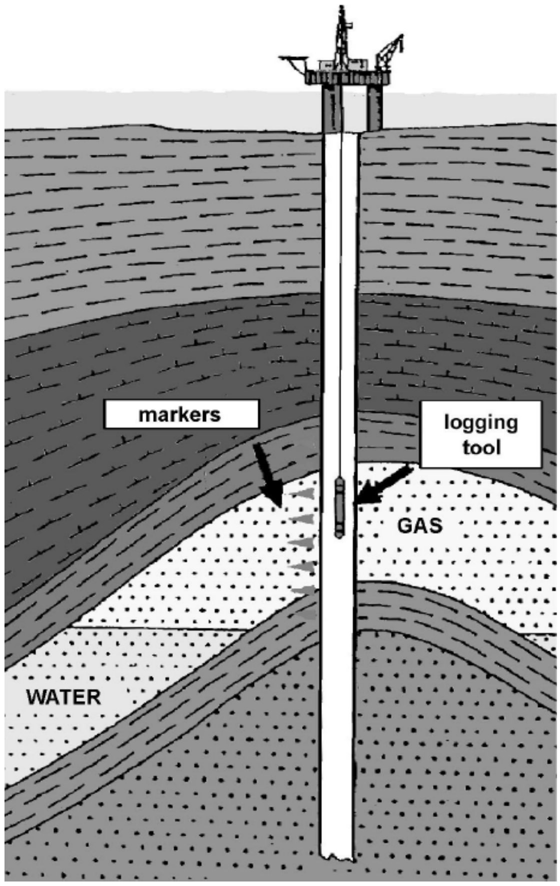

Figure 2.19: Schematic illustration of the radioactive marker technique

The nominal RMT precision, i.e., the expected average measurement error of the vertical strain measurement, is on the order of 10^{-4}, that is 1 mm for a vertical distance range of 10 m.

The advantages of the RMT are:

- the possibility of testing a large-scale sample in its natural environment;
- there is no need to assume initial conditions to be submitted to the specimen as it happens in the laboratory. Furthermore, it is possible to monitor the behavior of the material in the long period of its stress history.

while the disadvantages are:

- it is a very expensive method due to the fact that the markers must be installed in dedicated wells and not usable for production. Furthermore, this instrumentation must be installed before completing the casing operations of the well;
- measurement of marker displacements must be performed using tools that operate at high depths in difficult conditions;
- Attention should be paid to the measurement of C_m as it is very influenced by the degree of saturation of the deposit and by the cementating operations of the well after drilling.

The phase of casing cementation improves the mechanical characteristics of the rock near the well, area affected by marker measurements. Therefore the values of C_m may be lower than the real compressibility of the reservoir.

In the Oedometric test the specimen is always saturated while in situ tests these conditions are not always present like in gas reservoirs. In these latter conditions, only part of the pores is filled by gas while the remaining pore space is occupied by water, which forms menisci around the contact points of the grains. This phenomenon, defined capillary pressure, acts between the different phases increasing the inter-particle forces as shown in the Figure 2.20. These forces act in a roughly normal direction with respect to the particles' contact, acting as a binder between pores and grains. The net result is an increase of the resistance of the porous media to deformation and failure [20].

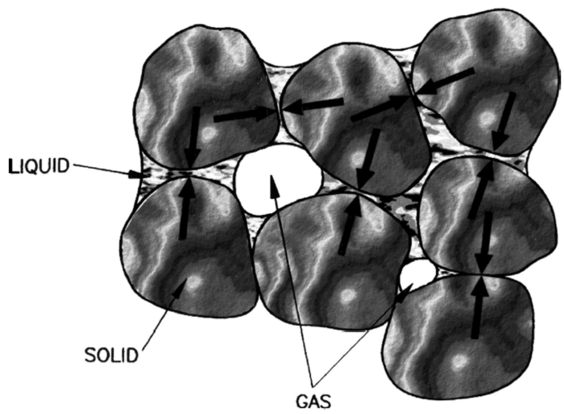

Figure 2.20: Schematic rappresentation of an unsaturated medium. Intergranular forces due to capillary effects are indicated [20]

As water content increases, the degree of saturation increases and lower will be the capillary forces. In fully saturated conditions these forces do not exist and the compressibility increases significantly. For this reason the values of C_m measured in the RMT tests are underestimated with respect to the real behavior of the entire reservoir. For a fixed value of the Poisson's coefficient, the Young's moduli that are obtained using these values of C_m are overestimated and are closer to the dynamic moduli erroneously. So it means that the real compressibility will be greater than the measured one so that the real value of the elastic modulus will be better represented by static elastic moduli.

2.2.3 Empirical law for Uniaxial compressibility

Analytical relationships are general but approximated simplified models while empirical relationship are accurate but of limited validity site/material dependent.

The large amount of data collected with the RMT tests done in the Po River Basin (Italy) has been statistically processed to generate a basin-scale compressibility law that links the vertical uniaxial compressibility C_m as an exponential function of the vertical effective stress σ_z [1]

$$C_m = 1.3696 \times 10^{-2} \sigma_z^{-1.1347}$$

where C_m is in $bars^{-1}$ and σ_z in $bars$.

This equation is valid for:

- Isotropic system;
- only for sand and clay typical of the Po Plain;
- rock compression in virgin loading conditions (I loading cycle);
- for a depth range between 1000 and 1500 m in normally pressurized conditions, tipical value of this basin.

While rock expansion is controlled by a new uniaxial compressibility called C'_m that describe the unloadind/reloading phase or the second loading cycle. In the oil field the first and second loading cycles can be assimilated to in situ loading conditions during primary production and subsequent storage activity, respectively. In fact C'_m plays a key role for the characterization of the geomechanical reservoir behavior during UGS operations when the seasonal fluctuations of the effective stress due to gas injection/removal usually occur at stresses less than the preconsolidation stress [23]. Being the formulation of Teatini deriving only from data obtained from RMT test, this presents the same criticality of the measurements made with the raioactive markers, then underestimates the value of C_m when the fully saturated conditions do not exist in reservoir.

In addition, Baù et al. [1] and Ferronato et al. [8] have observed that the correlation itself tends to underestimate the compressibility C_m for low values of effective stress, i.e. at relatively low depths. Therefore, it has been recommended as a precautionary measure, for depths that are less than 1500 m, the values of C_m calculated with the aforementioned formula should be corrected multiplying them by 2.

Moreover, comparing the data obtained with the RMT test and the results obtained from the odometer test, they argued that the ratio of virgin loading C_m to C'_m varies between 1.8 and 3.5 in a depth range between 1000 and 6000 m under hydrostatic condition.

2.3 Compaction and induced subsidence in reservoir rocks

Before any production the system is in equilibrium and is subjected to a lithostatic load due to the overlying formations called overburden. This load is carried partly by the solid skeleton of the reservoir rock and partly by fluids contained whitin the porous medium as a function of their elastic moduli and compressibility respectively. The pore fluid is acting in the pore spaces between the mineral grains and the rock structure and presses out against the overburden (vertical) and the horizontal reservoir stress.

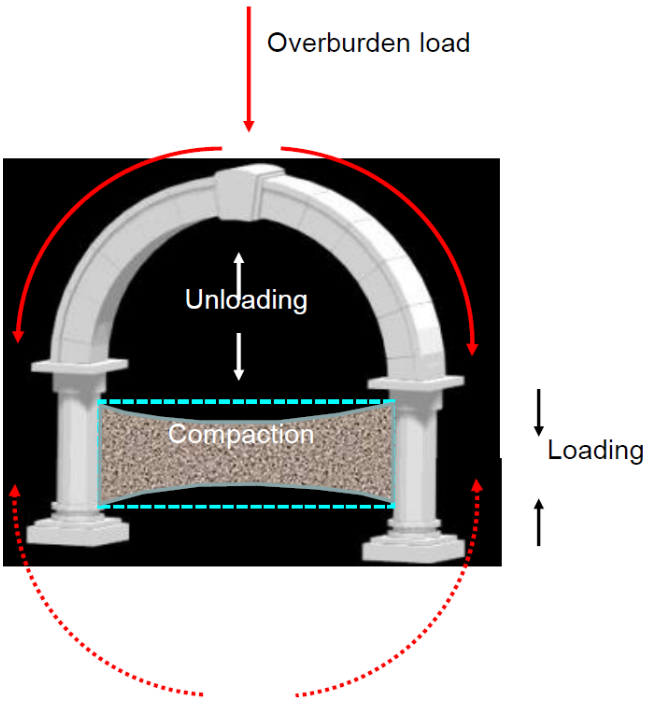

Figure 2.21: Stress arch effect [24]

The fluid extractions from the reservoir during production induce a pressure drop within the pores previously occupied by the fluids. At the same time, due to the fact that the weight of the overburden remains constant the variation of the total vertical stress is negligible only if the stress arch effect is not generated and, according to the Terzaghi's Principle, the effective stress on the solid skeleton icreases.

Instead, in the case where the stress arching effect is generated, partial weight of the overburden is transferred to the sideburden during reservoir compaction (see Figure 2.21). This phenomena occur frequently when the reservoir is soft compared to the surrounding rocks and increases when the reservoir approaches the shape of a sphere, or for high shape factor. The stress arching ratio is defined as the change of overburden pressure divided by the change of pore pressure, and it is controlled by reservoir geometry, rock properties of the reservoir and surrounding rock, and pore pressure distribution within the reservoir during production, [25].

The reservoir rock will be compressed (compacted) until a new equilibrium is reached.

However, in order to study the mechanical response of the reservoir we assume an uni-axial strain in vertical direction during compaction. This assumption is valid if the vertical extent of the reservoir is small compared to its lateral extent [15]. This simplification allows an easier characterization of rock properties using data from uni-axial lab measurement.

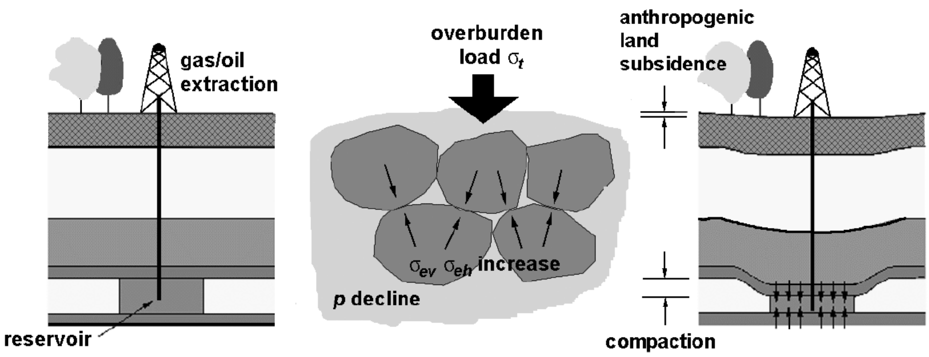

Figure 2.22: Schematization of a reservoir before, during and after production

The variation of the ground level is due to both natural and anthropogenic causes. The latter depend mainly on the fluid withdrawal from the underground (aquifers or producing hydrocarbon). For this reason it's important to verify if the potential subsidence induced by the extraction of fluids has no relevant impact on existing buildings and infrastructures in the area of interest. Therefore the extension of the cone of subsidence and the maximum displacements should be assessed [3].

Reservoir compaction and subsidence can cause wellbore-casing deformation and significant pipeline damage due to excess compressional or tensional strain [21], loss of the well and in the worst case fault reactivation generating earthquakes.

Many factors play an important role on subsidence magnitude. Necessary condition for the subsidence phenomena to occur is the high compaction of the reservoir and therefore the compressibility and the thickness of the rock are very important parameters. Moreover, the presence of a strong aquifer can keep constant the pressure of the reservoir even during production, reducing the occurrence of this phenomenon. Finally, the overburden may shield the reservoir and prevent subsidence according to its geometry, depth and the contrast in mechanical properties of the surrounding rocks.

2.3.1 Uniaxial reservoir compaction and uniaxial compressibility

In Petroleum applications the Oedometric test in drained conditions is thought to simulate the compaction of a reservoir during depletion.

So, as mentioned before, if the lateral extent of the reserovir is much larger than its thickness (ie if we can assume that the field is infinitely extended horizontally, we have geometric symmetries on the field of stresses and deformations) the analysis models show the absence of lateral deformations only along the center of the baricentric axis at which the longitudinal elastic modulus E' in drained conditions is reduced to the edometric.

So assuming that our model is Isotropic linear elastic, then the deformation of the reservoir can be expressed by the generalized Hooke's law and the uniaxial strain condition in terms of effective stresses [7]:

$$\varepsilon_h = \frac{1}{E'}[\Delta\sigma'_h - \nu(\Delta\sigma'_H + \Delta\sigma'_v)] = 0$$

$$\varepsilon_H = \frac{1}{E'}[\Delta\sigma'_H - \nu(\Delta\sigma'_h + \Delta\sigma'_v)] = 0$$

$$\varepsilon_v = \frac{1}{E'}[\Delta\sigma'_v - \nu(\Delta\sigma'_h + \Delta\sigma'_H)]$$

where H and h indicate the maximum and the minimum stress and strain respectively, orthogonal to the z axis.

If the change in reservoir thickness is:

$$\Delta h = -\varepsilon_v h$$

and in order to maintain uniaxial vertical compaction during depletion the effective horizontal stresses must increase:

$$\Delta\sigma'_h = \Delta\sigma'_H = \frac{\nu'}{1-\nu'}\Delta\sigma'_v$$

According to Terzaghi's principle, we assume that total vertical stress remains constant during production:

$$\Delta\sigma'_v = \Delta\sigma_v - \alpha\Delta u = -\alpha\Delta u$$

Combining all the equations we obtain the compaction formula:

$$\varepsilon_v = \frac{\Delta h}{h} = \frac{1}{E'}[\frac{(1+\nu')(1-2\nu')}{1-\nu')}]\alpha\Delta u$$

where

$$\frac{1}{E'}[\frac{(1+\nu')(1-2\nu')}{1-\nu')}] = \frac{1}{E_{oed}} = C_m$$

where C_m is the compaction coefficient or uniaxial compressibility.

Chapter 3

Case study

3.1 Geological context

The Italian peninsula and its surrounding marine areas have been subjected to a complex geological evolution that originated several hydrocarbon systems. The three main Italian tectono-stratigraphic systems can be classified as [4]:

1. Biogenic gas in the terrigenous Plio-Quaternary foredeep wedges;
2. Thermogenic gas in the thrusted terrigenous Tertiary foredeep wedges;
3. Oil and thermogenic gas in the carbonate Mesozoic substratum.

In Italy gas reservoirs contain mainly biogenic gas and they are located in the Po Plain and in the Northern and Central Adriatic Basin. Tectonostratigraphically, the area is composed by a carbonate substratum deposited during Permian-Mesozoic overlayed by a Cenozoic succession made of thick turbidite sequences with alternating sandstones and shales layers, which are interbedded combinations of sources and reservoirs [5].

The Biogenic gas is trapped in structural traps, generally anticlinal, in the internal part of the foredeep near to the Apennines chain; this kind of field is composed by a number of superimposed pools, which are made up of single or multiple reservoir intervals. While in more external parts of the foredeep the gas is accumulated in sandstone layers of stratigraphic traps. Going in the Adriatic foreland we have gentler anticlinal traps that are sealed by Pleistocene shales (Argille del Santerno). Structural traps with hydrodynamic component are commonly present while hydrodynamic traps are rare in the Adriatic basin. The latter are caused by the differences in water pressure, that are associated with water flow, creating a tilt of the hydrocarbon-water contact, like in Ravenna field where the GWC is tilted of about 40 meters. Reservoir rocks of biogenic gas in the Adriatic Basin are mainly

Pliocene-Pleistocene successions of turbidite sands and silts of several thousands meters thick. The biogenic gas was originated from organic matter of terrestrial origin and comes from turbiditic and hemipelagic shale and clay source rocks.

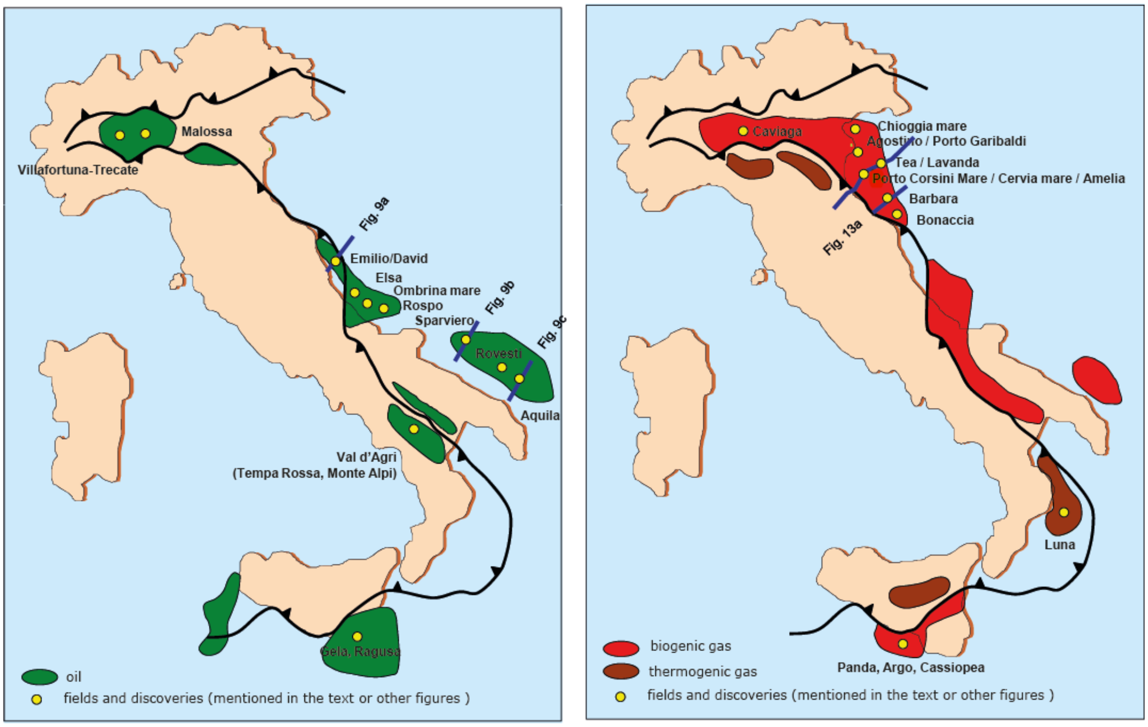

Figure 3.1: Oil and thermogenic gas occourence in the carbonate Mesozoic substratum, leftside; Gas occurences in the terrigenous foredeep wedges, rightside [4]

The others gas reservoirs contain thermogenic gas. This kind of system are made up of older turbidite deposit from the Southern Alps and of the Apennines. The deep burial of these deposits allowed an early thermogenic generation of gas from the deepest organic matter. This reservoirs are located mainly in the Southern Alps and in the Northern Apennines but the most important are in the Southern Apennines and in Sicily. Finally Oil and thermogenic gas reservoirs involve the Mesozoic carbonate substratum of the foredeep/foreland area and of the external thrust belts, Figures 3.1 and 3.2. Traps of crude oils and associated thermogenic gas can be both structural and hydrodynamic in the central and southern Adriatic. These hydrocarbons are contained in Mesozoic reservoir rocks that are mainly carbonates deposits with different genesis related to the Middle Triassic, Late Triassic/Early Jurassic and Early Cretaceous stages. In the Central Adriatic area there is heavy oil ranging from 5° to 22° API while the oil is lighter in the Southern Adriatic (e.g. 37° API at Aquila field).

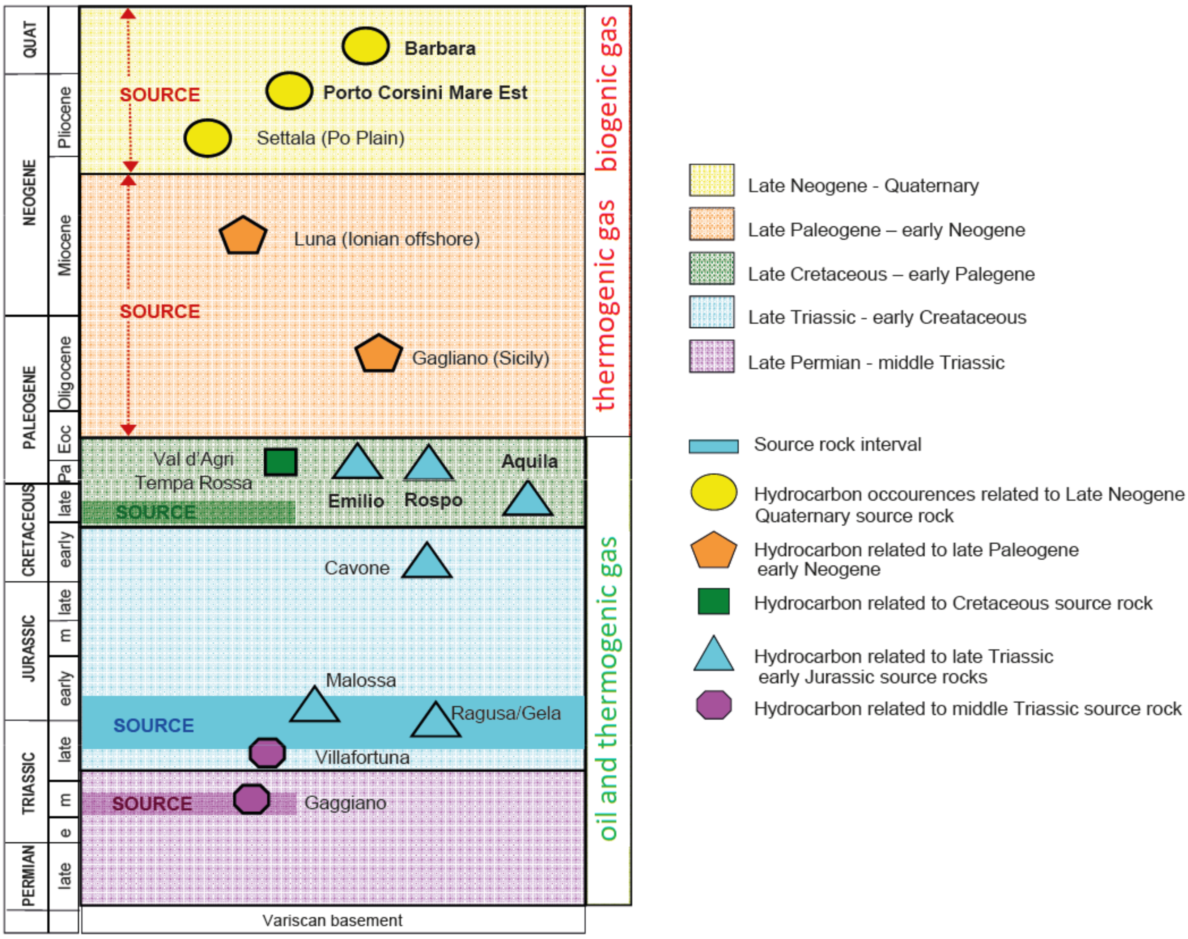

Figure 3.2: Stratigraphic distribution of source rocks and hydrocarbon occurrences in the Apennine-Adriatic area, Italy, [5]

Summarizing, the Biogenic gas has been produced at relatively shallow depths from the Apennine Plio-Quaternary foredeep basins, both onshore (Padana and Bradanica foredeeps) and offshore (central-northern Adriatic Sea), while oil and thermogenic gas are at greater depths in the Western Po Plain, in the Southern Italy and in the Adriatic foreland Basins.

3.2 Case 1

The synthetic case study is an offshore reservoir in the North-East of the Adriatic Basin where there is the greatest concentration of deposits of biogenic gas, as shown in Figure 3.1.

The analysed area is a stratigraphic alternation of sand and clay layers. This configuration allowed an accumulation of biogenic gas in a sandstone reservoir that lies at the depth of 1500 meters below the sea level. The sealing is guaranteed by a layer of clay overlying the deposit. The schematization of the stratigraphy of the case study is shown in Figure 3.3, while in the Table 3.1 are shown in detail the data related to each lithological unit and their stratigraphy. To be more precise, the gas is stored in a sand "lens" surrounded entirely by clayey deposits.

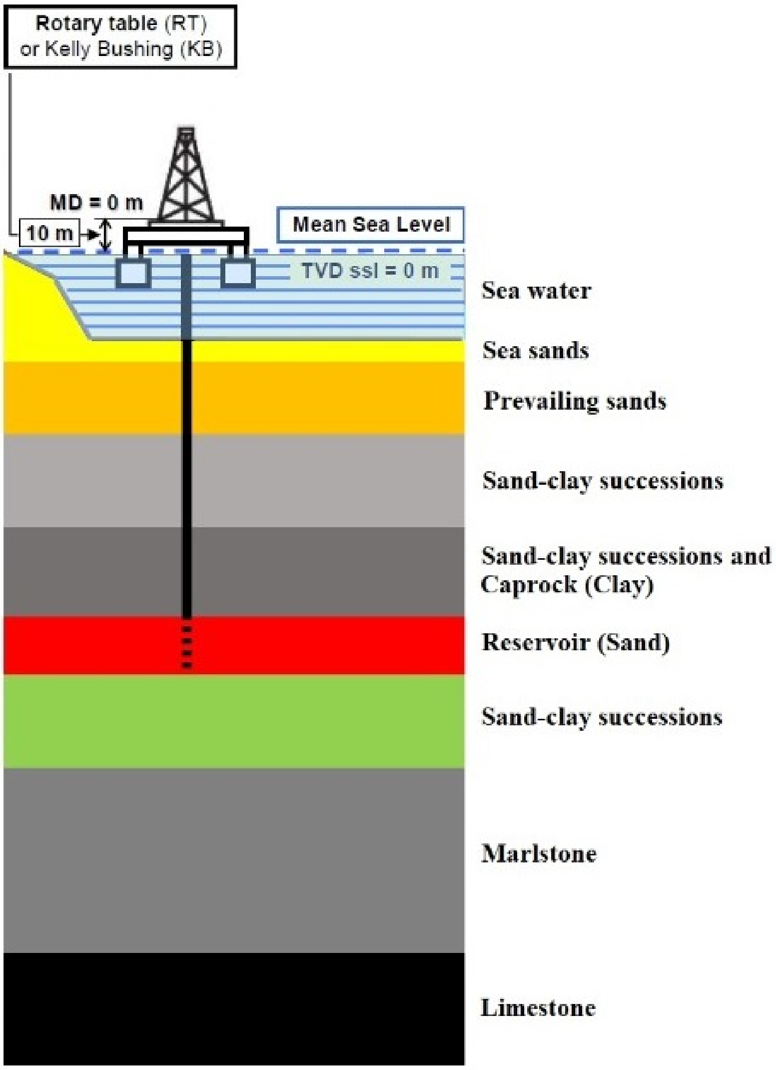

Figure 3.3: Scheme of typical biogenic gas reservoir in Northern Adriatic Basin

This configuration has been studied in this thesis work through the use of a mechanical simulator within the Petrel E&P software platform (Schlumberger) with which it is possible to construct a numerical model of the problem under examination. The software use a FEM (Finite Elemenet Method) 3 D numerical approach : the basic idea is to break down the domain of the modeling into a finite number of well-defined elements, called elementary cubes, which are connected to each other by nodes. All these elements form a grid and in this way the problem is discretized.

	Stratigraphy			
Lithological unit	**Top (m TVDss)**	**Bottom (m TVDss)**	**Average depth (m)**	**Thickness (m)**
Sea water	0	50		50
Sea sands	50	100	75	50
Prevailing sands	100	500	300	400
Sand-clay successions	500	1000	750	500
Sand-clay successions	1000	1430	1215	430
Caprock (Clay)	1430	1450	1440	20
Reservoir (Sand)	1450	1575	1513	125
Sand-clay successions	1575	2000	1787,5	425
Marlstone	2000	3000	2500	1000
Limestone	3000	5000	4000	2000

Table 3.1: Lithological units and stratigraphy

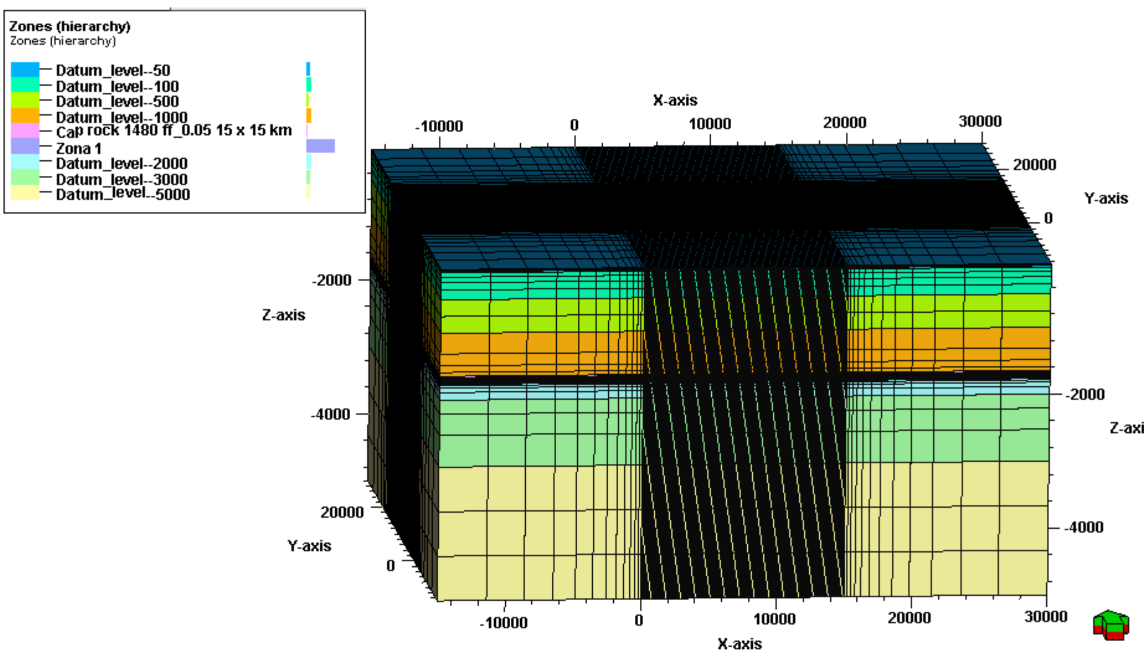

Figure 3.4: Regional scale model and relative stratigraphy (values in meter)

The phenomena of our interest are those that involve the compaction of the deposits and the potential subsidence induced during primary production. For this reason our geomechanical grid has been built on a regional scale in order to analyze the variations of strains, stresses and displacements not only of the reservoir but also of the neighboring areas such as overburden, sideburden and underburden formations, see Figure 3.4. Since the reservoir is the area where there is the greatest variation of effective stress due to the withdrawal of gas the grid is much packed around the reservoir in order to provide more accurate results.

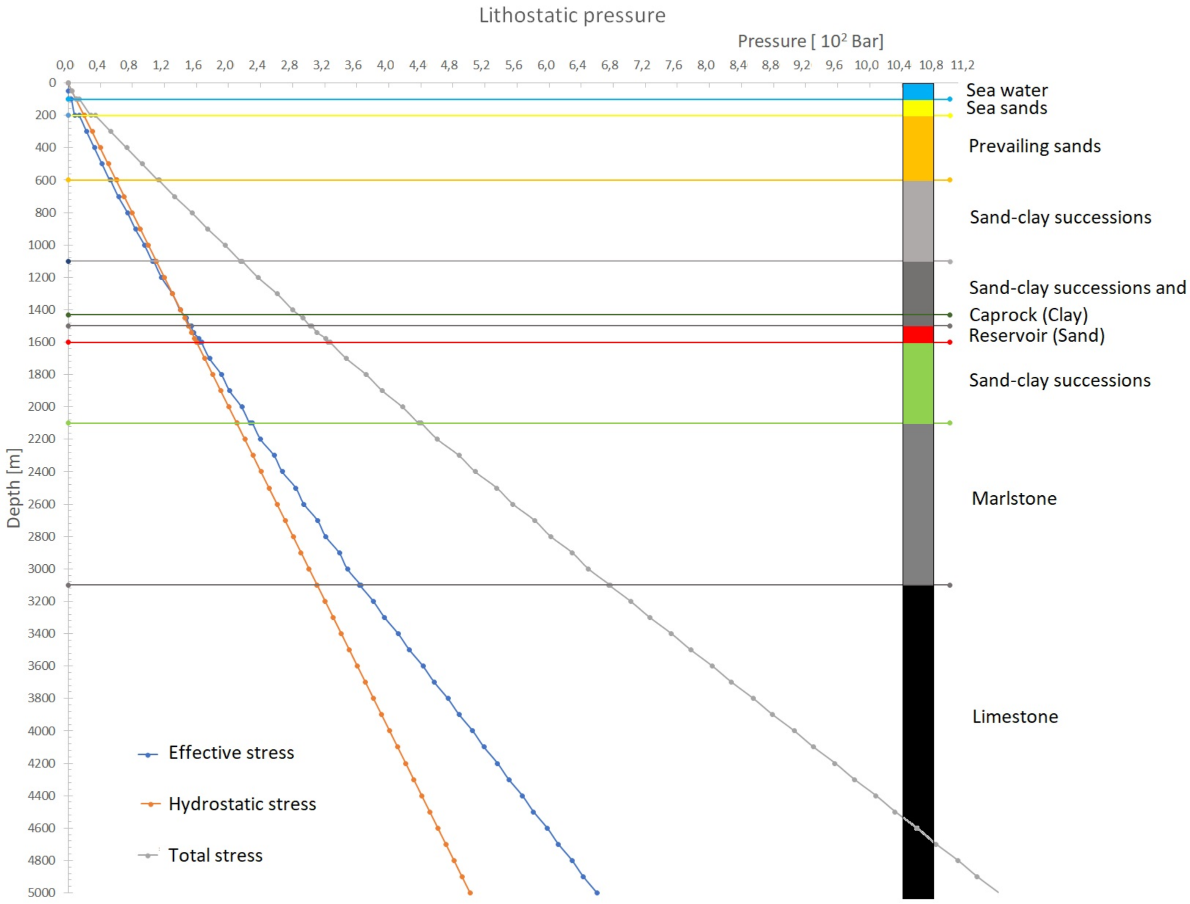

Figure 3.5: Lithostatic load and hydrostatic conditions of the model

For the entire model a constant porosity of 0.21 was considered both inside and outside the reservoir. We assume that the reservoir is saturated with gas and all the rest is saturated with water, the gas-water contact (GWC) is considered at a depth of 1575 meters or at the lower edge of the lens. The horizontal and vertical permeability in the reservoir are assumed equal to 50 and 5 mDarcy respectively and a Net To Gross equal to 0.8. There are neither faults nor active aquifers, all the layers are considered isotropic, homogeneous and continuous, and their mechanical properties vary only according to the depth using the empirical Teatini's formula described in chapter 2. In this case the initial state of stress of the reservoir and surrounding rocks is due to the simple lithostatic load and the fluid pressure is in hydrostatic conditions on the whole model assumed equal to 0.1 bar/m, see Figure 3.5.

Instead the reservoir has been modeled as a lens having a height of 75 meters and a radius of 1.5 kilometers inside which is contained an initial volume of gas (GOIP) equal to $4.295 \times 10^9 m^3_{sc}$. The average static pressure in the reservoir measured at a depth of 1500 meters is equal to 158.82 bar, see Figure 3.6.

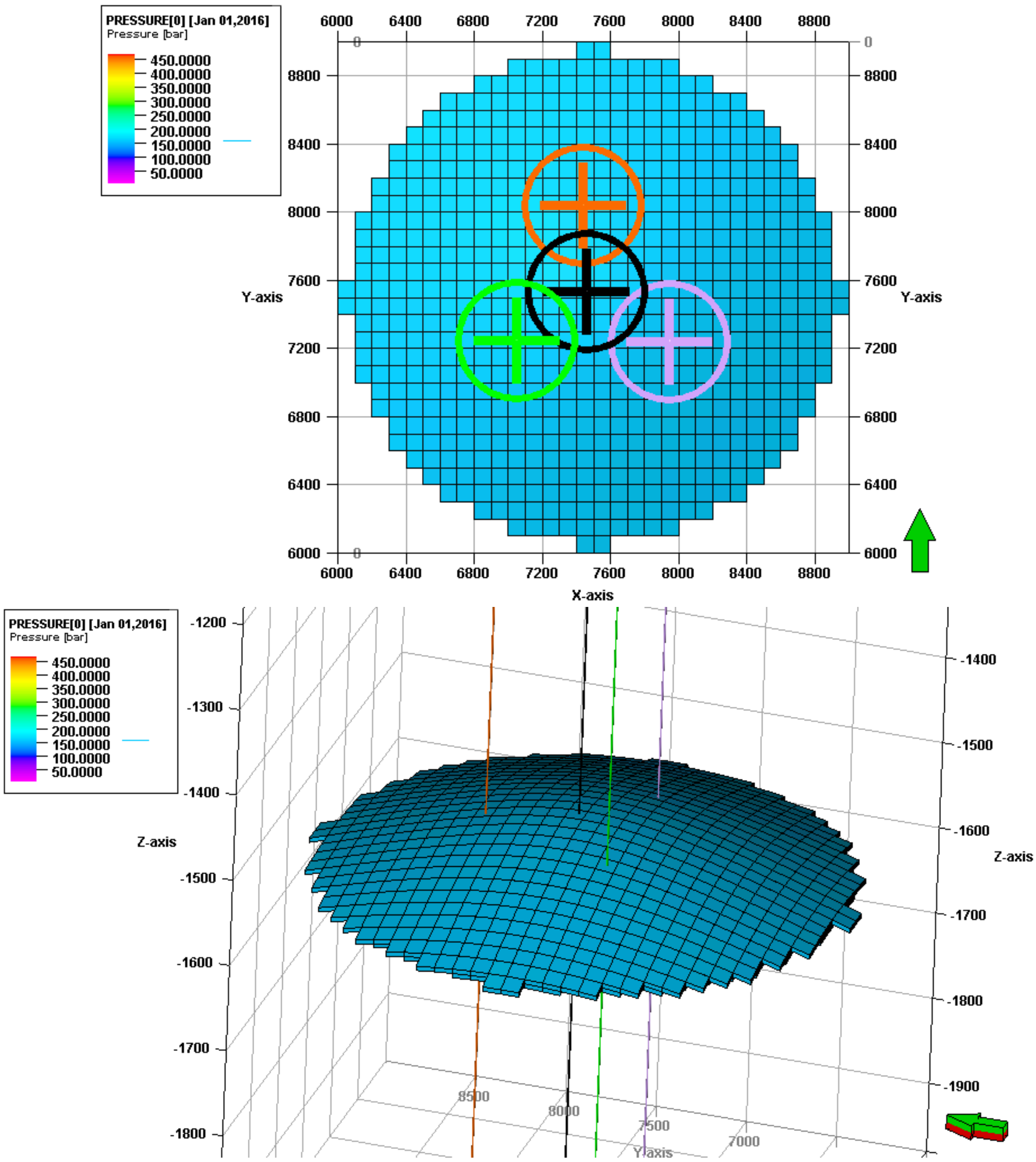

Figure 3.6: Distribution of the initial Pressure [bar] of the reservoir before production and position of the four production wells.

The model hypotheses consider the reservoir a closed system, or during production the pressure varies only within the reservoir and remains constant for all the sourrounding formations equal to the previously assigned hydrostatic value.

The production mechanism is a depletion drive and we assume a constant pore volume. Furthermore, no interaction between the formation induced by pressure variation and petrophysical parameters (i.e. porosity and permeability) is considered: i.e. during fluid flow simulation the petrophysical parameters remain constant. Generally for shallow gas reservoirs and for low degree of cementation of the reservoir rock, permeability and porosity vary during compaction phenomena, but in the analized case they are assumed constant, considering the study of this phenomena as a possible future continuation of the present work.

There are four production wells and production took place on January 1st 2016, while the end of production is planned for the end of April 2025 with a Recovery Factor of about 63%, Figure 3.7.

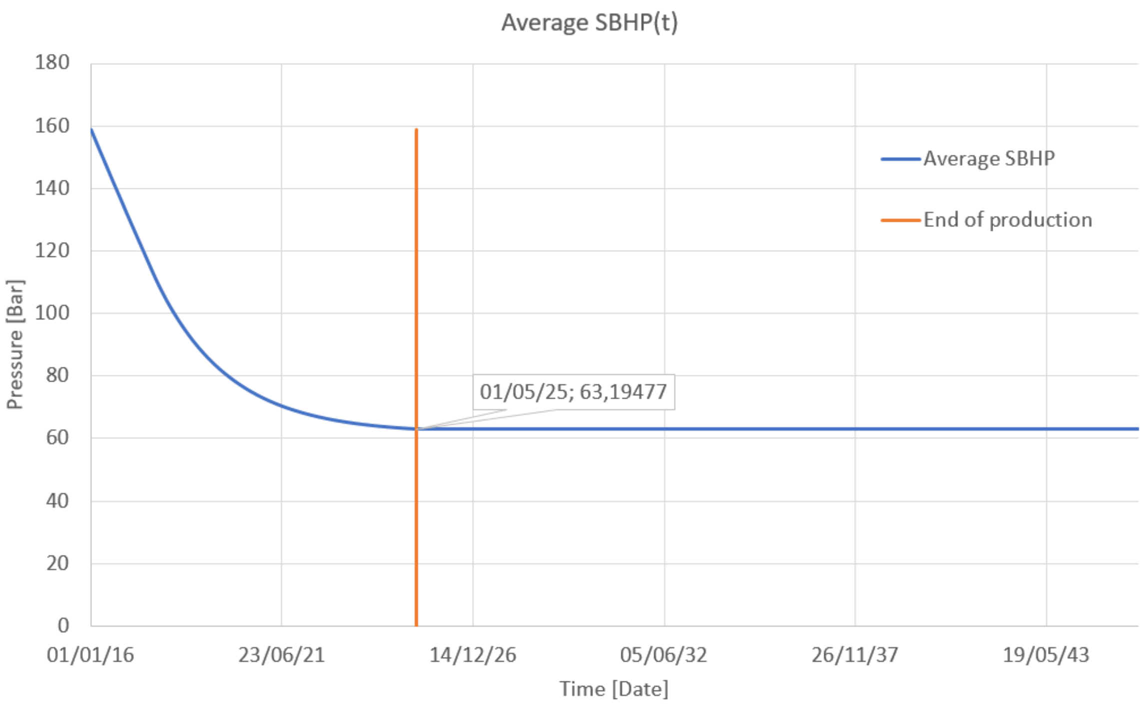

Figure 3.7: Average static bottom hole pressure

In order to populate the stratigraphies of the model with the relative mechanical characteristics we have assigned all the mechanical properties of each single material to a class and subsequently the latter have been associated to the relative hierarchical zone of the model, see Table 3.2.

Lithological unit	Class	Stratigraphy Average depth (m)	Thickness (m)	Mechanical properties Density (g/cm^3)	E (GPa)	v (-)	c (bar)	φ (°)	UCS (bar)
Sea water			50	1,027					
Sea sands	1	75	50	1,9	0,2	0,3	2	38	8,2
Prevailing sands	2	300	400	2	ƒ (z)	0,3	6	35	22,9
Sand-clay successions	3	750	500	2,1	ƒ (z)	0,3	10	32	36,1
Sand-clay successions	4	1215	430	2,2	ƒ (z)	0,3	10	32	36,1
Caprock (Clay)	5	1440	20	2,2	ƒ (z)	0,3	18	26	57,6
Reservoir (Sand)	6	1513	125	2,3	ƒ (z)	0,3	9	34	33,9
Sand-clay successions	7	1787,5	425	2,3	ƒ (z)	0,3	15	29	50,9
Marlstone	8	2500	1000	2,4	40	0,3	20	35	76,8
Limestone	9	4000	2000	2,6	50	0,3	40	45	193,1

Values obtained by weighting the properties of sands and clays: 2/3 sands and 1/3 clays
Values obtained by weighting the properties of sands and clays: 1/2 sands and 1/2 clays

Table 3.2: Geomechanical classes where f(z) is the stiffness modulus obtained from Teatini's formula

Our goal was to make a sensitivity analysis on different casess. Each case has been analyzed through three different mechanical configurations or models:

1. static configuration;
2. dynamic configuration;
3. dynamic initial configuration with additional information about the decay of the stiffness modulus inside the reservoir, the only area subject to large stress variations.

Since the study is focused on the entire primary production phase, the geomechanical model must be populated by assigning the first loading stiffness modulus. In this way the geomechanical model has been populated by assigning to each layer an average stiffness value through the use of the empirical Teatini's formula, Figure 3.8, where the value has been doubled for depths less than 1500 meters in accordance with the recommendations of Baù, 2.2.3. In this way we have assigned static characteristics for the entire model. Furthermore the geomechanical model was repopulated by assigning a dynamic stiffness (higher than the static one) to each layer equal to four times the value of static one, i.e. the ratio between the dynamic modulus at the first loading cycle and the static modulus at the first loading cycle was assumed to be equal to 4.

Since we want to extend in detail the study for the entire strain domain of the reservoir, a decay curve has been obtained from literature, Figure 2.14, assuming that the deposit is 100% sand and sampling 38 points from this curve. This new curve, called curve 1, was constructed starting from the static and dynamic moduli previously assigned to the reservoir, but adding the information of the decay of the stiffness modulus as a function of the strain level, see Figure 3.9.

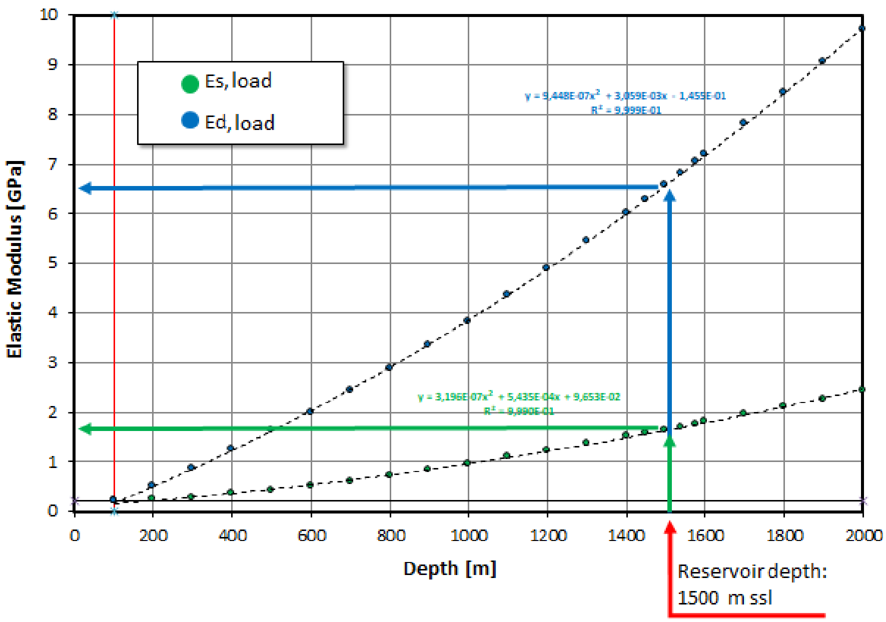

Figure 3.8: Young modulus variation as a function on depth

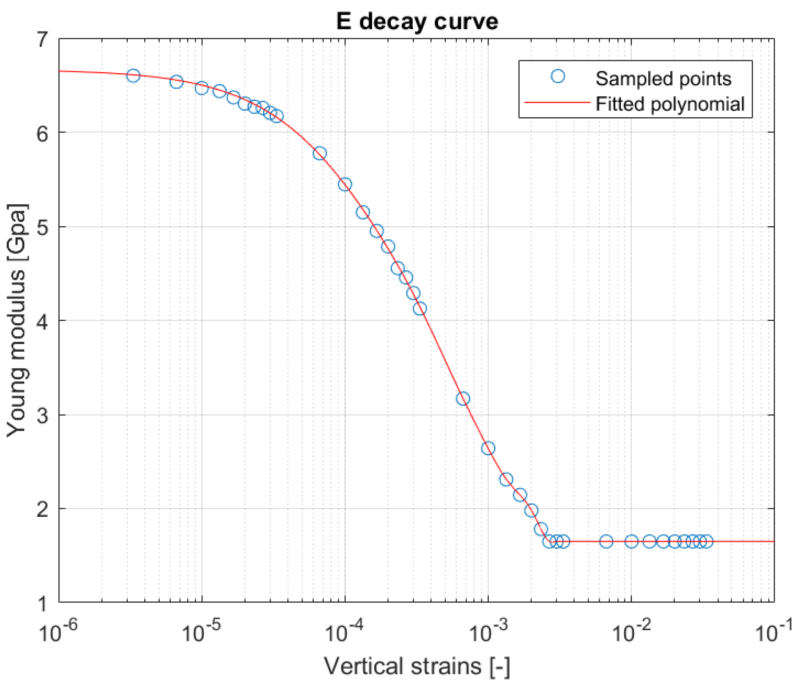

Figure 3.9: E decay curve

3.2.1 Static and Dynamic cases

A first comparison can be made between the results obtained by initializing the model in a static and dynamic way. Having assumed the hypotheses of ILE model, from the related theory we have seen how the strain level depends linearly on the stiffness modulus. Since the static stiffness modulus is four times smaller than the dynamic one, we expect to obtain greater strains in the static case than the dynamic. The goal of this thesis work is to study the mechanical response of the reservoir assuming a high pressure variation from an initial pressure of 158 bar with a continuous production until the abandonment pressure of 63 bar is reached causing a high variation of effective stress inside the reservoir.

How is visible from Table 3.3 and Figure 3.10, the results obtained show as the strain level of the static configuration is greater than the dynamic at the end of production, but they have the same order of magnitude and they are mainly in the transitional zone of the decay curve.

STATIC				
timestep	SBHP [bar] average	increasing Δp [bar]	σ'zz [bar] average	εzz [-] average
01/01/2016	158,83	0,00	156,51	0,00E+00
01/01/2018	107,74	51,08	205,38	2,10E-03
01/01/2020	79,43	79,40	232,47	3,30E-03
01/01/2022	68,53	90,30	242,89	3,80E-03
01/01/2024	64,36	94,47	246,87	4,00E-03
01/05/2025	63,19	95,63	247,99	4,00E-03

DYNAMIC				
timestep	SBHP [bar] average	increasing Δp [bar]	σ'zz [bar] average	εzz [-] average
01/01/2016	158,83	0,00	156,51	0,00E+00
01/01/2018	107,74	51,08	205,39	5,00E-04
01/01/2020	79,43	79,40	232,48	8,00E-04
01/01/2022	68,53	90,30	242,9	9,00E-04
01/01/2024	64,36	94,47	246,89	1,00E-03
01/05/2025	63,19	95,63	248,01	1,00E-03

Table 3.3: Case 1: static and dynamic results obtained using a two-year timestep (values in the domain of large strain in red)

The Figure 3.11 shows the comparison of the previous results with those obtained by initializing the model with the stiffness decay curve 1. The results obtained are encouraging since the stiffness modulus is quite identical to the value of dynamic modulus at very small strains and increasing the stress level over time we observe, a decay of the E modulus up to the static value approximately. It must be noticed that, at the end of production, using the curve 1 the average strain level in the reservoir is almost equal to the static configuration, but unlike the latter the large strains domain is never reached. So from this comparison we can suppose that the final strain level reached using the curve 1 is more similar to the static case than the dynamic.

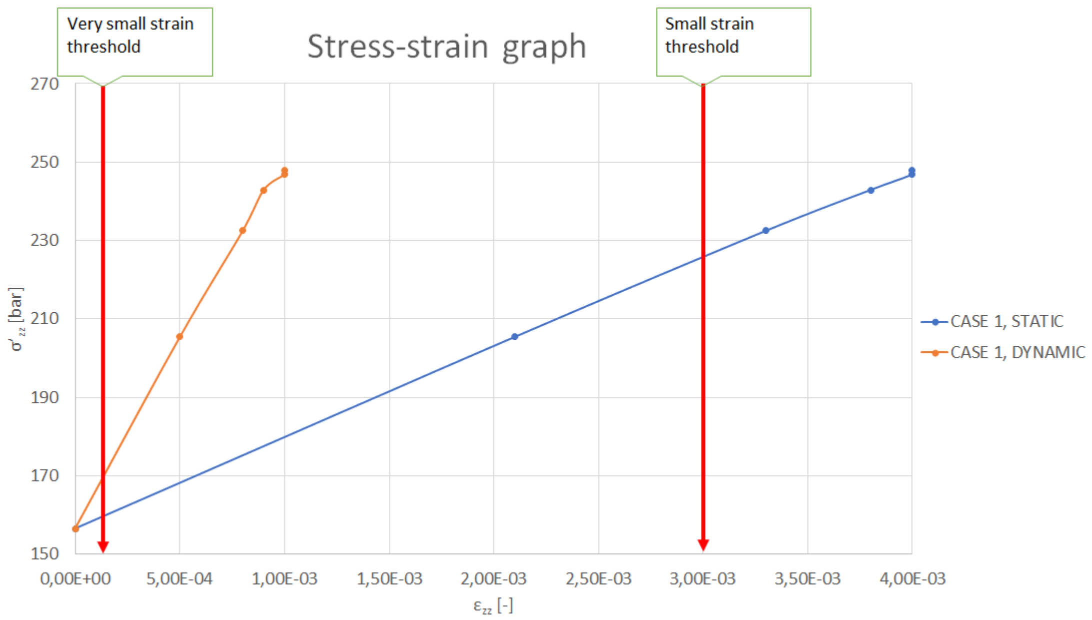

Figure 3.10: Case 1: average stress-strain graph of static and dynamic results obtained using a two-year timestep

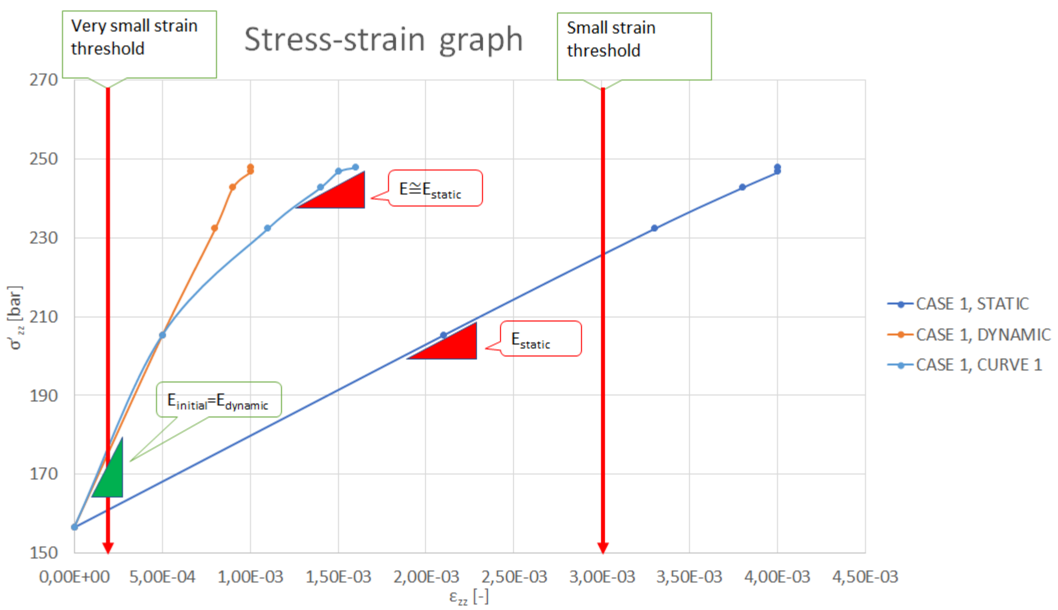

Figure 3.11: Case 1: average stress-strain graph of static, dynamic and curve 1 results calculated using a TWO-YEARS TIMESTEP

For the sake of completeness we report the evolution over time of the average effective stress inside the reservoir on the x-z plane of all three configurations to show that we are widely within the range of the admissible stress field in order to exclude failure phenomena, Figure 3.12. Moreover, in all the configurations there are no plastic strains.

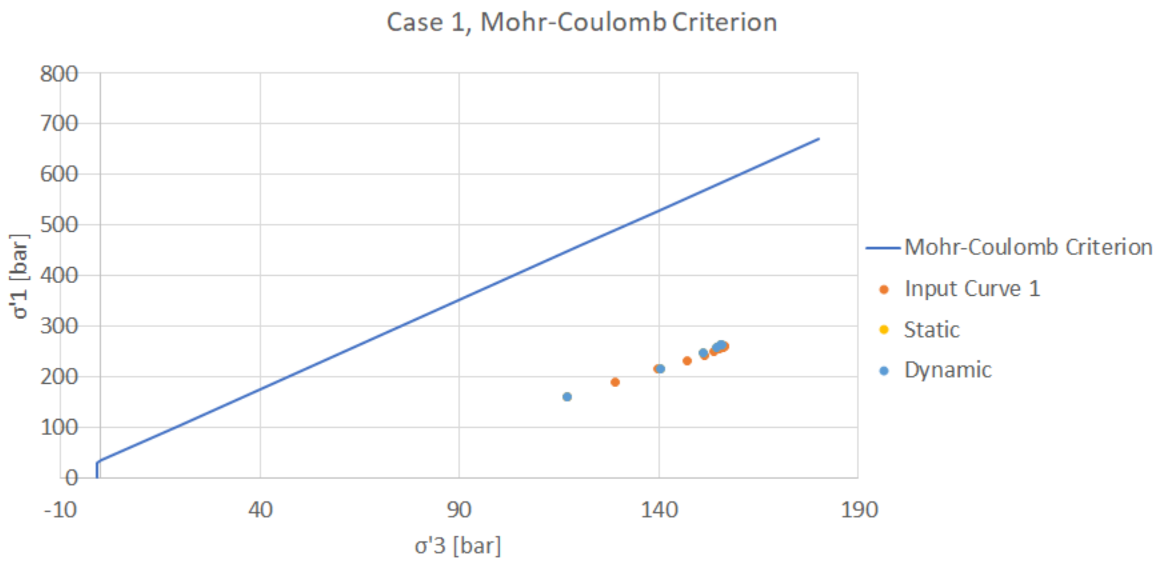

Figure 3.12: Case 1. Mohr-Coulomb Criterion

3.2.1.1 Sensitivity analysis on timesteps

Up to this point the results presented have been obtained using a two-year timestep. Now we want to understand if the choice of timestep influences the results by making a sensitivity analysis on this parameter.

The results of the static and dynamic cases are represented on the stress-strain graph by a straight line and therefore decreasing the timestep for these two cases would not lead to any additional information, but would get redundant information of the line drawn with a larger timestep. The same considerations can not be made for the case with a decay curve and therefore we have to made a study on the choice of timestep.

The Figure 3.13 shows that the results of the case with the decay curve obtained with different timesteps have generally similar trend or both have an initial stiffness modulus similar to the dynamic one and decreases increasing the stress level reaching almost the static value. In reality, the two-year timestep case overestimates the mechanical properties of the reservoir, especially in the first few years of production respect to the one-year timestep case, since the E modulus must decay immediately beyond the very small strain threshold.

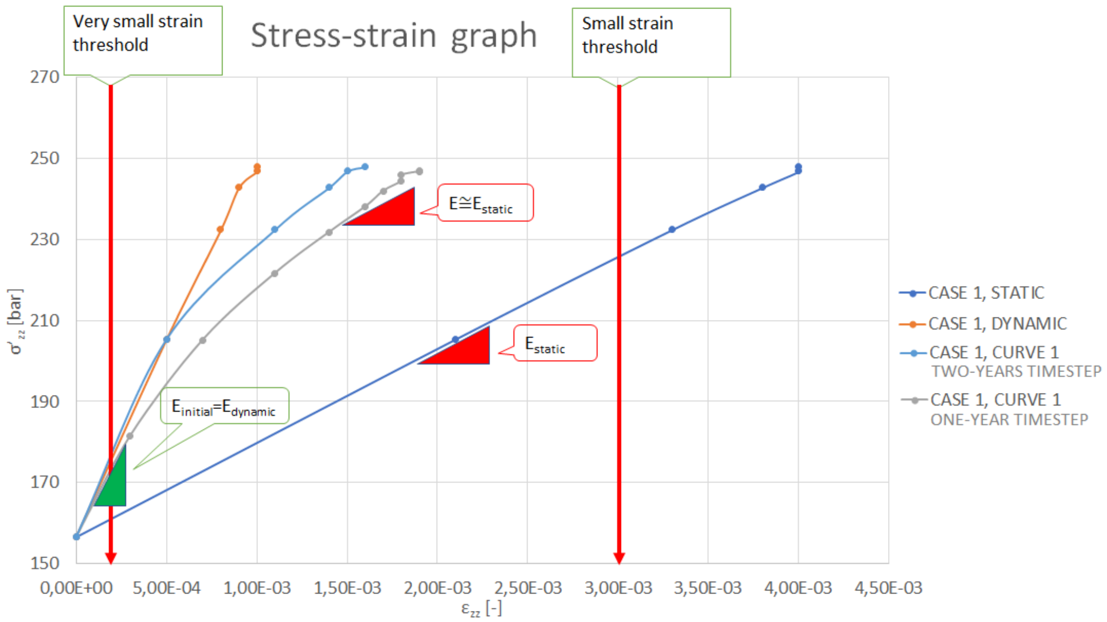

Figure 3.13: Case 1: average stress-strain graph of static, dynamic and curve 1 results calculated using a TWO-YEARS TIMESTEP and ONE-YEAR TIMESTEP

These results suggest that the analyzes performed using curve 1 with a one-year timestep are more reliable than those performed with a two-year timestep. As we have seen, decreasing the timestep for the case initialized with the curve means having more information about the non-linear trend of the results on the $\sigma'_{zz} - \varepsilon_{zz}$ graph.

3.2.1.2 Sensitivity analysis on number of sampled points of the curve

When the case is initialized with a E decay curve, which is described by a fixed number of value pairs of $\varepsilon_{zz} - E$ and not by a continuous law, the software, known the deformation, search within the same curve the respective value of the elastic modulus. When a precise pair of $\varepsilon_{zz} - E$ points is not associated with the known strain value, the value of the elastic modulus is approximated by the calculator. In order to reduce the approximation error of the elastic modulus, we increased the number of sampling points of the E decay curve creating two different variants of the curve 1 with 131 and 1503 pairs of points called curve 2 and curve 3 respectively.

We have observed that using input curve 2 and 3 for simulation is time consuming. The test with curve 2 gives results slightly lower than those obtained from the use of curve 1 as input and requires more time to complete the simulation. Instead, curve 3 did not allow to complete the simulation due to very long execution time. So we decided to carry out the following simulations using only the curve 1 as input and trying to do the sensitivity analysis using curve 2 and curve 3 directly as output. Or, from the ε_{zz} values obtained from the simulation the three different curves were used to recalculate the history of the respective associated values of E, as visible in Figure 3.14.

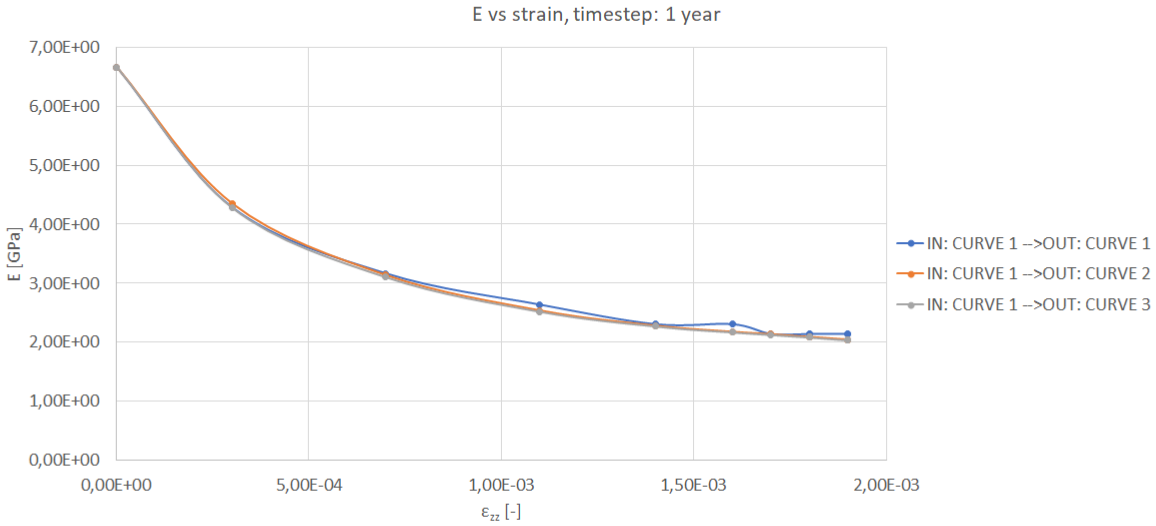

Figure 3.14: Case 1: E-axial strain graph using a one-year timestep, simulation run with Curve 1 in input and comparison between Curve 1, Curve 2, Curve 3 in output

From the $\varepsilon_{zz} - E$ graph obtained with a one-year timestep, it is clearly visible how the trends obtained using the input curve 1 and the output curve 2 and 3 are perfectly equal, while the trend deriving from the use of output curve 1 shows slight fluctuations after the early years of production. It should be kept in mind that in the field of small strains the E modulus must decrease continuously as axial deformation along z increases, but this does not happen in the configuration initialized with the input curve 1 and the output curve 1. Therefore, for this reason, one might think that the best solution to be used for the study of this synthetic case is to use curve 1 as input and curve 2 or curve 3 as output.

In reality, this comparison was also carried out in the same conditions with a two-year timestep. In this last case (Figure 3.15) the results obtained using curve 1 as input and curve 2 and 3 as output are again identical, while using the output curve 1 differ even more clearly than in the case studied with a one-year timestep overestimating the mechanical properties. Moreover, in the last time step we see again a smoothing of the stiffness modulus not only in the case of the curve 1 as output, but also using the curve 2 and 3 as output. This is in contrast with the theory and again suggests that the best solution to perform the analysis is to use the input curve 1 and the output curve 2 or 3 with a one-year timestep.

All of this confirms the fact that the timestep factor affecting the results.

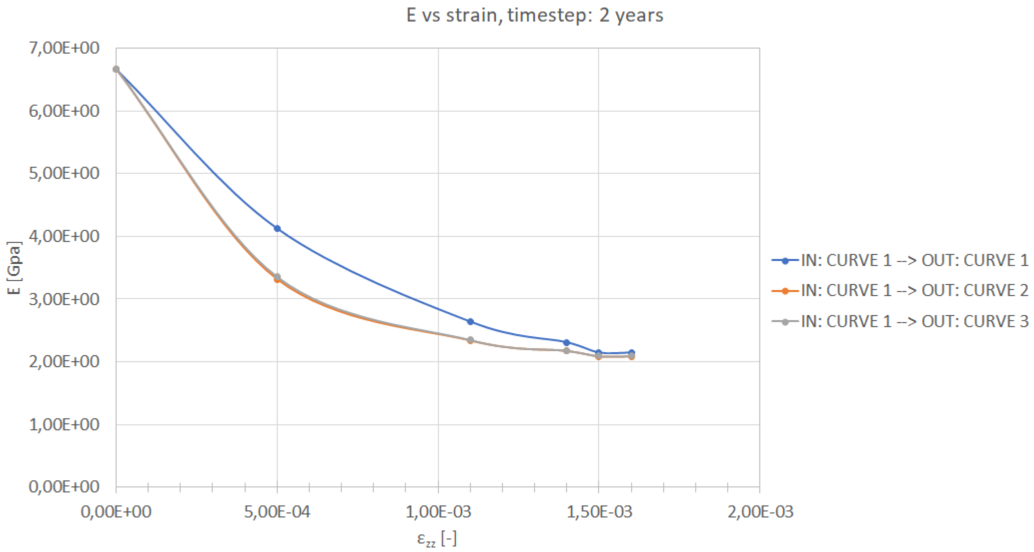

Figure 3.15: Case 1: E-axial strain graph using a two-year timestep, simulation run with Curve 1 in input and comparison between Curve 1, Curve 2, Curve 3 in output

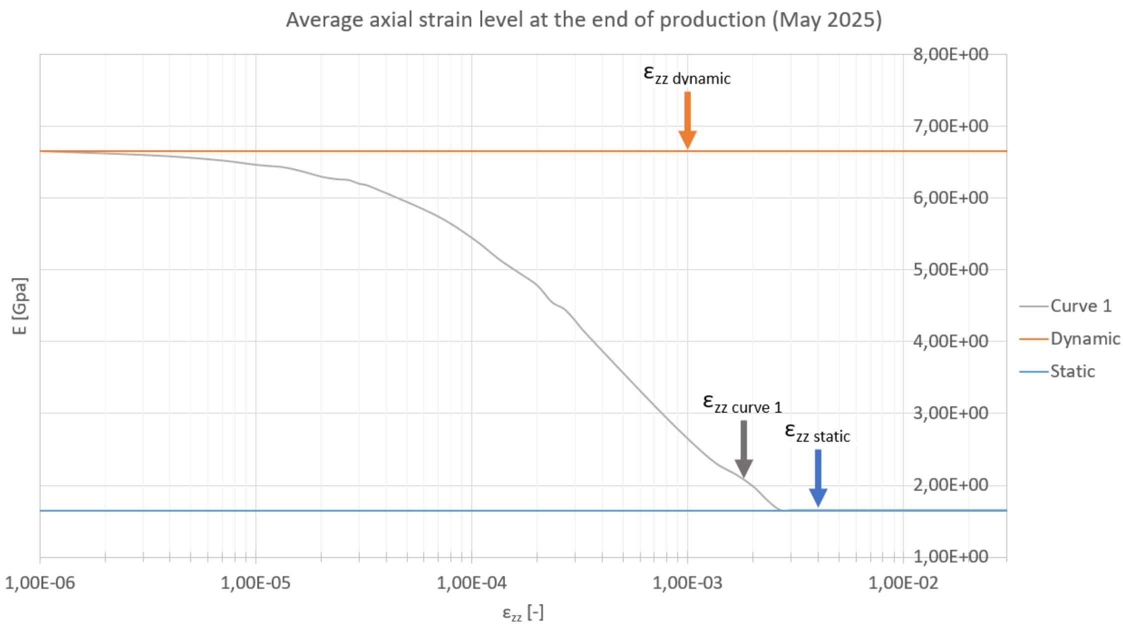

Figure 3.16: Case 1: E-strain graph of static, dynamic and curve 1 results. The arrows indicate respectively the average axial strain level of each model at the end of production

Concluding after all these considerations we assumed the definitive one-year timestep for the model with a E decay curve and two-years for the static and dynamic models and we compared the average deformation level in the reservoir at the end of production, as shown in Figure 3.16. In all three cases the mean deformation thresholds are of the same order of magnitude and are similar to the static configuration.

3.2.1.3 Displacements and induced subsidence

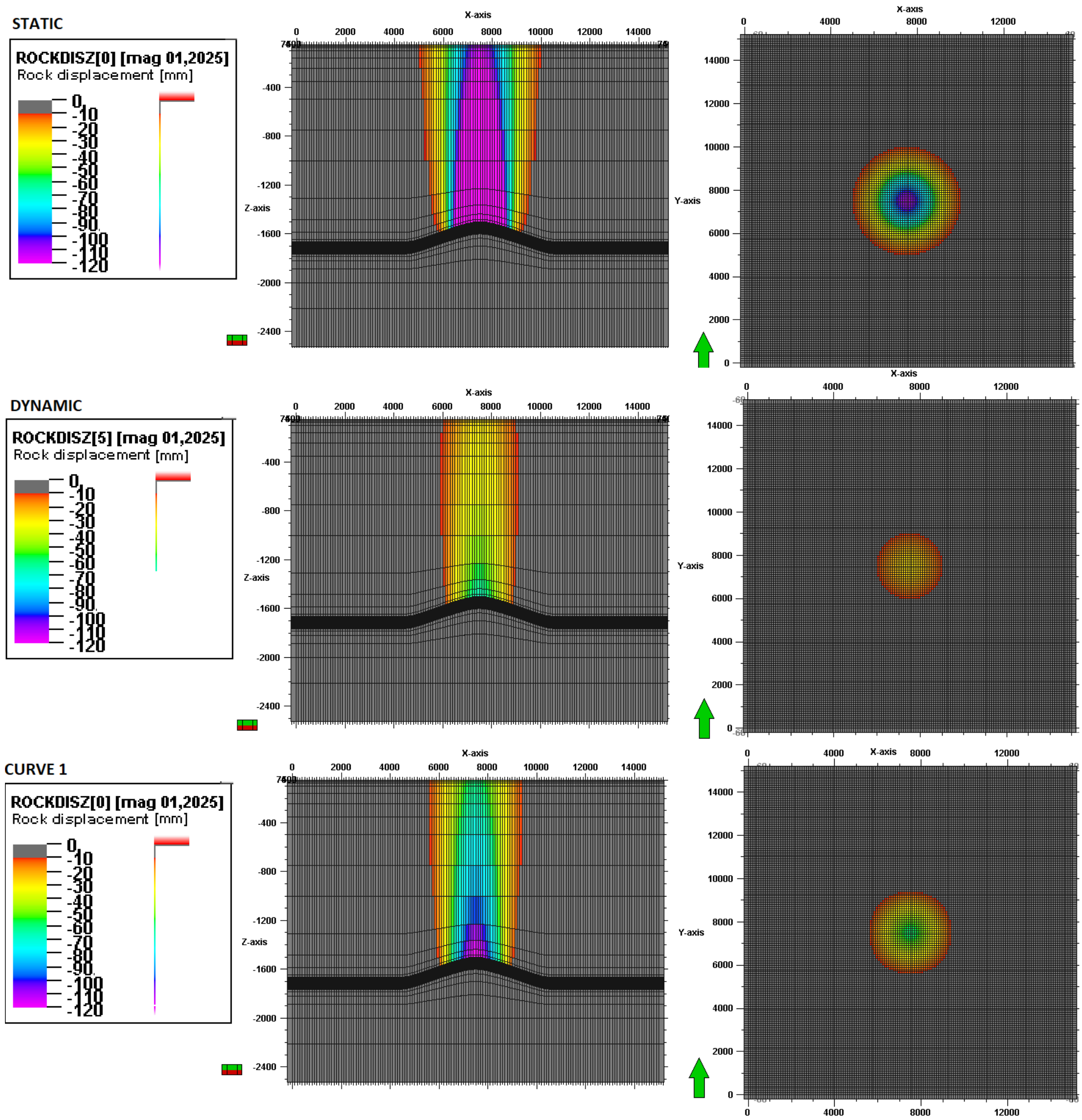

Figure 3.17: Case 1 if we consider an allowed vertical displacement less than 1 centimeter. South and top view, to the left and to the right respectively, of displacements along z-axis on a determined section of the model: static, dynamic and curve 1 cases

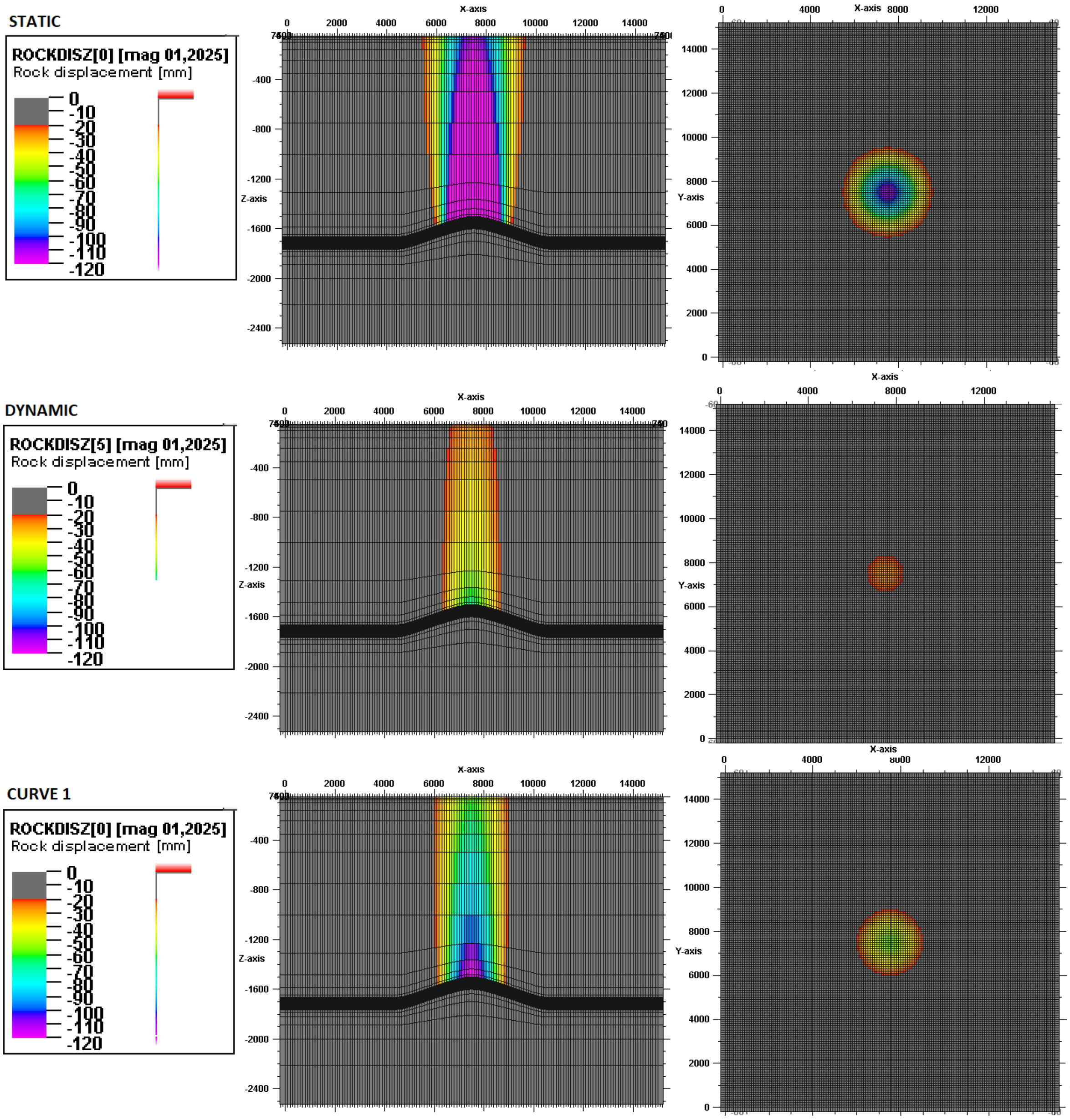

Figure 3.18: Case 1 if we consider an allowed vertical displacement less than 2 centimeter. South and top view, to the left and to the right respectively, of displacements along z-axis on a determined section of the model: static, dynamic and curve 1 cases

Observing the results obtained in Figure 3.17 and in Table 3.4, in all the analysed cases it is appreciable the development of a subsidence cone that extends from the reservoir, where the displacements are greater, up to the surface, where the displacements are less. However, the magnitude of the displacements and the extension of the subsidence cone are function of the elastic parameters assigned, or: the statically initialized model presents the absolute displacements greater compared to the other two configurations, while the dynamically initialized one has the lowest displacement values. In this way the induced subsidence is four times greater in the model statically initialized than the dynamic configuration and twice higher using the E decay curve. Horizontally the subsidence cone in the static configuration, as shown in Figure 3.17, is much more extensive than the other two configurations which have a radius of influence smaller than about 1 km from the static configuration value.

	CASE 1					
	TOP RESERVOIR, @1500 m TVD SSL		TOP SURFACE, @50 m TVD SSL			
	Max vertical displacement [cm]	Max horizontal displacement [cm]	Max vertical displacement [cm]	Max horizontal displacement [cm]	Radius with allowed subsidence [km]	
					1 cm	2 cm
Static	27	8	11	5	2,5	2,1
Dynamic	7	2	3	1	1,5	0,8
Curve 1	12	3	6	3	1,9	1,5

Table 3.4: Case 1. Overall displacements and areal extent of the subsidence cone expressend in terms of radius at the end of production (May 2025)

3.3 Shape Factor (SF) effect

Starting from case 1 as a reference case, we want to analyze how the shape of the reservoir changes the mechanical response of the model. To do this we maintain unchanged all the properties of the materials, the depth at which the deposit and stratigraphy is located, boundary conditions and reservoir pressure drop set for case 1 and we only modify the shape of the reservoir while maintaining constant the GOIP equal to $4.295x10^9 m^3_{sc}$.

CASE	OVERALL DIMENSIONS		SHAPE
1	SF = 0.05 (average)	H = 75 m R = 1.5 km	
2	SF = 0.01 (minimum)	H = 25 m R = 2.5 km	
3	SF = 0.1 (maximum)	H = 125 m R = 1.25 km	

Table 3.5: Overall dimension (H height and R radius) of reservoir in the tree different analyzed cases

We have thus created two more new cases with diametrically opposed reservoir shapes with respect to case 1. In case 2 we have a disk-shaped reservoir, so it is less thick and more extensive than case 1, whereas in case 3 the reservoir has a spherical shape and has a height greater than case 1, but a smaller extent. The different shapes of the analyzed reservoirs are visible in Table 3.5.

Since the pressure data are the same for all the analyzed cases, see Figure 3.19, it is possible to compare the results of the simulations at any point of the production history.

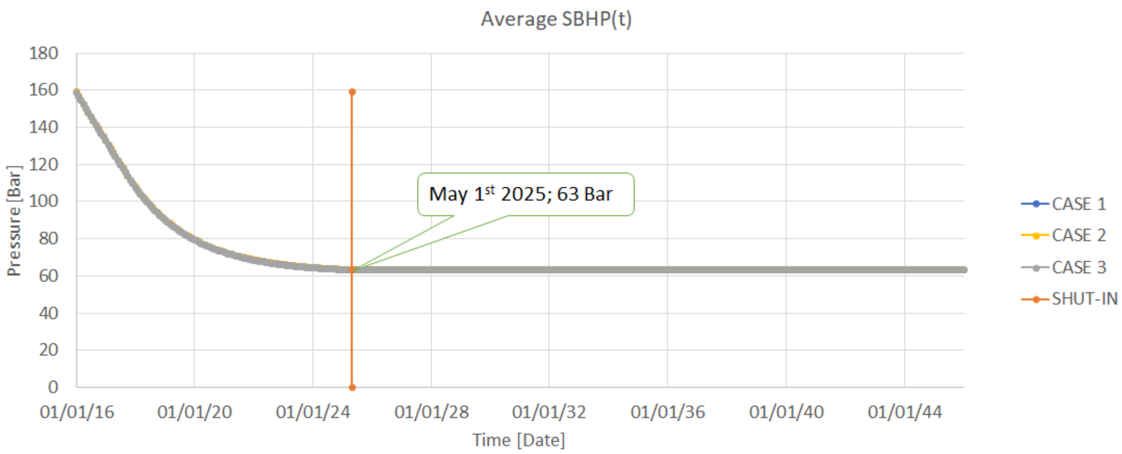

Figure 3.19: Average Static Bottom Hole Pressure as a function of time for all cases. Planned shut-in for all wells: May 1st 2025

Sensitivity analyses were performed on case 2 and case 3 considering all the possible input elastic parameters, i.e.: static values, dynamic values and decay curve. The results were critically compared in order to understand the influence of the shape factor on compaction and subsidence phenomena.

Figure3.20, show the comparison of the results obtained from the simulations made inputting the static and dynamic parameters in case 2 and in case 3: the shape factor does not affect in any way the deformation level. In fact, the stress-strain trends of all the dynamic configurations are the same except for the initial vertical effective stress. This discrepancy between the initial σ'_{zz} is due to the different distribution of effective stress on the reservoir influenced by the shape factor of it. In fact, in the disk-shaped reservoir there is a constant distribution of the effective stress over the entire field, while in the sphere and lens shape there is an increase of effective stress at the boundary of the reservoir due to the increase in depth of the reservoir moving away from the center, increasing the average value of the initial vertical effective stress for case 1 and case 3. The same considerations apply to the trends of all static configurations.

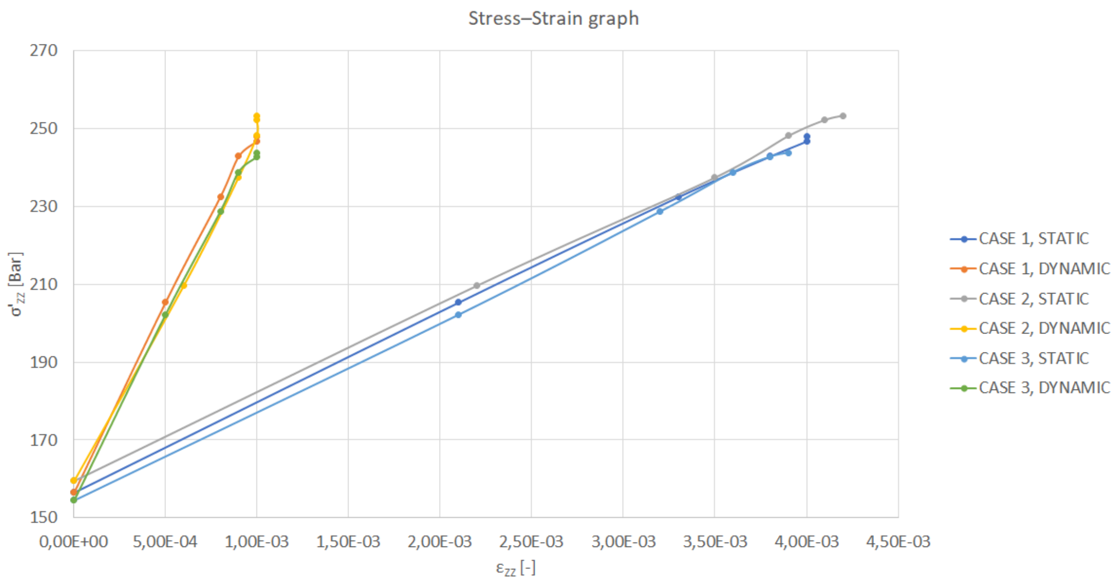

Figure 3.20: Average Stress-Strain graph of all static and dynamic cases

The comparison was made between the results obtained using the best configuration with input curve 1 and the curve 2 (or curve 3) as output with a one-year timestep. From Figure 3.21, the results show how in all cases there is a progressive decrease of the E modulus as the strain level increases and they have the same trend in all three cases. Again we note how the shape factor does not affect the strain level. From Table 3.6, the results show how in each case the average volumetric strain is always equal to the mean vertical axial strain since the mean horizontal strain is always equal to zero in the reservoir. However, in case 2 the compaction phenomena is exclusively linked to vertical axial deformation in the reservoir and it differs from case 1 and 3. In fact, only in case 2 the horizontal strain evaluated both on average and punctually (see maximum horizontal strain column in Table) is always equal to zero.

Moreover, in all cases and configurations there are no plastic strains.

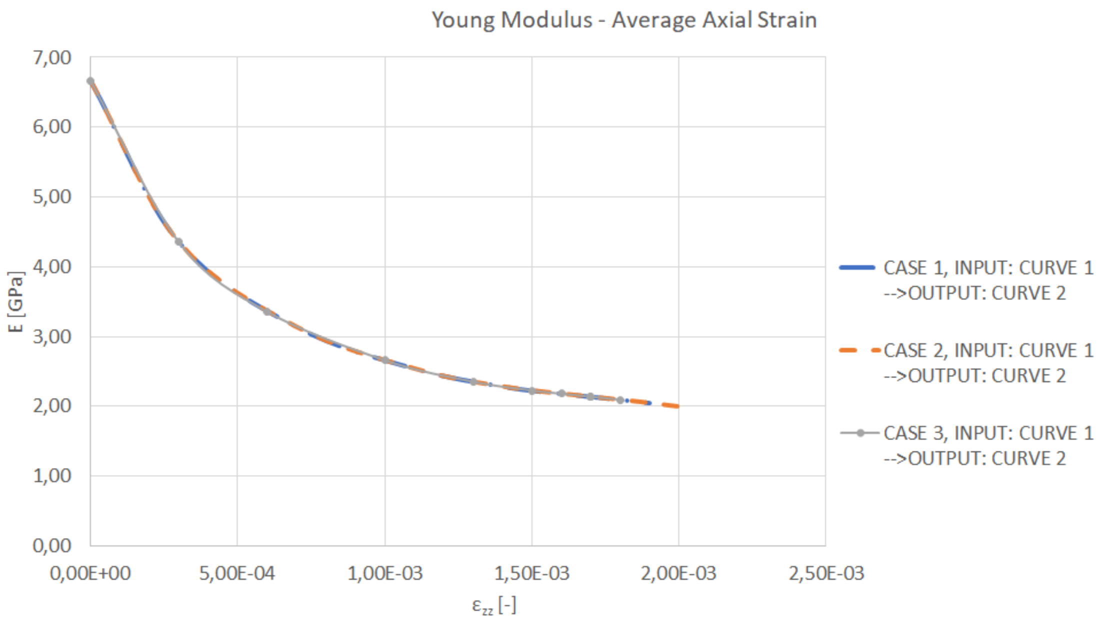

Figure 3.21: Young Modulus - Average Axial Strain for all cases obtained using curve 1 as input and curve 2 as output

CASE 1, INPUT: CURVE 1 -->OUTPUT: CURVE 2								
timestep	εzz [-]		εxx [-]		εv [-]		E (CURVE 2) [Gpa]	
	max	average	max	average	max	average	max	average
01/01/2016	0	0	0	0	0	0	6,66E+09	6,66E+09
01/01/2017	0,0003	0,0003	0	0	0,0003	0,0003	4,35E+09	4,35E+09
01/01/2018	0,0008	0,0007	0	0	0,0008	0,0007	2,95E+09	3,14E+09
01/01/2019	0,0012	0,0011	0	0	0,0012	0,0011	2,44E+09	2,54E+09
01/01/2020	0,0016	0,0014	0	0	0,0016	0,0014	2,18E+09	2,28E+09
01/01/2021	0,0018	0,0016	0,0001	0	0,002	0,0016	2,09E+09	2,18E+09
01/01/2022	0,0019	0,0017	0,0001	0	0,0021	0,0017	2,04E+09	2,13E+09
01/01/2023	0,0021	0,0018	0,0001	0	0,0023	0,0018	1,93E+09	2,09E+09
01/01/2024	0,0021	0,0018	0,0001	0	0,0023	0,0018	1,93E+09	2,09E+09
01/01/2025	0,0022	0,0019	0,0001	0	0,0024	0,0019	1,87E+09	2,04E+09
01/05/2025	0,0022	0,0019	0,0001	0	0,0024	0,0019	1,87E+09	2,04E+09

CASE 2, INPUT: CURVE 1 -->OUTPUT: CURVE 2								
timestep	εzz [-]		εxx [-]		εv [-]		E (CURVE 2) [Gpa]	
	max	average	max	average	max	average	max	average
01/01/2016	0	0	0	0	0	0	6,66E+09	6,66E+09
01/01/2017	0,0004	0,0003	0	0	0,0004	0,0003	3,95E+09	4,35E+09
01/01/2018	0,0008	0,0007	0	0	0,0008	0,0007	2,95E+09	3,14E+09
01/01/2019	0,0012	0,0011	0	0	0,0012	0,0011	2,44E+09	2,54E+09
01/01/2020	0,0016	0,0014	0	0	0,0016	0,0014	2,18E+09	2,28E+09
01/01/2021	0,0018	0,0017	0	0	0,0018	0,0017	2,09E+09	2,13E+09
01/01/2022	0,002	0,0018	0	0	0,002	0,0018	1,99E+09	2,09E+09
01/01/2023	0,0021	0,0019	0	0	0,0021	0,0019	1,93E+09	2,04E+09
01/01/2024	0,0021	0,0019	0	0	0,0021	0,0019	1,93E+09	2,04E+09
01/01/2025	0,0022	0,002	0	0	0,0022	0,002	1,87E+09	1,99E+09
01/05/2025	0,0022	0,002	0	0	0,0022	0,002	1,87E+09	1,99E+09

CASE 3, INPUT: CURVE 1 -->OUTPUT: CURVE 2								
timestep	εzz [-]		εxx [-]		εv [-]		E (CURVE 2) [Gpa]	
	max	average	max	average	max	average	max	average
01/01/2016	0	0	0	0	0	0	6,66E+09	6,66E+09
01/01/2017	0,0003	0,0003	0	0	0,0003	0,0003	4,35E+09	4,35E+09
01/01/2018	0,0008	0,0006	0	0	0,0008	0,0006	2,95E+09	3,36E+09
01/01/2019	0,0012	0,001	0,0001	0	0,0014	0,001	2,44E+09	2,66E+09
01/01/2020	0,0016	0,0013	0,0001	0	0,0018	0,0013	2,18E+09	2,35E+09
01/01/2021	0,0018	0,0015	0,0001	0	0,002	0,0015	2,09E+09	2,22E+09
01/01/2022	0,002	0,0016	0,0001	0	0,0022	0,0016	1,99E+09	2,18E+09
01/01/2023	0,0021	0,0017	0,0001	0	0,0023	0,0017	1,93E+09	2,13E+09
01/01/2024	0,0021	0,0017	0,0001	0	0,0023	0,0017	1,93E+09	2,13E+09
01/01/2025	0,0021	0,0017	0,0001	0	0,0023	0,0017	1,93E+09	2,13E+09
01/05/2025	0,0022	0,0018	0,0001	0	0,0024	0,0018	1,87E+09	2,09E+09

Table 3.6: Comparison between different kind of strains for all cases using input curve 1 and output curve 2

Let's now analyze the influence of the shape factor in the three cases in terms of displacements. From Table 3.7 and Table 3.4, is evident how the shape factor affects the amplitude of displacements and the relative induced subsidence in all cases and configurations. At low shape factors correspond low displacement and low induced subsidence values at the end of production and vice versa, Figure 3.26. In fact, there is a certain proportionality between the various configurations in all cases regardless of the shape factor. For any type of displacement the ratios between the configurations of the same case are constant and approximately equal to 2, or the ratio between the displacement in static configuration and that in configuration with curve is about two. The same proportionality is maintained between the curve configuration and the dynamic one.

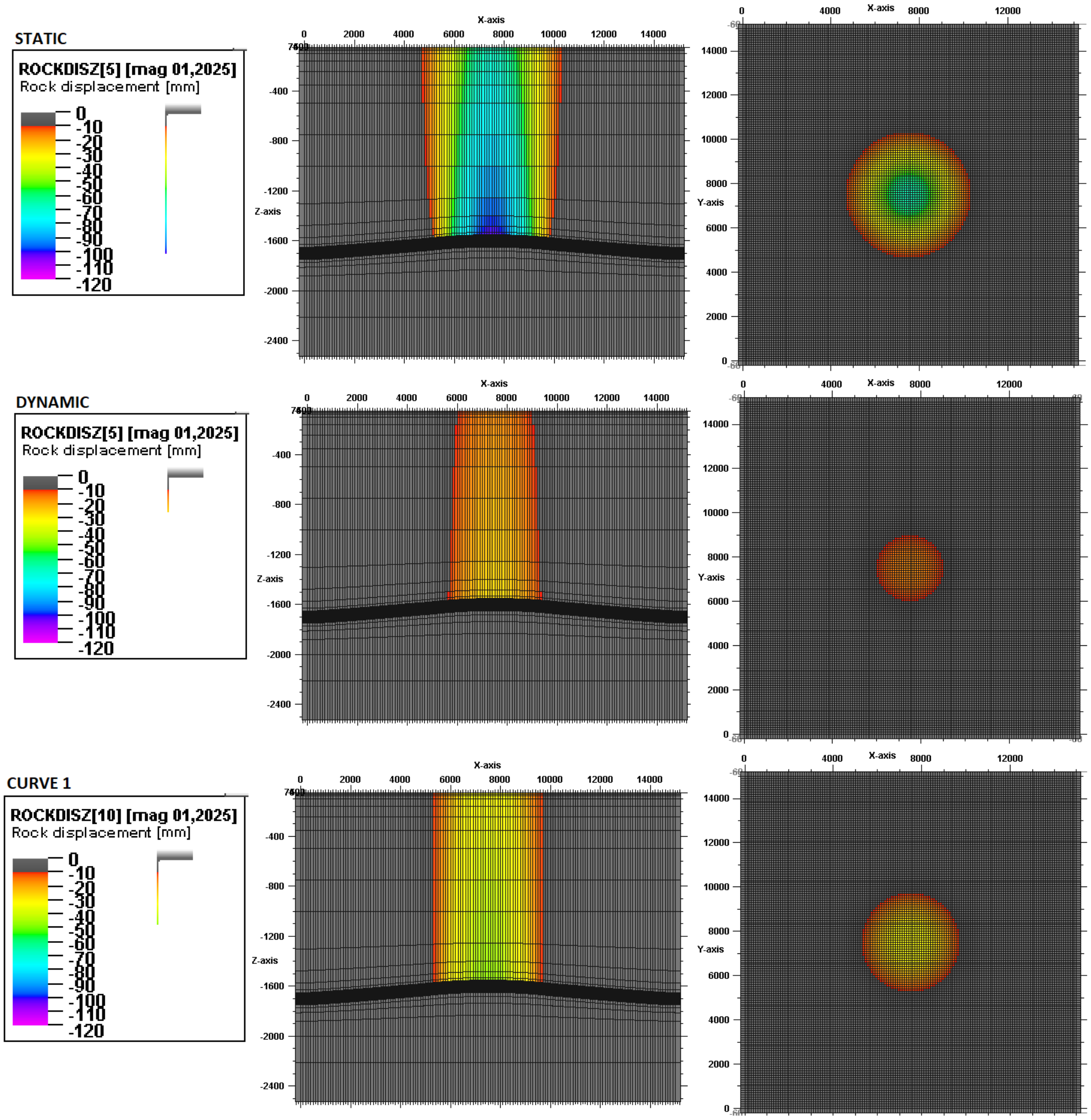

Figure 3.22: Case 2 if we consider an allowed vertical displacement less than 1 centimeter. South and top view, to the left and to the right respectively, of displacements along z-axis on a determined section of the model: static, dynamic and curve 1 cases

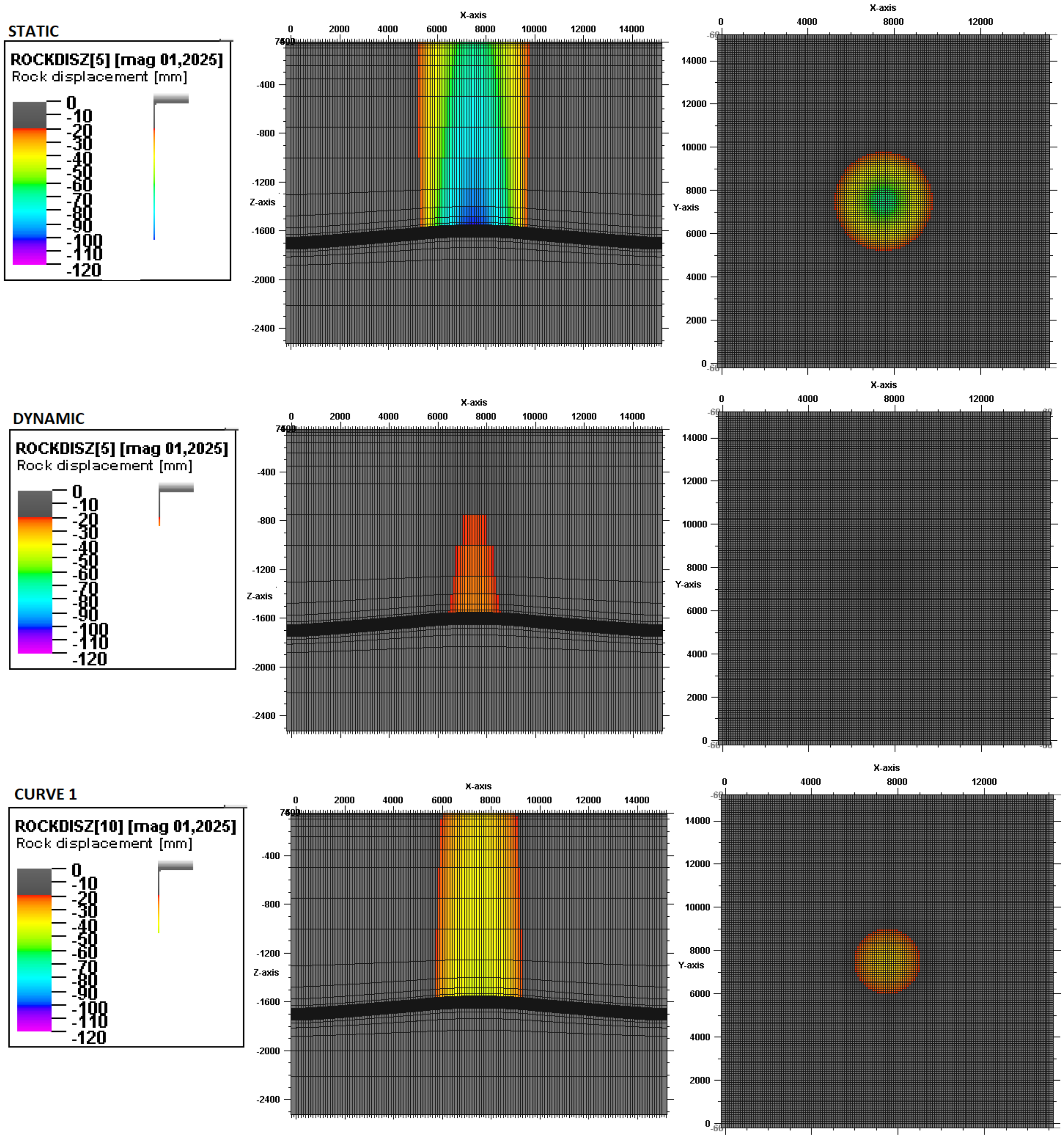

Figure 3.23: Case 2 if we consider an allowed vertical displacement less than 2 centimeter. South and top view, to the left and to the right respectively, of displacements along z-axis on a determined section of the model: static, dynamic and curve 1 cases

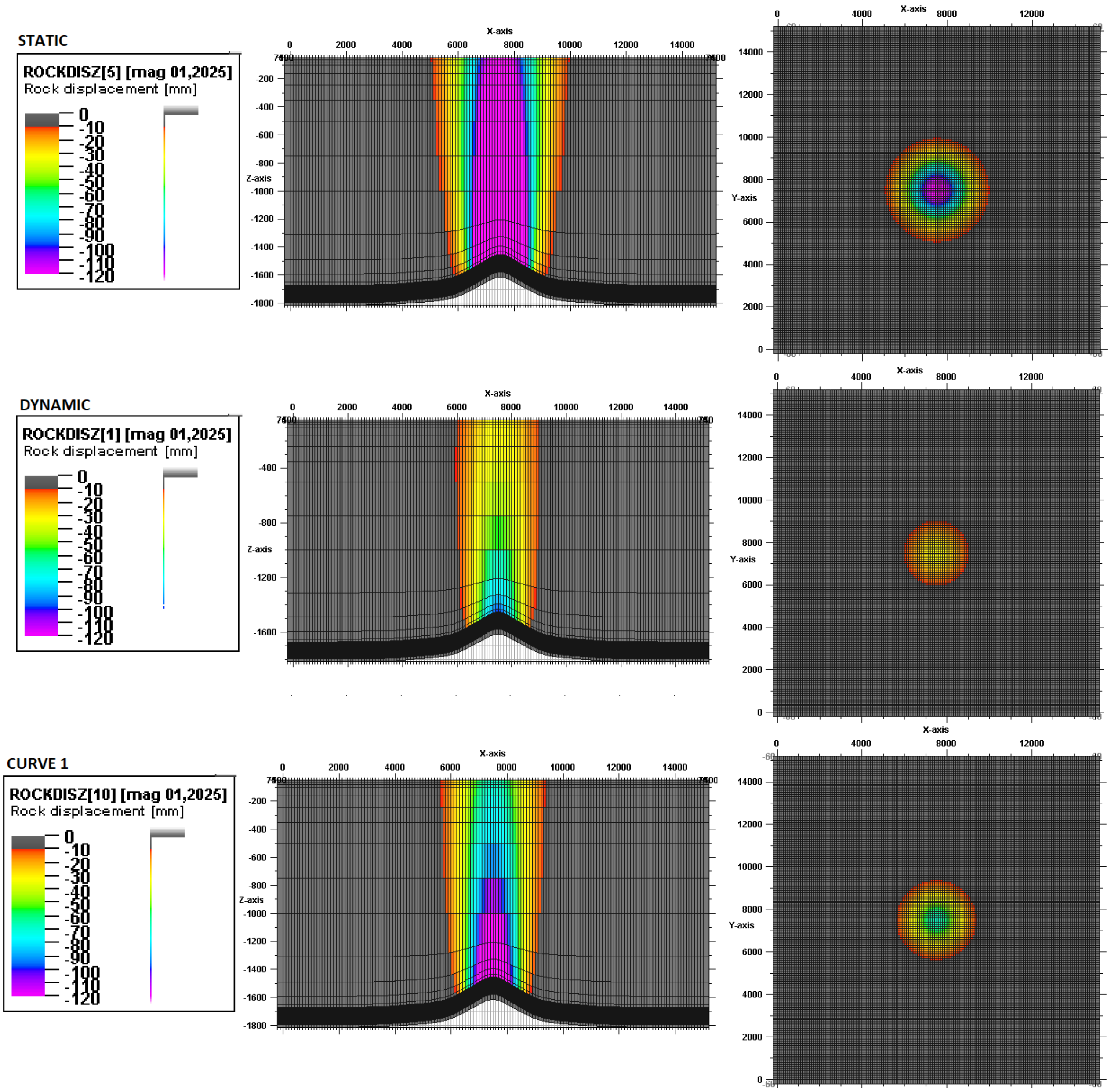

Figure 3.24: Case 3 if we consider an allowed vertical displacement less than 1 centimeter. South and top view, to the left and to the right respectively, of displacements along z-axis on a determined section of the model: static, dynamic and curve 1 cases

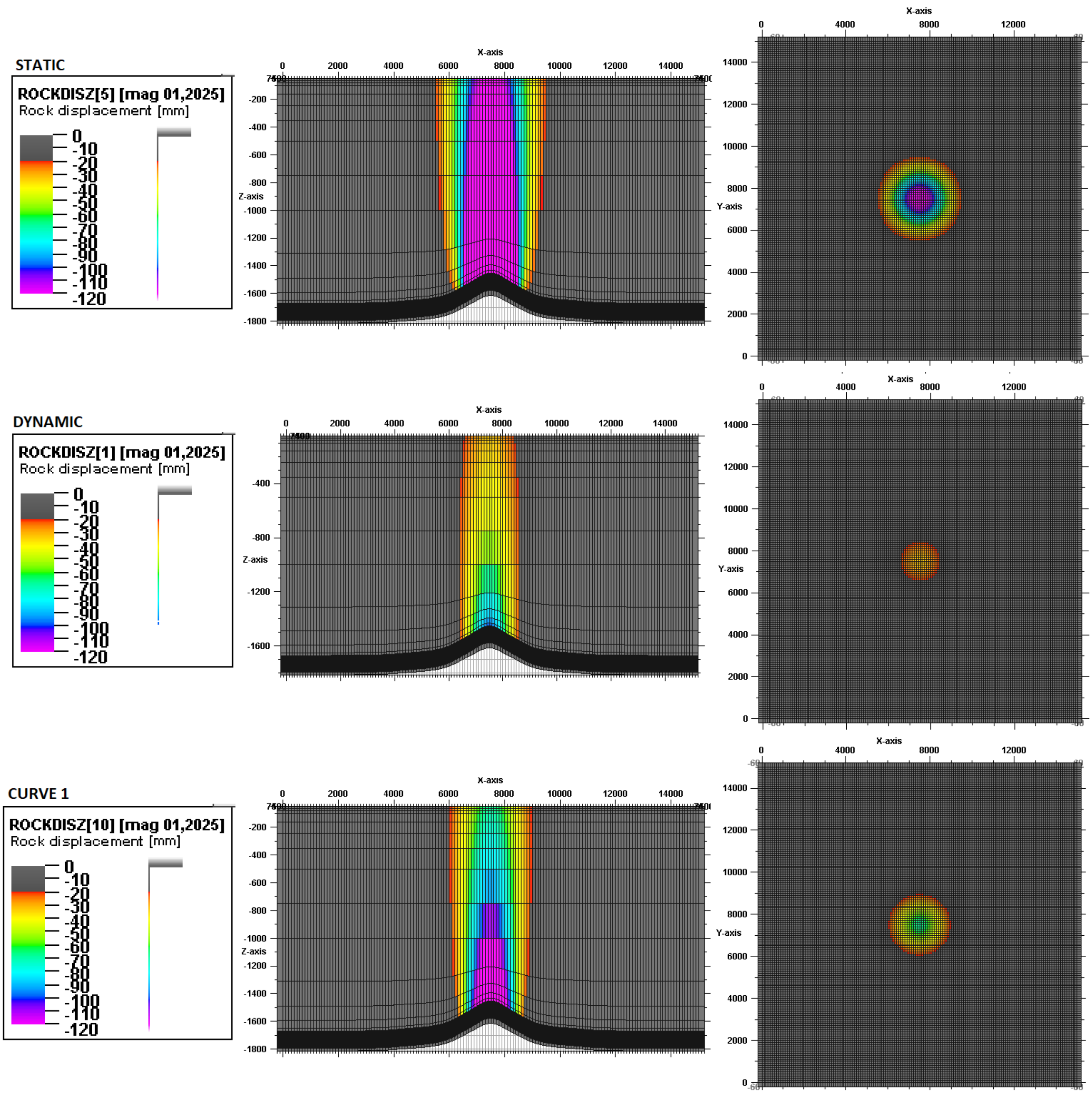

Figure 3.25: Case 3 if we consider an allowed vertical displacement less than 2 centimeter. South and top view, to the left and to the right respectively, of displacements along z-axis on a determined section of the model: static, dynamic and curve 1 cases

	CASE 2					
	TOP RESERVOIR, @1500 m TVD SSL		TOP SURFACE, @50 m TVD SSL			
	Max vertical displacement [cm]	Max horizontal displacement [cm]	Max vertical displacement [cm]	Max horizontal displacement [cm]	Radius with allowed subsidence [km]	
					1 cm	2 cm
Static	10	3	7	3	2,8	2,3
Dynamic	3	1	2	1	1,5	-
Curve 1	5	2	3	2	2,2	1,5

	CASE 3					
	TOP RESERVOIR, @1500 m TVD SSL		TOP SURFACE, @50 m TVD SSL			
	Max vertical displacement [cm]	Max horizontal displacement [cm]	Max vertical displacement [cm]	Max horizontal displacement [cm]	Radius with allowed subsidence [km]	
					1 cm	2 cm
Static	40	12	13	6	2,5	2,0
Dynamic	10	3	3	2	1,6	1,1
Curve 1	17	3	7	3	1,9	1,5

Table 3.7: Case 2 and 3. Overall displacements and areal extent of the subsidence cone expressend in terms of radius at the end of production (May 2025)

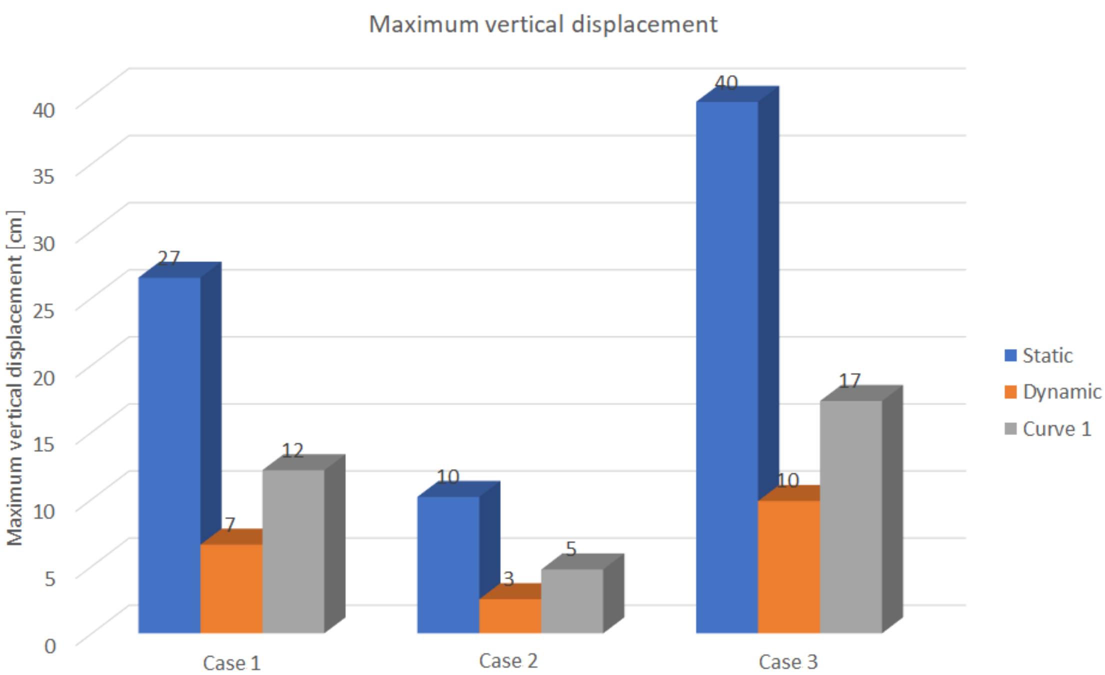

Figure 3.26: Maximum vertical displacements @top of reservoir of all cases in all configurations at the end of production (May 2025)

In conclusion we noticed that the shape factor:

- does not affect on strain magnitudo in all cases and configurations;

- affects on the amplitude of any kind of displacements both in reservoir and at surface in all cases and configurations: greater the shape factor value, greater the displacements.

Chapter 4

Conclusions

This thesis work focus on studying the evolution of the mechanical response over time of a reservoir clastic gas bearing formation present in the Adriatic Basin as a function of the assigned stiffness modulus and assessing the consequent impact on compaction and subsidence phenomena during primary production. In particular, different scenarios were simulated and analysed using a FEM 3 D numerical approach, considering basically static pseudo elastic parameters, dynamic pseudo elastic parameters and a transition curve between them.

In order to fully understand the mechanical behavior of soils one should take into account their discrete nature, but in numerical and analytical models they are treated according to the laws of continuous mechanics.

After a brief theoretical description of the ILE models we studied some factors that influence the elastic parameters. Among these the strain amplitude plays an important role. The entire field of strains can be subdivided into three sub-domains within which the material has three different mechanical responses. In this way we defined dynamic and static elastic modulus and its decay curve.

After a brief discussion of some laboratory and in situ tests to measure the static and dynamic moduli, in the absence of real data, in order to assign the mechanical properties to our synthetic model we used the empirical Teatini's formula which is valid for the whole Adriatic Basin and derives from in situ tests made through the use of radioactive markers. Radioactive markers allow to investigate the entire strain domain, but overestimate the stiffness modulus if the material is not saturated, like gas reservoirs, due to the presence of capillary forces.

We created the numerical model of a synthetic case study, called case 1, which represents a lens shaped gas reservoir at 1500 meters deep in hydrostatic condition in the Northern Adriatic Basin, where mainly there is a stratigraphic succession of sands and clays, through the use of a mechanical simulation software within the Petrel E&P software platform (Schlumberger). The model was adopted to analyse the effects in terms of compaction and subsidence phenomena of different factors, among with the effect of elastic modulus parameters. Three different mechanical configurations were simulated:

- static configurations with E modulus in the first loading cycle equal to 1.67 GPa (from Teatini's formula);
- dynamic configuration with E modulus in the first loading cycle equal to 6.66 GPa, or four time the static one, Figure 2.18;
- dynamic initial configuration with additional information about the decay of the stiffness modulus inside the reservoir. This E decay curve, curve 1, was constructed from a normalized curve of the same material present in literature, adapting it to the depth / pressure of our case study.

We analysed the base case, or case 1, with a two-year timestep and we observed that in all the configurations there are no plastic strains and that:

- using the static configuration a greater mean deformation level in reservoir is reached than the other two configurations and it is the only one that is beyond the small strain threshold;
- using the dynamic configuration the mean deformation level in reservoir is lower than the other two configurations;
- using the configuration with curve 1 the mechanical response of the reservoir is similar to the dynamic one in the first years of production, i.e. in the field of small strains when the stress is small, and similar to the static at the end of production, but it never reaches the static value and it does not exceed the small strain threshold.

For this reason we made a sensitivity analysis on the timestep and we observed that:

- the results of the static and dynamic cases are represented on the stress-strain graph by a straight line and therefore decreasing the timestep for these two cases would not lead to any additional information, but would get redundant information of the line drawn with a larger timestep;
- the results related to the configuration with curve 1 and one-year timestep show a decay of the E modulus on the stress-strain graph immediately after the very small strain threshold, confirming the theory.

We made a sensitivity analysis on the number of sampling points of the curve. When the case is initialized with a E decay curve the software, known the deformation, search within the same curve the respective value of the elastic modulus. When a precise pair of $\varepsilon_{zz} - E$ points is not associated with the known strain value, the value of the elastic modulus is approximated by the calculator. In order to reduce the approximation error of the elastic modulus, we increased the number of sampling points of the E decay curve creating two different variants of the curve 1 with 131 and 1503 pairs of points called curve 2 and curve 3 respectively. We observed that using more sensitive curves such as input curve 2 and 3 the simulation time just increases, but using them to convert the strain output in terms of Young modulus calculated by the simulator and adopted during simulation lead to more accurate results. So the best solution is to use input curve 1 and output curve 2 or 3 with a one-year timestep.

Finally, we have analysed the effect of input deformation parameters (static, dynamic and decay curve) on the entity of displacements both in the reservoir and on the surface and we noticed that they depend on the chosen configuration, i.e. they are maximum in the static configuration, average values in the configuration with curve and minimum in the dynamic one.

The last sensitivity analysis was the influence of the reservoir shape factor. We changed the shape of the reservoir by creating a disk-shaped and sphere-shaped reservoir, case 2 and case 3 respectively. For each of these two new case, stress-strain analyses were performed considering: static input parameters, dynamic input parameters and the decay curve. In all cases and configurations there are no plastic strains and we deduced that the shape factor:

- does not affect on deformations in all cases and configurations;
- affects on the amplitude of any kind of displacements both in reservoir and at surface in all cases and configurations: greater the shape factor value, greater the displacements. For this reason the worst case is case 3 in static configuration.

In this thesis work we have seen how timestep, number of sampling points of the decay curve and shape factor affect the mechanical response of the reservoir, but further sensitivity analysis can be done on:

- GOIP;
- reservoir depth because the mechanical properties vary according to the depth as well as the initial pressure in the reservoir and the maximum variation of pressure which can be impressed.

References

[1] D. Baú, M. Ferronato, G. Gambolati, and P. Teatini. Basin-scale compressibility of the Northern Adriatic by the radioactive marker technique. *Geotechique*, 52(8):605–616, 2002.

[2] G. Bava. Meccanica delle rocce. University Lecture, 2012.

[3] C. Benetatos, G. Codegone, G. Giani, V. Rocca, and F. Verga. Approccio integrato per l'analisi della subsidenza indotta dalla coltivazione dei giacimenti di idrocarburi. Techreport, Politecnico di Torino, C.so Duca degli Abruzzi 24, 10129, Torino.

[4] F. Bertello, R. Fantoni, and R. Franciosi. Overview on Italy's petroleum systems and related oil and gas occurrences. 2008.

[5] F. Cazzini, O. Dal Zotto, R. Fantoni, M. Ghielmi, P. Ronchi, and P. Scotti. Oil and gas in the Adriatic Foreland, Italy. *Journal of Petroleum Geology*, 38(3):255–279, 2015.

[6] L.I. Gonzalez de Vallejo, M. Ferrer, L. Ortuno, and C. Oteo. *Geoingegneria*. Pearson Education Italia S.r.l., 2005.

[7] C. Deangeli. Reservoir Geomechanics. University Lecture, 2016.

[8] M. Ferronato, G. Gambolati, and P. Teatini. Unloading-reloading uniaxial compressibility of deep reservoirs by marker measurements. *11th FIG Symposium on Deformation Measurements, Santorini, Greece*, 2003.

[9] M. Ferronato, G. Gambolati, P. Teatini, and D. Baú. Radioactive Marker Measurements in Heterogeneous Reservoirs: Numerical Study. *Geomechanics*, 4(2), 2004.

[10] S. Foti. Comportamento dinamico dei terreni e prove di laboratorio. University Lecture, 2015.

[11] J. M. Head and F. M. Jardine. *Ground-Borne Vibrations Arising from Piling*, volume 142. 1992.

[12] R. J. Jardine, D. M. Potts, A. B. Fourie, and J. B. Burland. Studies of the influence of non-linear stress-strain characteristics in soil-structure interaction. *Geotechnique*, 36 (3):377–396, 1986.

[13] R.J. Jardine. Some observation on the kinematic nature of soil stiffness. *Soils and Fundations*, 32(2):111–124, June 1992.

[14] R.J. Jardine, M.J. Symes, and J.B. Burland. The measurement of soil stiffness in the triaxial apparatus. *Geotechnique*, 34(3):323–340, January 1984.

[15] M.E. Jones, M.J. Leddra, and A.S. Goldsmith. *The Geomechanical characteristics of reservoir and reservoir rocks*. Health and Safety Executive, 1992.

[16] T.W. Lambe and R.V. Whitman. *Meccanica dei terreni*. Dario Flaccovio editore S.r.l., London, 1997.

[17] R. Lancellotta. *Geotecnica*. Zanichelli editore S.p.A., New York, 2012.

[18] S. Likitlersuang, S. Teachavorasinskun, C. Surarak, E. Oh, and A. Balasubramaniam. Small strain stiffness and stiffness degradation curve of Bangkok Clays. *Soils and Foundations*, pages 498–509, 2013. Birkhäuser Verlag.

[19] P. Macini, E. Mesini, V.A. Salomoni, and B.A. Schrefler. Casing influence while measuring in situ reservoir compaction. *Petroleum Science and Engineering*, 50:40–54, 2006.

[20] A. Menin, V. A. Salomoni, R. Santagiuliana, L. Simoni, A. Gens, and B. A. Schrefler. A mechanism contributing to subsidence above gas reservoirs and its application to a case study. *International Journal for Computational Methods in Engineering Science and Mechanics*, 9(5):270–287, 2008.

[21] N. Nagel. Compaction and subsidence issues within the petroleum industry: From Wilmington to Ekofisk and beyond. *Physics and Chemistry of the Earth, Part A Solid Earth and Geodesy*, 26(1):3–14, 2001.

[22] T.J. Plona and J.M. Cook. Effects of stress cycles on static and dynamic Young's moduli in Castlegate sandstone. *Rock Mechanics*, 1995.

[23] P. Teatini, N. Castelletto, M. Ferronato, G. Gambolati, C. Janna, E. Cairo, D. Marzorati, D. Colombo, A. Ferretti, A. Bagliani, and F. Bottazzi. Geomechanical response to seasonal gas storage in depleted reservoirs: A case study in the Po River basin, Italy. *Geophysical Research*, 116, 2011.

[24] F. Verga. Reservoir Engineering. University lecture, 2016.

[25] F. Wang, X. Li, G. Couples, J. Shi, J. Zhang, Y. Tepinhi, and L.Wu. Stress arching effect on stress sensitivity of permeability and gas well production in Sulige gas field. *Journal of Petroleum Science and Engineering*, 125:234–246, 2015.

[26] N. Yagi and Y. Ishii. On the relationship of the mechanical properites of soils and rocks to the velocity of elastic waves. *Disaster Prevention Research Institute, Kyoto University*, 18(147), 1969.

Appendix

Examples of P-wave velocities

Material	V_P (m/s)
Air	330
Water	1450–1530
Petroleum	1300–1400
Loess	300–600
Soil	100–500
Snow	350–3000
Solid glacier ice*	3000–4000
Sand (loose)	200–2000
Sand (dry, loose)	200–1000
Sand (water saturated, loose)	1500–2000
Glacial moraine	1500–2700
Sand and gravel (near surface)	400–2300
Sand and gravel (at 2 km depth)	3000–3500
Clay	1000–2500
Estuarine muds/clay	300–1800
Floodplain alluvium	1800–2200
Permafrost (Quaternary sediments)	1500–4900
Sandstone	1400–4500
Limestone (soft)	1700–4200
Limestone (hard)	2800–7000
Dolomites	2500–6500
Anhydrite	3500–5500
Rock salt	4000–5500
Gypsum	2000–3500
Shales	2000–4100
Granites	4600–6200
Basalts	5500–6500
Gabbro	6400–7000
Peridotite	7800–8400
Serpentinite	5500–6500
Gneiss	3500–7600
Marbles	3780–7000
Sulphide ores	3950–6700
Pulverised fuel ash	600–1000
Made ground (rubble etc.)	160–600
Landfill refuse	400–750
Concrete	3000–3500
Disturbed soil	180–335
Clay landfill cap (compacted)	355–380

* Strongly temperature dependent (Kohnen 1974)

Table 1: P-wave velocity values

Problem	Friction Angle	Depends Upon
Internal strength of sand at small strains	Peak friction angle ϕ	Composition of soil; initial void ratio; initial confining stress
Internal strength of sand at very large strains	Ultimate friction angle ϕ_{cv}	Composition of soil; void ratio in ultimate condition

Table 2: Types of friction angle for sands

	Friction Angles							
	Slope Angle of Repose		At Ultimate Strength		At Peak Strength			
					Medium Dense		Dense	
Classification	$i(°)$	Slope (vert. to hor.)	$\phi_{cv}(°)$	$\tan \phi_{cv}$	$\phi(°)$	$\tan \phi$	$\phi(°)$	$\tan \phi$
Silt (nonplastic)	26 to 30	1 on 2 / 1 on 1.75	26 to 30	0.488 / 0.577	28 to 32	0.532 / 0.625	30 to 34	0.577 / 0.675
Uniform fine to medium sand	26 to 30	1 on 2 / 1 on 1.75	26 to 30	0.488 / 0.577	30 to 34	0.577 / 0.675	32 to 36	0.675 / 0.726
Well-graded sand	30 to 34	1 on 1.75 / 1 on 1.50	30 to 34	0.577 / 0.675	34 to 40	0.675 / 0.839	38 to 46	0.839 / 1.030
Sand and gravel	32 to 36	1 on 1.60 / 1 on 1.40	32 to 36	0.625 / 0.726	36 to 42	0.726 / 0.900	40 to 48	0.900 / 1.110

Table 3: Summary of friction angle data for use in preliminary design Lambe and Whitman [16]

			E_s [kg/cm^2 x 10^2]		E_d [kg/cm^2 x 10^2]		E_s AVERAGE [psi]	E_{d_MIN} / E_{s_MIN}	E_{d_MAX} / E_{s_MAX}	v			Average Compressibility of Es MIN [psi^{-1}]	Average Compressibility of Es MAX [psi^{-1}]
			min	max	min	max				min	max	average		
SOILS	Sand	loose	1,0	3,0	4,47	32,78	2,1E-05	4,5	10,9	0,48	0,50	0,49	4,2E-05	1,4E-05
		medium	3,0	5,0	20,72	74	2,1E-05	6,9	14,8	0,47	0,49	0,48	2,8E-05	1,7E-05
		dense	5,0	8,0	67	293	2,3E-05	13,4	36,6	0,45	0,48	0,47	3,0E-05	1,8E-05
	Clay	loose	0,1	0,5	2,97	19,3	2,3E-04	59,4	38,6	0,47	0,50	0,49	1,3E-03	1,3E-04
		medium	0,5	1,2	16	56	7,4E-05	32,0	46,7	0,47	0,50	0,49	1,3E-04	5,3E-05
		dense	1,2	6,0	47	133	1,8E-05	39,2	22,2	0,47	0,50	0,49	5,3E-05	1,1E-05
	Silt	loose	0,3	0,8										
		medium	1,0	2,0										
		dense	2,0	8,0										
	Gravel	loose	3,0	8,0										
		medium	8,0	10,0			1,2E-04			0,15	0,35	0,25	1,3E-04	1,1E-04
		dense	10,0	20,0										

		Porosity φ [%]	E_s [kg/cm^2 x 10^2]		E_d [kg/cm^2 x 10^2]		E_s AVERAGE [psi]	E_{d_MIN} / E_{s_MIN}	E_{d_MAX} / E_{s_MAX}	v			Average Compressibility of Es MIN [psi^{-1}]	Average Compressibility of Es MAX [psi^{-1}]
			min	max	min	max				min	max	average		
INTACT ROCKS	Andesite	10 - 15	3000	4000			2,0E-07			0,23	0,32	0,28	3,2E-07	2,4E-07
	Amphibolite	-	1300	9200	4600	10500		3,5	1,1					
	Sandstone	5 - 25	300	6100	500	5600	2,2E-07	1,7	0,9	0,10	0,40	0,25		
	Basalt	0.1 - 2	3200	10000	4100	8700	1,1E-07	1,3	0,9	0,19	0,38	0,29	2,8E-07	9,1E-08
	Limestone	5 - 20	1500	9000	800	9900	1,3E-07	0,5	1,1	0,12	0,33	0,23	7,7E-07	1,3E-07
	Coal	10												
	Quartzite	0.1 - 0.5	2200	10000			1,2E-07			0,08	0,24	0,16	6,5E-07	1,4E-07
	Dolerite	0.1	6900	9600	6000	9800	8,5E-08	0,9	1,0	0,28	0,28	0,28	1,3E-07	9,7E-08
	Diorite	-	200	1700	2500	4400		12,5	2,6					
	Dolostone	0.5 - 10	400	5100	2200	8600	2,6E-07	5,5	1,7	0,29	0,34	0,32	2,0E-06	1,5E-07
	Schist	3	600	3900			3,1E-07			0,01	0,31	0,16	2,4E-06	3,7E-07
	Gabbro	0.1 - 0.2	100	6500			2,1E-07			0,12	0,20	0,16	1,4E-05	2,2E-07
	Gneiss	0.5 - 1.5	1700	8100	2500	10500	1,4E-07	1,5	1,3	0,08	0,40	0,24	6,5E-07	1,4E-07
	Granite	0.5 - 1.5	1700	7700	1000	8400	1,5E-07	0,6	1,1	0,10	0,40	0,25	6,2E-07	1,4E-07
	Greywacke	3	4700	6300	2300	10700		0,5	1,7					
	Marble	0.3 - 2	2800	7200			1,4E-07			0,10	0,40	0,25	3,8E-07	1,5E-07
	Argillite	2 - 15	300	2200	1000	7000	5,6E-07	3,3	3,2	0,25	0,29	0,27	3,2E-06	4,4E-07
	Slate	0.1 - 1	500	3000			4,0E-07			0,25	0,30	0,28	1,9E-06	3,2E-07
	Rhyolite	4 - 6	1000	5000			2,3E-07			0,20	0,40	0,30	8,4E-07	1,7E-07
	Salt	5	500	2000			5,6E-07			0,22	0,22	0,22	2,4E-06	5,9E-07
	Tuff	14 - 40	300	7600			1,8E-07			0,24	0,29	0,27	3,3E-06	1,3E-07
	Chalk	5	1500	3600			2,8E-07			0,35	0,35	0,35	4,2E-07	1,8E-07
	Conglomerate		1000	9000			1,4E-07			0,10	0,15	0,13	1,6E-06	1,8E-07
	Marlstone		400	3400	1000	4900		2,5	1,4					
	Anhydrate		1500	7600										
	Siltstone		5300	7500	700	6500	1,1E-07	0,1	0,9	0,25	0,25	0,25	2,0E-07	1,4E-07
	Shale	20 - 50	500	3000			4,0E-07			0,20	0,40	0,30	1,7E-06	2,8E-07
	Mudstone	-	500	7000			1,9E-07			0,15	0,15	0,15	3,0E-06	2,1E-07

Typical rocks and soils in oil field

Table 4: Collected data of some of the mechanical properties of soils and rocks, de Vallejo et al. [6], Lambe and Whitman [16]. In blue calculated values

		UCS average values [kg/cm^2]		Tensile strength [kg/cm^2]		c [kg/cm^2]		phi [°]		V_p [m/s]		V_s [m/s]	
		average	range	min	max	min	max	min	max	min	max	min	max
INTACT ROCKS	Andesite	2100 - 3200	1000 - 5000	70,0	70,0	280,0	280,0	45,0	45,0				
	Amphibolite	2800	2100 - 5300	230,0	230,0								
	Sandstone	550 - 1400	300 - 2350	50,0	200,0	80,0	350,0	30,0	50,0	1400,0	4200,0	1200,0	1800,0
	Basalt	800 - 2000	600 - 3500	50,0	250,0	200,0	600,0	48,0	55,0	4500,0	6500,0	300,0	900,0
	Limestone	600 - 1400	500 - 2000	40,0	300,0	50,0	400,0	35,0	50,0	2500,0	6000,0	1200,0	3000,0
	Coal												
	Quartzite	2000 - 3200	1000 - 5000	100,0	300,0	250,0	700,0	40,0	55,0	5000,0	6500,0		
	Dolerite	2400 - 3500	1300 - 3650	550,0	550,0	900,0	1200,0	40,0	50,0	5500,0	7000,0		
	Diorite	1800 - 2450	1200 - 3350	80,0	300,0	150,0	150,0	50,0	55,0				
	Dolostone	600 - 2000	500 - 3500	50,0	250,0	220,0	600,0	25,0	35,0	5000,0	6000,0		
	Schist	300 - 600	200 - 1600	20,0	55,0	250,0	250,0	25,0	30,0				
	Gabbro	2100 - 2800	1800 - 3000	140,0	300,0	300,0	300,0	35,0	35,0	4500,0	6500,0		
	Gneiss	600 - 2000	500 - 2500	20,0	200,0	140,0	400,0	30,0	40,0	3100,0	5500,0	1700,0	3500,0
	Granite	700 - 2000	500 - 3000	70,0	250,0	150,0	500,0	45,0	58,0	4500,0	6000,0	1700,0	3500,0
	Greywacke	1000 - 1500	800 - 2200	55,0	150,0	60,0	100,0	45,0	50,0				
	Marble	1200 - 2000	600 - 2500	65,0	200,0	150,0	350,0	35,0	45,0	3500,0	6000,0	2000,0	3500,0
	Argillite	200 - 400	100 - 900	15,0	100,0	30,0	350,0	40,0	60,0	1400,0	3000,0		
	Slate	400 - 1500	300 - 2000	70,0	200,0	100,0	500,0	40,0	55,0	3500,0	5000,0	2000,0	3500,0
	Rhyolite	800 - 1600		50,0	100,0								
	Salt	120	50 - 300							4500,0	6000,0		
	Tuff		100 - 460	10,0	40,0	7,0	7,0					500,0	700,0
	Chalk	250	100 - 400	10,0	25,0			30,0	30,0	3000,0	4000,0	230,0	1100,0
	Conglomerate	300 - 2300		30,0	100,0					2500,0	5000,0		
	Marlstone	300 - 700	200 - 900							1800,0	3200,0		
	Anhydrate	900	800 - 1300	60,0	120,0								
	Siltstone		350 - 2500	27,0	27,0							2400,0	2700,0

Typical rocks and soils in oil field

Table 5: Strength parameters, longitudinal and transversal waves velocities of some intact rocks, de Vallejo et al. [6]

			Peak strength		Residual strength	
		Description	**c [kg/cm^2]**	**ϕ [°]**	**c [kg/cm^2]**	**ϕ [°]**
ROCKS WITH DISCONTINUITIES	Basalt	Clay-rich breccia with rocky fragments	2.4	42		
	Limestone	Filling with clay of 6 mm			0	13
		Id. from 1 to 2 cm	1	13 - 14		
		Id. < 1 mm	0.5 - 2	17 - 21		
		Marlstone of 2 cm	0	25	0	15 - 24
	Diorite	Filling with clay	0	26.5		
	Dolostone	Filling with clay of 15 cm thick	0.41	14.5	0.22	17
	Schist and Quartzite	Filling with clay 10 - 15 cm thick	0.3 - 0.8	32		
		Filling with thin clay in layers of stratifications	6.1 - 7.4	41		
		Filling with thick clay in layers of stratifications	3.8	31		
	Granite	Faults filling with clay	0 - 1.0	24 - 25		
		Faults filling with sand	0.5	40		
		Fault plane zone, disjointed rock, filling with clay	2.42	42		
	Greywacke	Filling with clay 1 - 2 mm in layers of stratifications			0	21
	Argillite	Filling with clay	0.6	32		
		Clay in layers of stratifications			0	19.5
	Slate	Altered and laminated	0.5	33		

Figure 1: Strength parameters of some rocks with discontinuities, de Vallejo et al. [6]

	Depth	σ_v		p		σ'_v		$c_{m,load}$		$E_{s,load}$	$E_{s,load}$	E_d
	(m)	(MPa)	(bar)	(MPa)	(bar)	(MPa)	(bar)	(Mpa^{-1})	(bar^{-1})	(GPa)	(GPa)	(GPa)
	0	0,000	0,000	0,000	0,000	0,000	0,00	-	-	-	-	-
	50	0,501	5,011	0,501	5,011	0,000	0,00	-	-	-	-	-
	100	1,433	14,331	1,002	10,023	0,431	4,31	2,61E-02	0,002611482	0,20	0,20	0,20
	200	3,395	33,951	2,005	20,046	1,391	13,91	6,91E-03	0,000690946	0,24	0,45	0,50
	300	5,357	53,571	3,007	30,069	2,350	23,50	3,81E-03	0,000380897	0,28	0,70	0,85
	400	7,319	73,191	4,009	40,092	3,310	33,10	2,58E-03	0,000258265	0,36	0,94	1,26
	500	9,281	92,811	5,011	50,114	4,270	42,70	1,93E-03	0,000193464	0,41	1,23	1,64
	600	11,341	113,412	6,014	60,137	5,327	53,27	1,50E-03	0,000150496	0,49	1,48	1,97
	700	13,401	134,013	7,016	70,160	6,385	63,85	1,23E-03	0,000122538	0,61	1,82	2,42
	800	15,461	154,614	8,018	80,183	7,443	74,43	1,03E-03	0,000102974	0,72	2,16	2,89
	900	17,521	175,215	9,021	90,206	8,501	85,01	8,86E-04	8,8561E-05	0,84	2,52	3,36
	1000	19,582	195,816	10,023	100,229	9,559	95,59	7,75E-04	7,7526E-05	0,96	2,87	3,83
	1100	21,740	217,398	11,025	110,252	10,715	107,15	6,81E-04	6,8107E-05	1,09	3,27	4,36
	1200	23,898	238,980	12,027	120,275	11,871	118,71	6,06E-04	6,06324E-05	1,23	3,68	4,90
	1300	26,056	260,562	13,030	130,297	13,026	130,26	5,46E-04	5,45649E-05	1,36	4,08	5,45
	1400	28,214	282,144	14,032	140,320	14,182	141,82	4,95E-04	4,9547E-05	1,50	4,50	6,00
	1450	29,293	292,935	14,533	145,332	14,760	147,60	4,74E-04	4,73515E-05	1,57	4,71	6,28
	1500	30,422	304,216	15,034	150,343	15,387	153,87	4,52E-04	4,51682E-05	1,64	4,93	6,58
Datum	*1540*	31,324	313,242	15,435	154,352	15,889	158,89	4,36E-04	4,35536E-05	1,71	5,12	6,82
	1575	32,114	321,139	15,786	157,860	16,328	163,28	4,22E-04	4,22276E-05	1,76	5,28	7,04
	1600	32,678	326,779	16,0366	160,366	16,641	166,41	4,13E-04	4,13261E-05	1,80	5,39	7,19
	1700	34,934	349,342	17,03889	170,3889	17,895	178,95	3,81E-04	3,80559E-05	1,95	5,86	7,81
	1800	37,191	371,905	18,04118	180,4118	19,149	191,49	3,52E-04	3,52408E-05	2,11	6,32	8,43
	1900	39,447	394,468	19,04347	190,4347	20,403	204,03	3,28E-04	3,27935E-05	2,27	6,80	9,06
	2000	41,703	417,031	20,04575	200,4575	21,657	216,57	3,06E-04	3,06475E-05	2,42	7,27	9,70
	2100	44,058	440,575	21,04804	210,4804	23,010	230,10	1,86E-05	1,86E-06	40		
	2200	46,412	464,119	22,05033	220,5033	24,362	243,62					
	2300	48,766	487,663	23,05262	230,5262	25,714	257,14					
	2400	51,121	511,207	24,0549	240,549	27,066	270,66					
	2500	53,475	534,751	25,05719	250,5719	28,418	284,18					
	2600	55,830	558,295	26,05948	260,5948	29,770	297,70					
	2700	58,184	581,839	27,06177	270,6177	31,122	311,22					
	2800	60,538	605,383	28,06406	280,6406	32,474	324,74					
	2900	62,893	628,927	29,06634	290,6634	33,826	338,26					
	3000	65,247	652,471	30,06863	300,6863	35,179	351,79					
	3100	67,798	677,977	31,07092	310,7092	36,727	367,27	1,49E-05	1,49E-06	50		
	3200	70,348	703,483	32,07321	320,7321	38,275	382,75					
	3300	72,899	728,989	33,07549	330,7549	39,823	398,23					
	3400	75,450	754,495	34,07778	340,7778	41,372	413,72					
	3500	78,000	780,001	35,08007	350,8007	42,920	429,20					
	3600	80,551	805,507	36,08236	360,8236	44,468	444,68					
	3700	83,101	831,013	37,08464	370,8464	46,017	460,17					
	3800	85,652	856,519	38,08693	380,8693	47,565	475,65					
	3900	88,203	882,025	39,08922	390,8922	49,113	491,13					
	4000	90,753	907,531	40,09151	400,9151	50,662	506,62					
	4100	93,304	933,037	41,0938	410,938	52,210	522,10					
	4200	95,854	958,543	42,09608	420,9608	53,758	537,58					
	4300	98,405	984,049	43,09837	430,9837	55,307	553,07					
	4400	100,956	1009,555	44,10066	441,0066	56,855	568,55					
	4500	103,506	1035,061	45,10295	451,0295	58,403	584,03					
	4600	106,057	1060,567	46,10523	461,0523	59,952	599,52					
	4700	108,607	1086,073	47,10752	471,0752	61,500	615,00					
	4800	111,158	1111,579	48,10981	481,0981	63,048	630,48					
	4900	113,709	1137,085	49,1121	491,121	64,596	645,96					
	5000	116,259	1162,591	50,11439	501,1439	66,145	661,45					

Table 6: Case study stratigraphy along z axis, total stress and total effective stress distributions with relative elastic moduli obtained applying Teatini's formula

	timestep	σ'zz [bar]			σ'xx [bar]			σ'zx [bar]			εzz [-]			εxx [-]		
		min	max	average	min	max	average	min	max	average	min	max	average	min	max	average
Case 1 STATIC	01/01/2016	146,19	161,27	156,51	116,95	129,01	125,21	0	0	0	0	0	0	0	0	0
	01/01/2017															
	01/01/2018	194,76	215,82	205,38	140,27	153,4	147	-1,81	1,81	0	0,0014	0,0025	0,0021	-0,0001	0,0001	0
	01/01/2019															
	01/01/2020	213,03	245,83	232,47	151,2	167,08	159,08	-2,84	2,84	0	0,0022	0,0038	0,0033	-0,0001	0,0002	0
	01/01/2021															
	01/01/2022	220,03	257,33	242,89	154,37	172,33	163,73	-3,24	3,24	0	0,0024	0,0043	0,0038	-0,0001	0,0002	0
	01/01/2023															
	01/01/2024	222,71	261,71	246,87	155,59	174,33	165,5	-3,39	3,39	0	0,0026	0,0045	0,004	-0,0001	0,0002	0
	01/01/2025															
	01/05/2025	223,45	262,92	247,99	155,93	174,88	166	-3,43	3,43	0	0,0026	0,0045	0,004	-0,0001	0,0002	0

	timestep	σ'zz [bar]			σ'xx [bar]			σ'zx [bar]			εzz [-]			εxx [-]		
		min	max	average	min	max	average	min	max	average	min	max	average	min	max	average
Case 1 DYNAMIC	01/01/2016	146,19	161,27	156,51	116,95	129,01	125,21	0	0	0	0	0	0	0	0	0
	01/01/2017															
	01/01/2018	194,78	215,84	205,39	140,31	153,45	147,04	-1,8	1,8	0	0,0003	0,0006	0,0005	0	0	0
	01/01/2019															
	01/01/2020	213,05	245,86	232,48	151,21	167,16	159,13	-2,82	2,82	0	0,0005	0,0009	0,0008	0	0	0
	01/01/2021															
	01/01/2022	220,07	257,36	242,9	154,39	172,41	163,79	-3,22	3,22	0	0,0006	0,0011	0,0009	0	0,0001	0
	01/01/2023															
	01/01/2024	222,74	261,75	246,89	155,61	174,42	165,57	-3,37	3,37	0	0,0006	0,0011	0,001	0	0,0001	0
	01/01/2025															
	01/05/2025	223,48	262,96	248,01	155,96	174,97	166,07	-3,41	3,41	0	0,0006	0,0011	0,001	0	0,0001	0

	timestep	σ'zz [bar]			σ'xx [bar]			σ'zx [bar]			εzz [-]			εxx [-]		
		min	max	average	min	max	average	min	max	average	min	max	average	min	max	average
Case 1 CURVE 1	01/01/2016	146,19	161,27	156,51	116,95	129,01	125,21	0	0	0	0	0	0	0	0	0
	01/01/2017	172,45	189,14	181,6	129,11	141,28	136,41	-0,92	0,91	0	0,0002	0,0003	0,0003	0	0	0
	01/01/2018	194,39	214,94	205,21	139,9	152,67	146,79	-1,72	1,72	0	0,0004	0,0008	0,0007	0	0	0
	01/01/2019	205,28	232,38	221,7	147,17	160,23	153,98	-2,25	2,25	0	0,0006	0,0012	0,0011	0	0	0
	01/01/2020	211,91	243,03	231,86	151,59	164,91	158,39	-2,55	2,55	0	0,0008	0,0016	0,0014	0	0	0
	01/01/2021	215,98	249,68	238,16	153,78	167,84	161,12	-2,73	2,73	0	0,0008	0,0018	0,0016	0	0,0001	0
	01/01/2022	218,47	253,77	242,04	155	169,64	162,8	-2,84	2,84	0	0,0009	0,0019	0,0017	0	0,0001	0
	01/01/2023	220,01	256,32	244,45	155,76	170,76	163,84	-2,91	2,91	0	0,0009	0,0021	0,0018	0	0,0001	0
	01/01/2024	220,94	257,95	245,92	156,22	171,45	164,48	-2,95	2,95	0	0,001	0,0021	0,0018	0	0,0001	0
	01/01/2025	221,51	258,97	246,83	156,51	171,87	164,87	-2,98	2,97	0	0,001	0,0022	0,0019	0	0,0001	0
	01/05/2025	221,62	259,19	247,01	156,57	171,95	164,95	-2,98	2,98	0	0,001	0,0022	0,0019	0	0,0001	0

Table 7: Case 1 results of static, dynamic and using input curve 1 configurations. All values refer to the reservoir only

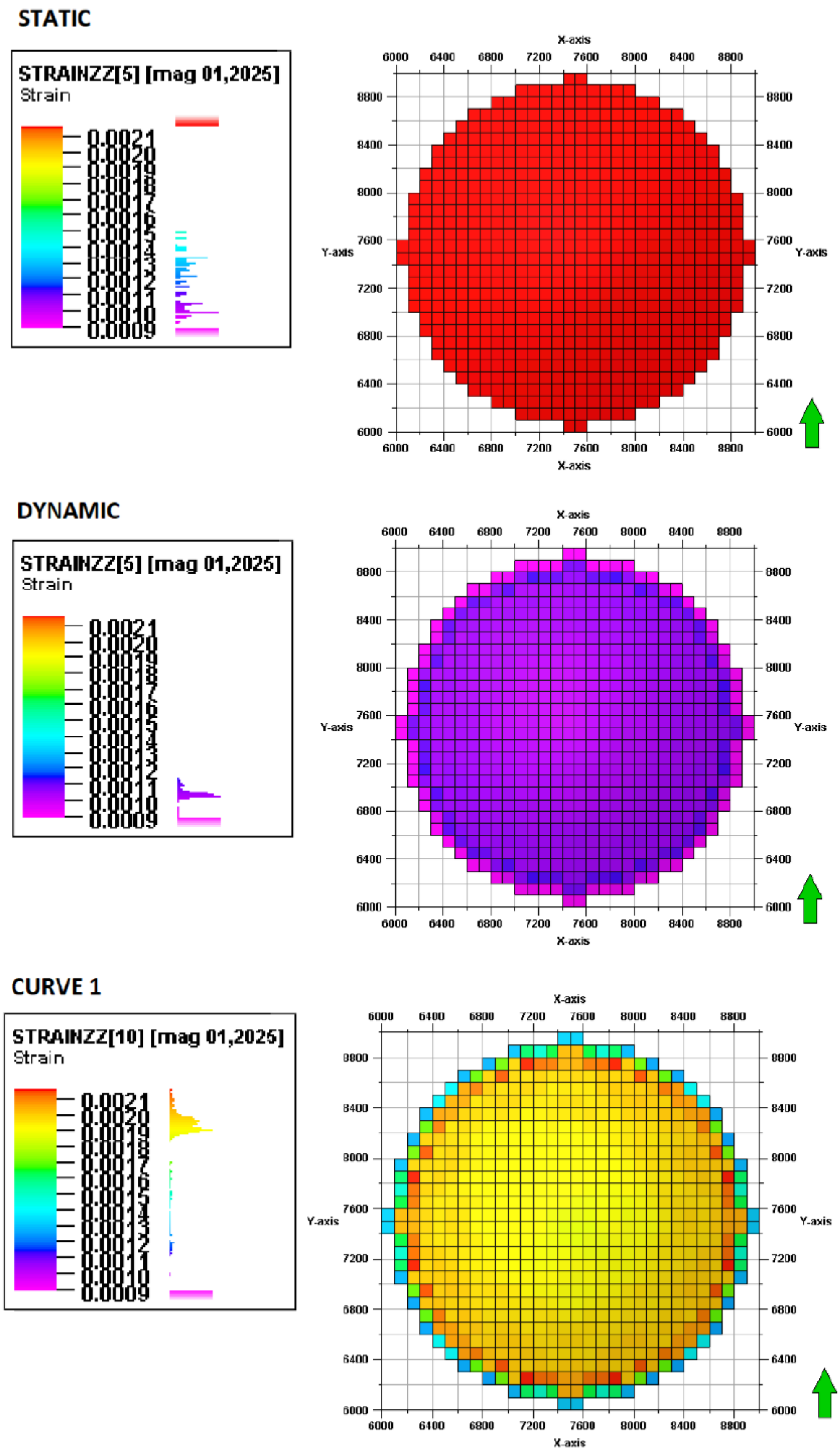

Figure 2: Case 1: vertical strain distribution at the end of production of static, dynamic and input curve 1 configurations

CURVE 1	
ε_{zz} [-]	E [Gpa]
0	6,66E+09
3,33E-06	6,60E+09
6,67E-06	6,53E+09
1,00E-05	6,47E+09
1,33E-05	6,44E+09
1,67E-05	6,37E+09
2,00E-05	6,30E+09
2,33E-05	6,27E+09
2,67E-05	6,26E+09
3,00E-05	6,20E+09
3,33E-05	6,17E+09
6,67E-05	5,78E+09
1,00E-04	5,45E+09
1,33E-04	5,15E+09
1,67E-04	4,95E+09
2,00E-04	4,79E+09
2,33E-04	4,55E+09
2,67E-04	4,46E+09
3,00E-04	4,29E+09
3,33E-04	4,13E+09
6,67E-04	3,17E+09
1,00E-03	2,64E+09
1,33E-03	2,31E+09
1,67E-03	2,15E+09
2,00E-03	1,98E+09
2,33E-03	1,78E+09
2,67E-03	1,65E+09
3,00E-03	1,65E+09
3,33E-03	1,65E+09
6,67E-03	1,65E+09
1,00E-02	1,65E+09
1,33E-02	1,65E+09
1,67E-02	1,65E+09
2,00E-02	1,65E+09
2,33E-02	1,65E+09
2,67E-02	1,65E+09
3,00E-02	1,65E+09
3,33E-02	1,65E+09
3,00E-01	1,65E+09

CURVE 2					
ε_{zz} [-]	E [Gpa]	ε_{zz} [-]	E [Gpa]	ε_{zz} [-]	E [Gpa]
0	6,66E+09	1,13E-03	2,48E+09	2,26E-03	1,83E+09
3,33E-05	6,16E+09	1,16E-03	2,46E+09	2,28E-03	1,81E+09
5,83E-05	5,85E+09	1,18E-03	2,44E+09	2,31E-03	1,80E+09
8,33E-05	5,59E+09	1,21E-03	2,41E+09	2,33E-03	1,78E+09
1,08E-04	5,37E+09	1,23E-03	2,39E+09	2,36E-03	1,77E+09
1,33E-04	5,18E+09	1,26E-03	2,37E+09	2,38E-03	1,75E+09
1,58E-04	5,01E+09	1,28E-03	2,35E+09	2,41E-03	1,74E+09
1,83E-04	4,85E+09	1,31E-03	2,33E+09	2,43E-03	1,73E+09
2,08E-04	4,71E+09	1,33E-03	2,31E+09	2,46E-03	1,72E+09
2,33E-04	4,59E+09	1,36E-03	2,30E+09	2,48E-03	1,70E+09
2,58E-04	4,46E+09	1,38E-03	2,28E+09	2,51E-03	1,69E+09
2,83E-04	4,35E+09	1,41E-03	2,27E+09	2,53E-03	1,68E+09
3,08E-04	4,24E+09	1,43E-03	2,25E+09	2,56E-03	1,68E+09
3,33E-04	4,14E+09	1,46E-03	2,24E+09	2,58E-03	1,67E+09
3,58E-04	4,04E+09	1,48E-03	2,22E+09	2,61E-03	1,66E+09
3,83E-04	3,95E+09	1,51E-03	2,21E+09	2,63E-03	1,66E+09
4,08E-04	3,86E+09	1,53E-03	2,20E+09	2,66E-03	1,65E+09
4,33E-04	3,78E+09	1,56E-03	2,19E+09	2,68E-03	1,65E+09
4,58E-04	3,70E+09	1,58E-03	2,18E+09	2,71E-03	1,65E+09
4,83E-04	3,62E+09	1,61E-03	2,17E+09	2,73E-03	1,65E+09
5,08E-04	3,55E+09	1,63E-03	2,16E+09	2,76E-03	1,65E+09
5,33E-04	3,48E+09	1,66E-03	2,15E+09	2,78E-03	1,65E+09
5,58E-04	3,42E+09	1,68E-03	2,13E+09	2,81E-03	1,65E+09
5,83E-04	3,36E+09	1,71E-03	2,12E+09	2,83E-03	1,65E+09
6,08E-04	3,30E+09	1,73E-03	2,11E+09	2,86E-03	1,65E+09
6,33E-04	3,24E+09	1,76E-03	2,10E+09	2,88E-03	1,65E+09
6,58E-04	3,19E+09	1,78E-03	2,09E+09	2,91E-03	1,65E+09
6,83E-04	3,14E+09	1,81E-03	2,08E+09	2,93E-03	1,65E+09
7,08E-04	3,09E+09	1,83E-03	2,07E+09	2,96E-03	1,65E+09
7,33E-04	3,04E+09	1,86E-03	2,06E+09	2,98E-03	1,65E+09
7,58E-04	3,00E+09	1,88E-03	2,04E+09	3,00E-03	1,65E+09
7,83E-04	2,95E+09	1,91E-03	2,03E+09	3,33E-03	1,65E+09
8,08E-04	2,91E+09	1,93E-03	2,02E+09	6,67E-03	1,65E+09
8,33E-04	2,87E+09	1,96E-03	2,01E+09	1,00E-02	1,65E+09
8,58E-04	2,83E+09	1,98E-03	1,99E+09	1,33E-02	1,65E+09
8,83E-04	2,80E+09	2,01E-03	1,98E+09	1,67E-02	1,65E+09
9,08E-04	2,76E+09	2,03E-03	1,96E+09	2,00E-02	1,65E+09
9,33E-04	2,72E+09	2,06E-03	1,95E+09	2,33E-02	1,65E+09
9,58E-04	2,69E+09	2,08E-03	1,93E+09	2,67E-02	1,65E+09
9,83E-04	2,66E+09	2,11E-03	1,92E+09	3,00E-02	1,65E+09
1,01E-03	2,63E+09	2,13E-03	1,90E+09	3,33E-02	1,65E+09
1,03E-03	2,60E+09	2,16E-03	1,89E+09	3,00E-01	1,65E+09
1,06E-03	2,57E+09	2,18E-03	1,87E+09		
1,08E-03	2,54E+09	2,21E-03	1,86E+09		
1,11E-03	2,51E+09	2,23E-03	1,84E+09		

Table 8: Curve 1 and curve 2 sampling points

INPUT CURVE 1 (38 PT)					OUTPUT CURVE CURVA 1	CURVA 2	CURVA 3
timestep	SBHP [bar] average	increasing Δp [bar]	σ'zz [bar] average	εzz [-] average	E (1) [Gpa]	E (2) [Gpa]	E (3) [Gpa]
	158,83	0,00	156,51	1,00E-06	6,66E+09	6,66E+09	6,66E+09
01/01/2017	132,61	26,21	181,6	3,00E-04	4,29E+09	4,35E+09	4,28E+09
01/01/2018	107,74	51,08	205,21	7,00E-04	3,17E+09	3,14E+09	3,10E+09
01/01/2019	90,26	68,56	221,7	1,10E-03	2,64E+09	2,54E+09	2,52E+09
01/01/2020	79,43	79,40	231,86	1,40E-03	2,31E+09	2,28E+09	2,27E+09
01/01/2021	72,68	86,14	238,16	1,60E-03	2,31E+09	2,18E+09	2,17E+09
01/01/2022	68,53	90,30	242,04	1,70E-03	2,15E+09	2,13E+09	2,13E+09
01/01/2023	65,94	92,88	244,45	1,80E-03	2,15E+09	2,09E+09	2,08E+09
01/01/2024	64,36	94,47	245,92	1,80E-03	2,15E+09	2,09E+09	2,08E+09
01/01/2025	63,39	95,44	246,83	1,90E-03	2,15E+09	2,04E+09	2,04E+09
01/05/2025	63,19	95,63	247,01	1,90E-03	2,15E+09	2,04E+09	2,04E+09

Table 9: Case 1, input curve 1, one-year timestep: Young modulus calculated using output curve 1, 2 and 3

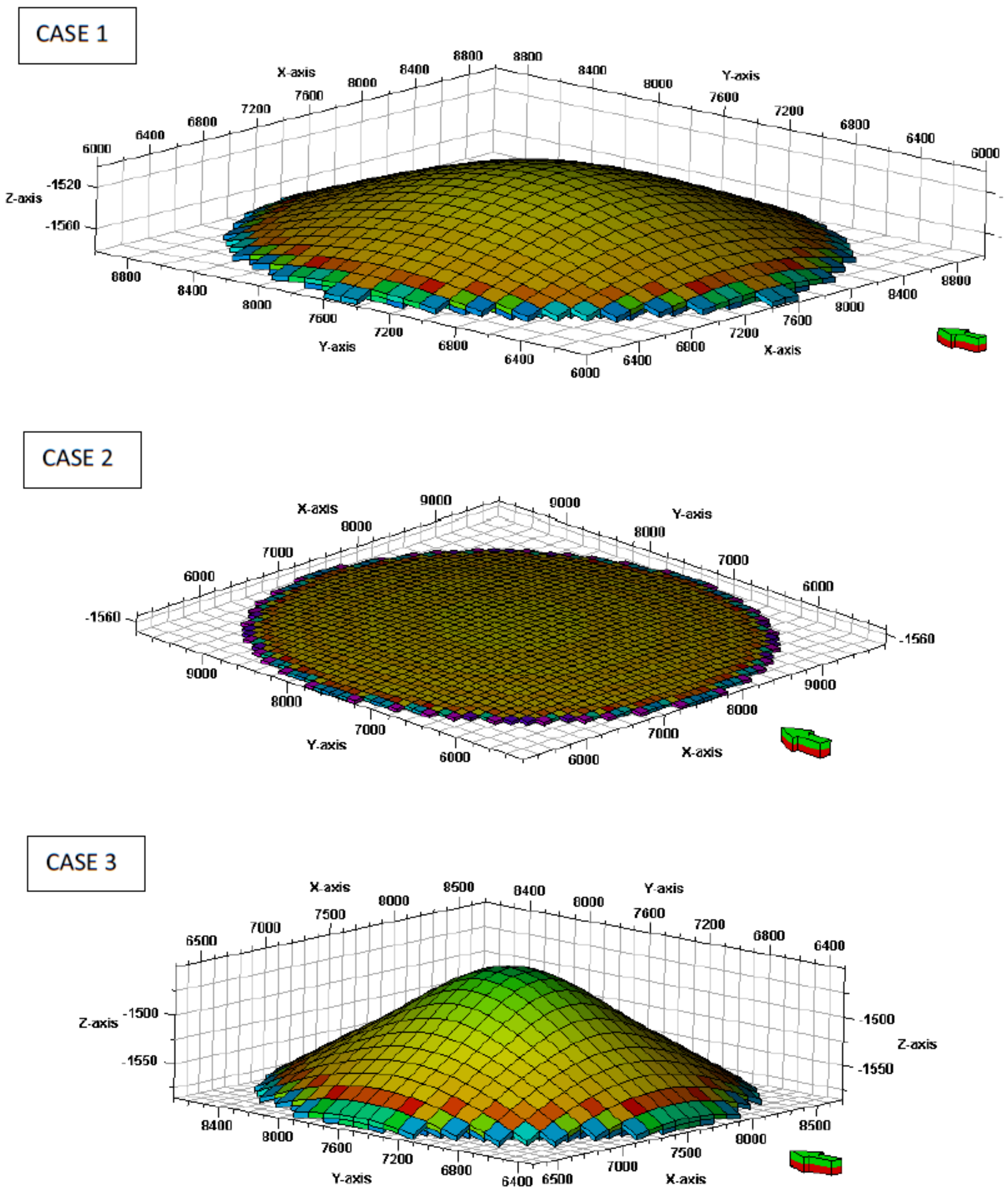

Figure 3: Reservoir shape of case 1, 2 and 3. The representation is on different scales, but it is useful to visualize the reservoir shape of the different cases

	timestep	σ'zz [bar]			σ'xx [bar]			σ'zx [bar]			εzz [-]			εxx [-]		
		min	max	average	min	max	average	min	max	average	min	max	average	min	max	average
Case 2 STATIC	01/01/2016	156,54	161,27	159,54	125,23	129,01	127,63	0	0	0	0	0	0	0	0	0
	01/01/2017															
	01/01/2018	195,72	219,24	209,69	144,43	154,36	149,34	-0,88	0,88	0	0,0015	0,0026	0,0022	-0,0001	0,0001	0
	01/01/2019															
	01/01/2020	216,37	246,06	237,46	153,73	165,76	161,36	-1,4	1,4	0	0,0024	0,0038	0,0035	-0,0001	0,0001	0
	01/01/2021															
	01/01/2022	222,29	256,16	248,14	157,36	169,95	165,98	-1,6	1,6	0	0,0027	0,0043	0,0039	-0,0001	0,0001	0
	01/01/2023															
	01/01/2024	227,34	260,81	252,23	158,76	171,58	167,75	-1,67	1,67	0	0,0029	0,0045	0,0041	-0,0001	0,0001	0
	01/01/2025															
	01/05/2025	228,21	262,15	253,37	159,16	172,09	168,25	-1,7	1,7	0	0,0029	0,0045	0,0042	-0,0001	0,0001	0

	timestep	σ'zz [bar]			σ'xx [bar]			σ'zx [bar]			εzz [-]			εxx [-]		
		min	max	average	min	max	average	min	max	average	min	max	average	min	max	average
Case 2 DYNAMIC	01/01/2016	156,54	161,27	159,54	125,23	129,01	127,63	0	0	0	0	0	0	0	0	0
	01/01/2017															
	01/01/2018	195,71	217,84	209,95	144,43	154,36	149,34	-0,88	0,88	0	0,0004	0,0006	0,0006	0	0	0
	01/01/2019															
	01/01/2020	216,45	244,09	237,97	153,73	165,76	161,36	-1,4	1,4	0	0,0006	0,0009	0,0009	0	0	0
	01/01/2021															
	01/01/2022	224,56	256,15	248,75	157,36	169,5	166,17	-1,6	1,6	0	0,0007	0,0011	0,001	0	0	0
	01/01/2023															
	01/01/2024	227,69	260,81	252,88	158,76	171,58	167,75	-1,67	1,67	0	0,0007	0,0011	0,001	0	0	0
	01/01/2025															
	01/05/2025	228,59	262,15	254,03	159,16	172,09	168,25	-1,7	1,7	0	0,0007	0,0011	0,001	0	0	0

	timestep	σ'zz [bar]			σ'xx [bar]			σ'zx [bar]			εzz [-]			εxx [-]		
		min	max	average	min	max	average	min	max	average	min	max	average	min	max	average
Case 2 CURVE 1	01/01/2016	156,54	161,26	159,41	125,23	129,01	127,53	0	0	0	0	0	0	0	0	0
	01/01/2017	178,2	192,75	185,33	136,57	142,78	138,74	-0,44	0,44	0	0,0002	0,0004	0,0003	0	0	0
	01/01/2018	195,64	217,73	209,91	144,32	153,54	149,33	-0,86	0,86	0	0,0005	0,0008	0,0007	0	0	0
	01/01/2019	208,42	233,44	227,14	149,95	160,23	156,74	-1,15	1,15	0	0,0007	0,0012	0,0011	0	0	0
	01/01/2020	216,29	242,96	237,82	153,41	164,32	161,33	-1,33	1,33	0	0,0009	0,0016	0,0014	0	0	0
	01/01/2021	221,16	250,11	244,45	155,56	167,09	164,18	-1,43	1,43	0	0,001	0,0018	0,0017	0	0	0
	01/01/2022	224,14	254,63	248,54	156,88	168,83	165,93	-1,5	1,5	0	0,0011	0,002	0,0018	0	0	0
	01/01/2023	225,99	257,45	251,08	157,7	170,04	167,03	-1,54	1,54	0	0,0011	0,0021	0,0019	0	0	0
	01/01/2024	227,13	259,18	252,64	158,21	170,77	167,7	-1,56	1,56	0	0,0012	0,0021	0,0019	0	0	0
	01/01/2025	227,83	260,23	253,6	158,52	171,23	168,11	-1,58	1,58	0	0,0012	0,0022	0,002	0	0	0
	01/05/2025	227,99	260,47	253,79	158,59	171,33	168,19	-1,58	1,58	0	0,0012	0,0022	0,002	0	0	0

Table 10: Case 2 results of static, dynamic and using input curve 1 configurations. All values refer to the reservoir only

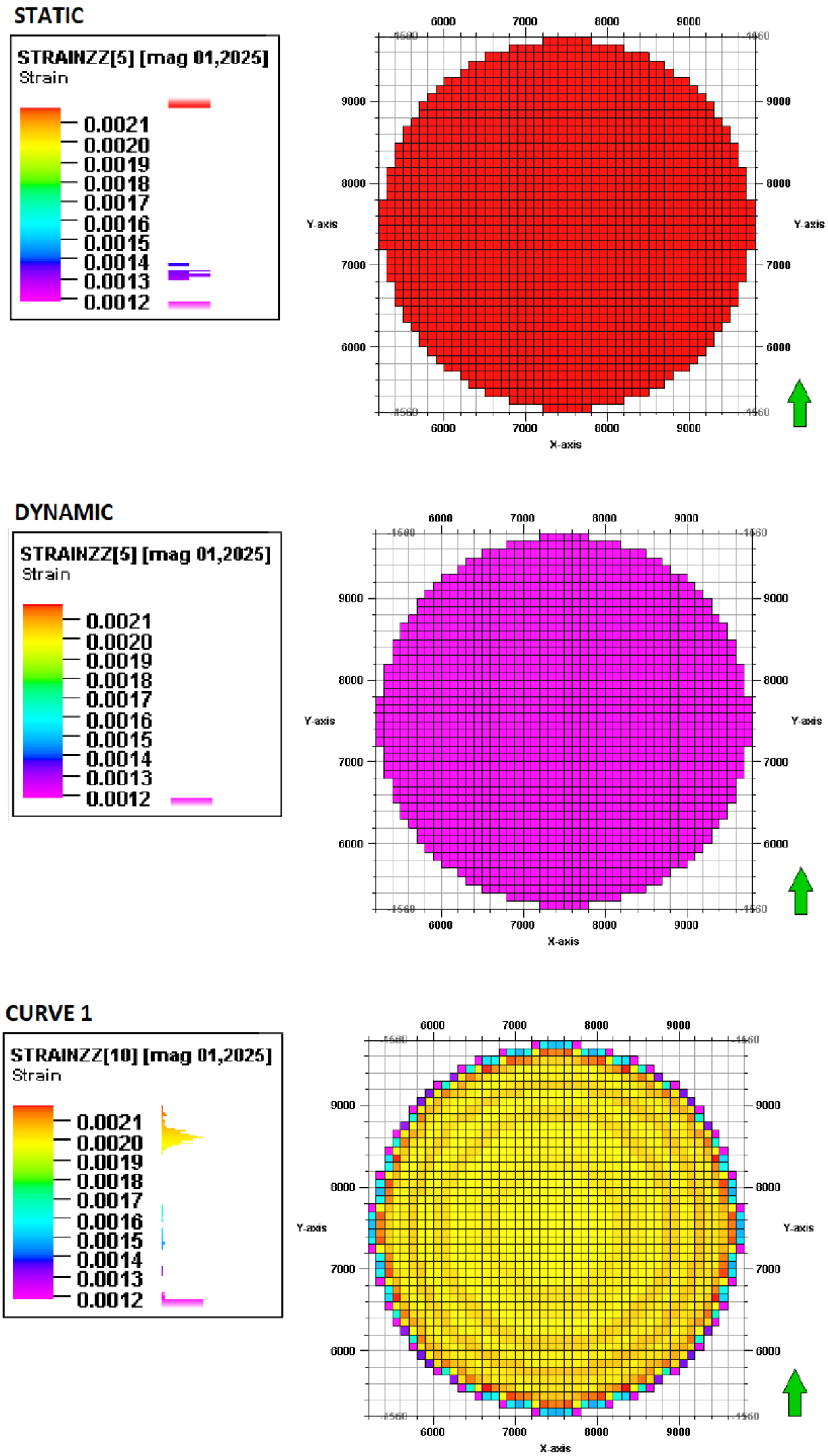

Figure 4: Case 2: vertical strain distribution at the end of production of static, dynamic and input curve 1 configurations

	timestep	σ'zz [bar] min	σ'zz [bar] max	σ'zz [bar] average	σ'xx [bar] min	σ'xx [bar] max	σ'xx [bar] average	σ'zx [bar] min	σ'zx [bar] max	σ'zx [bar] average	εzz [-] min	εzz [-] max	εzz [-] average	εxx [-] min	εxx [-] max	εxx [-] average
Case 3 STATIC	01/01/2016	136,47	161,96	154,5	109,18	129,57	123,6	0	0	0	0	0	0	0	0	0
	01/01/2017															
	01/01/2018	184,44	213,25	202,2	133,66	153,55	145,72	-2,7	2,62	0	0,0013	0,0024	0,0021	-0,0001	0,0002	0
	01/01/2019															
	01/01/2020	210,51	243,01	228,65	147,01	167,48	157,98	-4,22	4,09	0	0,002	0,0037	0,0032	-0,0002	0,0003	0
	01/01/2021															
	01/01/2022	217,59	254,66	238,83	152,13	172,89	162,7	-4,81	4,66	0	0,0023	0,0042	0,0036	-0,0002	0,0003	0
	01/01/2023															
	01/01/2024	220,16	259,13	242,73	154,05	174,96	164,5	-5,03	4,87	0	0,0024	0,0044	0,0038	-0,0002	0,0003	0
	01/01/2025															
	01/05/2025	220,87	260,39	243,81	154,57	175,73	165	-5,09	4,93	0	0,0024	0,0045	0,0039	-0,0003	0,0003	0

	timestep	σ'zz [bar] min	σ'zz [bar] max	σ'zz [bar] average	σ'xx [bar] min	σ'xx [bar] max	σ'xx [bar] average	σ'zx [bar] min	σ'zx [bar] max	σ'zx [bar] average	εzz [-] min	εzz [-] max	εzz [-] average	εxx [-] min	εxx [-] max	εxx [-] average
Case 3 DYNAMIC	01/01/2016	136,47	161,96	154,5	109,18	129,57	123,6	0	0	0	0	0	0	0	0	0
	01/01/2017															
	01/01/2018	184,48	213,28	202,22	133,71	153,61	145,76	-2,69	2,6	0	0,0003	0,0006	0,0005	0	0	0
	01/01/2019															
	01/01/2020	210,57	243,01	228,68	147,08	167,57	158,05	-4,2	4,07	0	0,0005	0,0009	0,0008	-0,0001	0,0001	0
	01/01/2021															
	01/01/2022	217,65	254,66	238,87	152,21	172,99	162,77	-4,78	4,63	0	0,0006	0,0011	0,0009	-0,0001	0,0001	0
	01/01/2023															
	01/01/2024	220,21	259,13	242,76	154,14	175,07	164,58	-5,01	4,85	0	0,0006	0,0011	0,001	-0,0001	0,0001	0
	01/01/2025															
	01/05/2025	220,93	260,38	243,85	154,66	175,64	165,09	-5,07	4,91	0	0,0006	0,0011	0,001	-0,0001	0,0001	0

	timestep	σ'zz [bar] min	σ'zz [bar] max	σ'zz [bar] average	σ'xx [bar] min	σ'xx [bar] max	σ'xx [bar] average	σ'zx [bar] min	σ'zx [bar] max	σ'zx [bar] average	εzz [-] min	εzz [-] max	εzz [-] average	εxx [-] min	εxx [-] max	εxx [-] average
Case 3 CURVE 1	01/01/2016	136,47	161,96	154,5	109,18	129,57	123,6	0	0	0	0	0	0	0	0	0
	01/01/2017	161,33	187,27	178,99	121,85	141,45	134,97	-1,37	1,32		0,0002	0,0003	0,0003	0	0	0
	01/01/2018	183,98	212,47	201,91	132,93	152,61	145,33	-2,56	2,48	0	0,0004	0,0008	0,0006	0	0	0
	01/01/2019	199,44	230,72	217,84	140,29	159,95	152,42	-3,33	3,23		0,0006	0,0012	0,001	0	0,0001	0
	01/01/2020	208,84	242,03	227,61	144,69	164,45	156,73	-3,77	3,66	0	0,0007	0,0016	0,0013	-0,0001	0,0001	0
	01/01/2021	212,99	249,14	233,66	147,38	167,23	159,38	-4,03	3,92		0,0008	0,0018	0,0015	-0,0001	0,0001	0
	01/01/2022	215,29	253,52	237,37	149,01	168,92	161	-4,19	4,07	0	0,0008	0,002	0,0016	-0,0001	0,0001	0
	01/01/2023	216,72	256,24	239,68	150,02	169,98	162,02	-4,29	4,16		0,0009	0,0021	0,0017	-0,0001	0,0001	0
	01/01/2024	217,59	257,9	241,09	150,64	170,63	162,64	-4,35	4,22	0	0,0009	0,0021	0,0017	-0,0001	0,0001	0
	01/01/2025	218,12	258,92	241,96	151,02	171,02	163,02	-4,39	4,26		0,0009	0,0021	0,0017	-0,0001	0,0001	0
	01/05/2025	218,22	259,14	242,13	151,08	171,1	163,09	-4,39	4,27	0	0,0009	0,0022	0,0018	-0,0001	0,0001	0

Table 11: Case 3 results of static, dynamic and using input curve 1 configurations. All values refer to the reservoir only

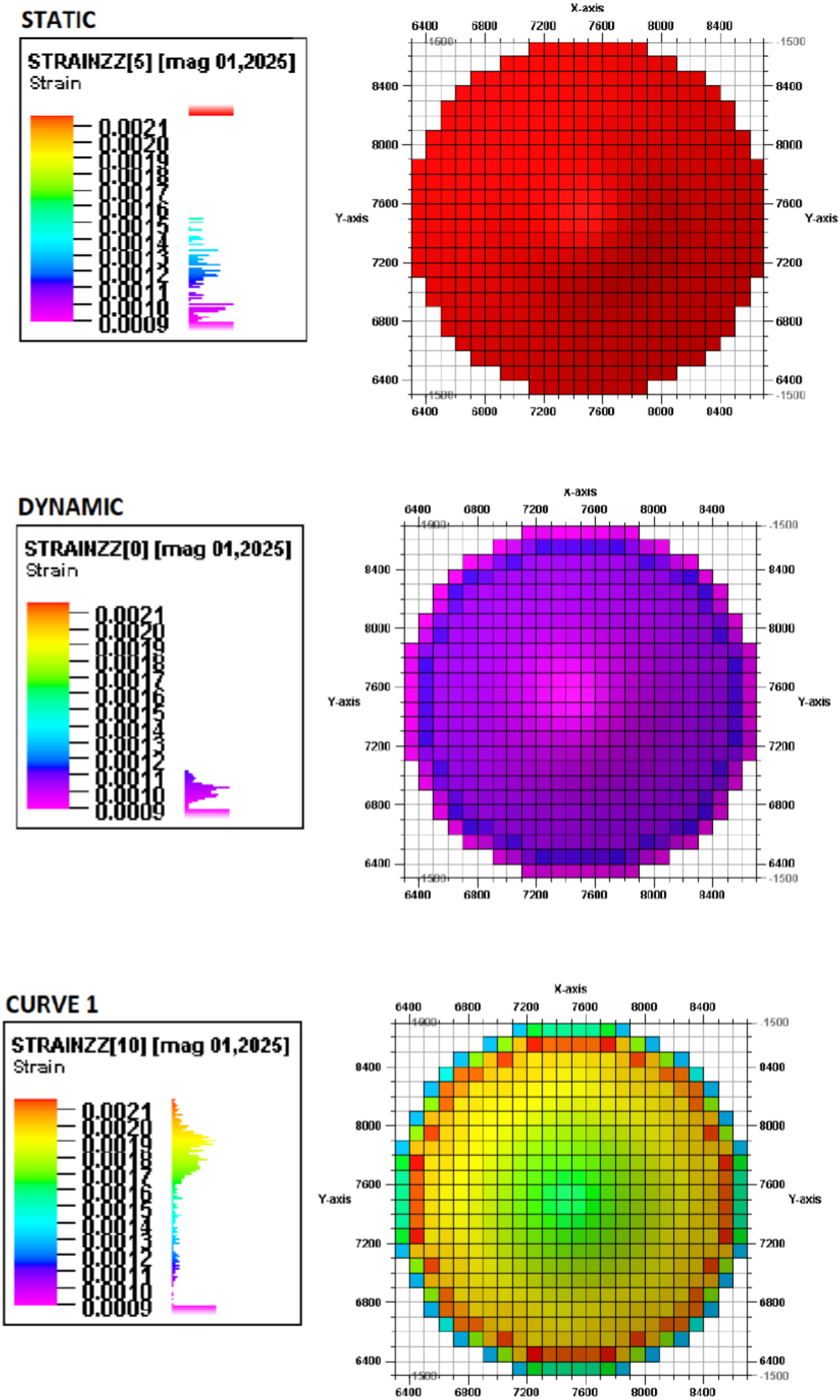

Figure 5: Case 3: vertical strain distribution at the end of production of static, dynamic and